

REE mobility and fractionation during shale weathering along a climate gradient

Lixin Jin^{a,*}, Lin Ma^a, Ashlee Dere^{b,c}, Timothy White^b, Ryan Mathur^d, Susan L. Brantley^b

^a Department of Geological Sciences, University of Texas at El Paso, El Paso, TX 79968, United States

^b Earth and Environmental Systems Institute and Department of Geosciences, Pennsylvania State University, State College, PA 16803, United States

^c Department of Geography and Geology, University of Nebraska at Omaha, Omaha, NE 68182, United States

^d Department of Geology, Juniata College, Huntingdon, PA 16652, United States

ARTICLE INFO

Keywords:

Dissolution kinetics
Sulfides
Organic matter
Sorption
Redox

ABSTRACT

We systematically investigated six soil profiles developed on a climosequence of gray shale to constrain the mobility and fractionation of rare earth elements (REE) during chemical weathering processes. In addition, one site developed on black shale (Marcellus Formation) was included to document REE behaviors in organic-rich versus organic-poor shale end members under the same environmental conditions. Our study shows that REE are mobilized intensively during shale weathering and the extent of depletion is larger under warm/humid climates. However, the integrated release rates calculated from six soil profiles are not directly correlated to mean annual precipitation or temperature. Instead, the primary control might be the REE concentrations in the most reactive minerals. REE-bearing phases in shale (sulfides, phosphates and organic matter) probably react quickly at first, mobilizing REE. Following that, REE are then released more slowly during dissolution reactions of clay minerals. Consistent with this interpretation, black shale weathers much faster and releases more REE than gray shale under the same climate conditions, due to the higher organic matter and sulfide contents and lower soil pH. REE are not 100% depleted in any of the investigated soil sites; in northern sites, depletion is minimal whereas in the southern (warm and humid) sites, surface depletion is higher and re-deposition is observed at depth. Retention of REE is likely caused by adsorption to mineral surfaces as pH increases and dissolved organic matter content decreases with depth. This case study quantified loss, redistribution and fractionation of REE during shale weathering, improved our understanding of REE mobility in surficial environments, and contributed to the exploration of REE as strategic mineral resources.

1. Introduction

Rare earth elements (REE) have been identified as crucial and strategic natural resources. The demand for REE in the United States is increasing rapidly, especially as industrial compounds for novel electronic and green-energy products (e.g., USGS, 2011). REE are relatively abundant in Earth's crust, but REE deposits with minable concentrations are uncommon. Traditionally, exploitable REE concentrations are found in igneous rocks such as carbonatites and alkaline rocks (Chakhmouradian and Wall, 2012), as well as placer deposits, pegmatites, iron-oxide copper-gold deposits, and even in marine phosphates (Long, 2010; Mariano and Mariano Jr., 2012). Recently, REE have been explored at Earth's land surface, especially in laterites developed on felsic igneous rocks (Kynicky et al., 2012). REE in these surficial ores may be low in concentration, but are easily accessible and have a high proportion of more valuable heavy rare earth elements (HREE), making

these deposits profitable. Within laterites, REE are present in accessory minerals of weathering residuals, in secondary phases such as fluorocarbonate and phosphate, and adsorbed onto clay surfaces. One recent study also pointed to deep-sea REE-rich muds in the Pacific Ocean as a new potential REE resource (Kato et al., 2011). The formation of these muds is related to adsorption and concentration of REE from seawater by hydrothermal iron-oxyhydroxides and phillipsite (Kato et al., 2011).

Finding new REE deposits will be facilitated by characterizing global REE cycles from sources to sinks and especially by understanding how REE are released, retained, and transported under different conditions at Earth's surface. During the transformation of bedrock into soils, REE are leached into natural waters and transported to oceans. The REE hosted in easily weathered minerals become depleted in soil profiles early during rock alteration, while those in relatively stable mineral phases remain in the soils for longer duration. The adsorption of dissolved REE in soils also depends on their affinity to mineral surfaces,

* Corresponding author at: 500 W. University Ave., El Paso, TX 79912, United States.

E-mail address: ljin2@utep.edu (L. Jin).

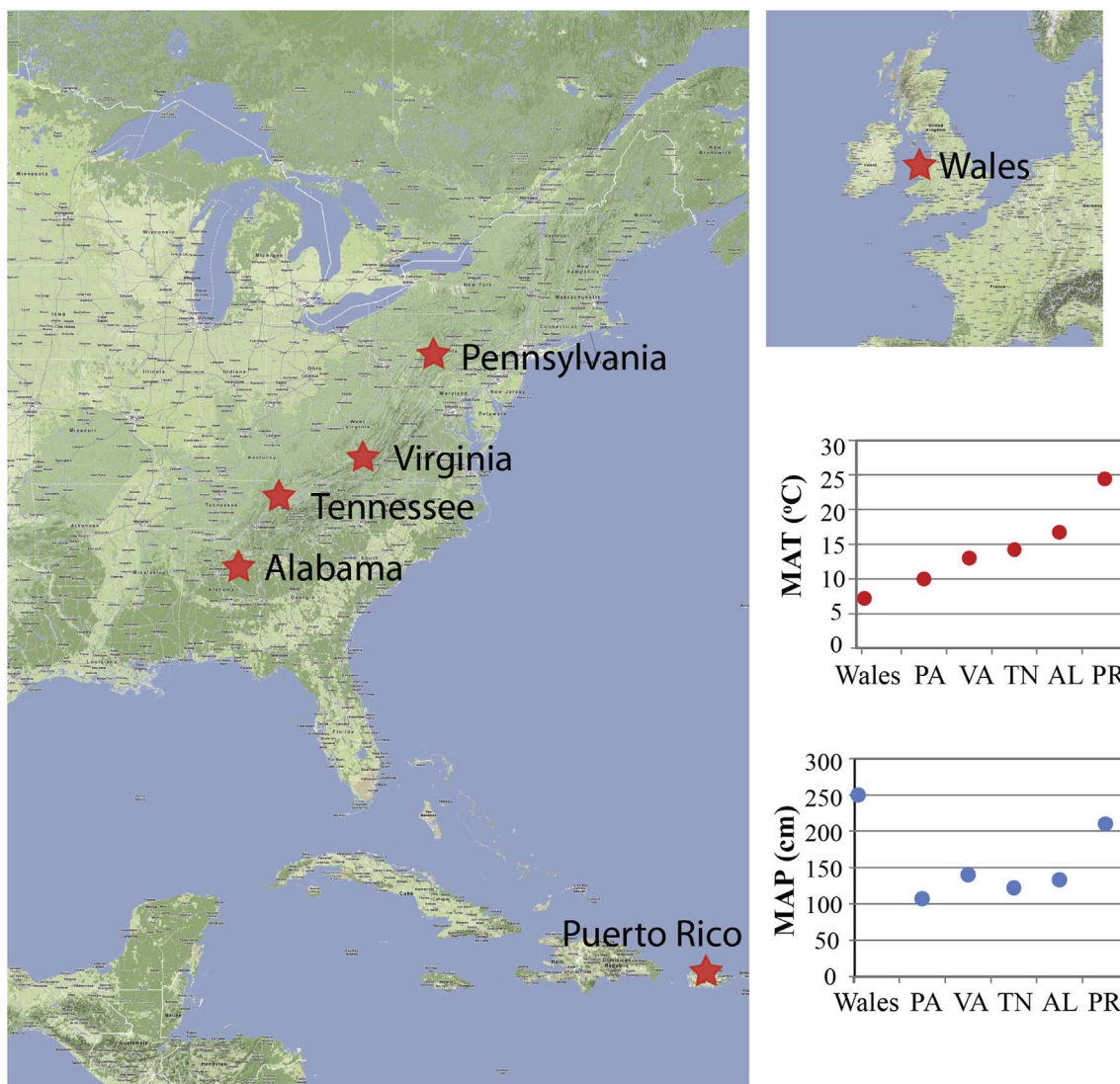


Fig. 1. Location and climate information for sites along the shale weathering transect reported in this study (after Dere et al., 2013). Two sites are both in Pennsylvania but 20 km apart, one on Silurian gray Rose Hill shale and the other on Devonian Marcellus black shale. The Wales soil is developed on a stratigraphically equivalent shale to the Rose Hill; the soil in Puerto Rico is developed on a different shale that has a very similar composition to the Rose Hill, except for Ca.

especially Fe/Al oxyhydroxide and phosphate phases. Controls on the REE mobility and fractionation have been extensively studied during weathering of different lithology (e.g., Millero, 1992; Johannesson and Zhou, 1999; Moller and Bau, 1993; Johannesson et al., 2000; Ohlander et al., 1996; Aubert et al., 2001; Compton et al., 2003; Galan et al., 2007; Yusoff et al., 2013; Vázquez-Ortega et al., 2015), but few studies have focused on the fate of REE in soils developed on shale (e.g. Ma et al., 2011). It is crucial to fill this knowledge gap because shale underlies up to 25% of Earth's land surface (Amiotte-Suchet et al., 2003) and has greater REE abundances than any other sedimentary rocks such as carbonate, sandstone, and evaporite (Rudnick and Gao, 2003).

This study of REE mobilization during rock-water interaction builds on an old paradigm that soil forms as a function of climate, topography, organisms, parent material type, and soil age, the so-called state factors (Jenny, 1941). In particular, we use a gradient approach that has often been used to investigate the influence of different variables on weathering (such as chronosequences, lithosequences and climosequences) (Bockheim, 1980; Birkeland, 1999; White and Blum, 1995; Chadwick et al., 1999; Gaillardet et al., 1999; Jacobson et al., 2003; West et al., 2005; Williams et al., 2010; Rasmussen et al., 2011; Dere et al., 2013).

Here, we systematically studied soil profiles in six watersheds developed on a previously described sequence of gray shales along a climate transect in the eastern USA, Puerto Rico and Wales (Fig. 1; Dere et al., 2013) to constrain the mobility and fractionation of REE during different stages of shale weathering. In addition, one site on Marcellus black shale in Pennsylvania was included and compared to the gray shale site to examine the REE behavior in organic-rich versus organic-poor shale end members under the same environmental conditions. Our main objectives were to investigate: 1) REE abundances in shale-derived soils and REE depletion rates along the climosequence, 2) the biogeochemical, and hydrological conditions (e.g., cation exchange capacity, redox conditions, dissolved organic carbon, REE-bearing phases, and pH) that dictate the mobility, retention, and fractionation of REE in surface and subsurface environments, 3) the lithological controls on REE release rates by comparing soils developed on the black and gray shales, and 4) the difference in long-term versus short-term REE release rates in shale weathering. This study will contribute to our understanding of REE geochemical behavior during continental shale weathering and potential sites for exploration of REE resources.

Table 1
Characteristics of the shale transect sites^a.

Site	Latitude	Longitude	Elevation (m)	MAT (°C)	MAP (cm yr ⁻¹)	PET (cm yr ⁻¹)	P _{eff} (cm yr ⁻¹)	Soil thickness (cm)	Soil residence time (ka)	Samples collected
Gray Shale (Rose Hill Shale) Wales, UK	N52° 28.416	W3° 41.575	417	7.2	250	45	205	35	10	Soil profile and rock fragments, saprolite does not exist
Pennsylvania (PA)	N40°	W77°	297	10	107	53	54	28	17	Soil profile, saprolite and bedrocks
Virginia (VA)	N39.31	W79°	752	11	106	57	49	80	47	Soil profile with rock fragments, soils developed on shales but underlain by sandstone
Tennessee (TN)	N35° 55.625	W83°	418	14	138	64	74	398	234	Soil profile with rock fragments, saprolite was not sampled
Alabama (AL)	N34° 25.375	W86° 12.400	241	16	136	70	66	220	129	Soil profile with rock fragments, saprolite was not sampled
Puerto Rico (PR)	N18° 18.050	W66° 54.401	366	24	234	81	153	613	253	Soil profile with rock fragments, saprolite was not sampled
Black Shale (Marcellus Shale) Pennsylvania (PA)			10	107	53	54				Three soil profiles along a hillslope, rock fragments, three nests of soil waters

PET = potential evapotranspiration, P_{eff} = effective precipitation (MAP-PET).

^a Site information from Dere et al. (2013) and Dere et al. (2016); the gray and black shale sites in PA are assumed to have the same climate conditions.

2. Geological setting

2.1. Site descriptions

The Susquehanna Shale Hills Critical Zone Observatory (SSHO) is established on Silurian Rose Hill gray shale formation, an oxidized shale, in central Pennsylvania within the Appalachian Basin. This Critical Zone Observatory (CZO) has improved our understanding of the interaction of physical, chemical, hydrological, and biological processes that shape shale-dominated landscapes (e.g., Jin et al., 2010, 2011a, 2011b; Yesavage et al., 2012; Brantley et al., 2013; Dere et al., 2013; Thomas et al., 2013; West et al., 2013; Ma et al., 2015a, 2015b; Dere et al., 2016). Three additional field sites in Virginia (VA), Tennessee (TN), and Alabama (AL) were selected as transect sites for the SSHO along a climate gradient on the same shale unit within the Appalachian Mountains, holding other variables as constant as possible (Fig. 1; Table 1). To expand the climate range, two more sites were included: a tropical site in Puerto Rico (PR) and a cold/wet site in Wales, United Kingdom.

In these studies, efforts have been intentionally focused on the same parent material bedrock composition by choosing sites that are located on Silurian gray shale, known as the Rose Hill Formation of the Clinton Group in PA and VA, the Rockwood Formation in TN, the Red Mountain Formation in AL, and the Gwestyn Formation in Wales. The Oligocene San Sebastian Formation was identified as the most geochemically similar formation in PR to the Rose Hill Formation (Dere et al., 2013). All study sites are located on mountain ridge-tops or relatively flat terrains. We have previously referred to these as “1-D weathering sites” because they were selected to avoid the complexity of downslope sediment transport, thus changes in soil chemistry and mineralogy are entirely due to in situ shale weathering (Jin et al., 2010). These sites have been previously studied for major elemental chemistry and mineralogical transformation relating to the degree of shale weathering (Dere et al., 2013; Dere et al., 2016). Ma et al. (2011) investigated the concentrations and patterns of REE during shale weathering in rocks, soils and water samples for the PA site in SSHO and reported differential weathering, especially dissolution of phosphate phases, controlling the release of REE and dictating REE patterns in soil waters and residual soils. They also showed REE precipitated when soil water recharged to streams with an increase in pH and a decrease in REE solubility (Ma et al., 2011).

One site developed on Devonian black shale (Marcellus Formation) was selected in Huntington, PA to compare REE behaviors in organic-rich and organic-poor shale end-members under the same environmental conditions as the PA gray shale site (SSHO). Chemical weathering reactions and associated isotopic variation (Cu) on this Marcellus site have been previously reported (Mathur et al., 2012; Jin et al., 2013); evolution of soil chemistry and mineralogy as well as accompanied changes in porosity and mineral surface area have been modeled using reactive transport codes and major mineral dissolution reactions to identify shale transformation to soil (Heidari et al., 2017).

2.2. Climate gradient

Mean annual temperature (MAT) and mean annual precipitation (MAP; cm yr⁻¹) were estimated for each site using data from proximal weather stations at similar elevations with at least 20 years of records (Dere et al., 2013; Table 1). Along the east coast of the United States, the climate is characterized by a temperate end-member in Pennsylvania and a warm and wet end-member in Puerto Rico (Fig. 1). Wales is an outlier, with low MAT but high MAP. Potential evapotranspiration (PET; cm yr⁻¹) was estimated for each site by the Thornthwaite method (Thornthwaite, 1948) and effective precipitation (P_{eff}; cm yr⁻¹) was calculated as the difference between MAP and PET and reported by Dere (2014) (Table 1).

Table 2
REE and Zr concentrations (ppm) in outcrop, rock fragment and deepest soil samples at the study sites.

Site	Sample name	IGSN ^a	Type	La	Ce	Pr	Nd	Sm	Eu	Gd	Tb	Dy	Ho	Er	Tm	Yb	Lu	REE	Zr
Wales	Pn431-35	SSH00001HH	Deepest soil	54	132	13	47	8.3	1.9	6.5	1.0	5.6	1.2	3.4	0.5	3.3	0.5	279	166
	Q-RF	SSH0000GG	Shale chip ^b	55	6	23	4.9	1.2	5.1	0.8	5.4	1.1	3.5	0.5	3.3	0.5	131	164	
	ALD-10-01	Local outcrop ^b	35	74	8	26	5.4	1.4	5.2	0.9	5.5	1.2	3.2	0.5	3.1	0.5	168	157	
	ALD-10-02	Local outcrop ^b	212	454	54	177	29.4	5.8	15.0	1.7	8.2	1.4	3.7	0.5	3.4	0.5	966	164	
	ALD-10-03	Local outcrop ^b	18	44	5	18	3.9	1.0	3.6	0.6	4.2	0.9	2.6	0.4	2.8	0.4	106	164	
	ALD-10-04	Local outcrop ^b	70	163	19	66	12.1	2.5	7.5	1.0	5.9	1.2	3.3	0.5	3.3	0.5	356	219	
	ALD-10-06	Local outcrop ^b	56	103	11	34	6.0	1.4	5.0	0.9	5.4	1.1	3.2	0.5	3.3	0.5	231	190	
	ALD-10-07	Local outcrop ^b	19	42	5	17	4.3	1.1	4.6	0.8	5.4	1.2	3.4	0.5	3.5	0.5	109	207	
	ALD-10-08	Local outcrop ^b	18	36	4	13	3.1	0.9	4.1	0.8	5.1	1.1	3.2	0.5	3.2	0.5	93	180	
	ALD-10-09	Local outcrop ^b	20	45	6	20	4.8	1.2	4.7	0.8	4.9	1.1	2.9	0.5	3.0	0.5	115	169	
	ALD-10-33	SSH000STU	Local outcrop ^b	39	87	10	34	6.8	1.6	5.3	0.8	5.1	1.1	2.9	0.5	3.1	0.5	197	137
	Average	SSH000SUU	Local outcrop ^b	51	110	13	43	8.1	1.8	6.0	0.9	5.5	1.1	3.2	0.5	3.2	0.5	247	175
	Sidev	SSH000STZ	Local outcrop ^b	59	127	15	49	7.9	1.5	3.3	0.3	1.0	0.1	0.3	0.0	0.2	0.0	266	24
	Parent ^b	SSH00001JS	Deepest soil	33	72	8	28	5.7	1.4	5.0	0.8	5.2	1.1	3.1	0.5	3.2	0.5	167	176
PA-Gray Shale	SPRT 2030	SSH0000SVF	Deepest soil	37	71	9	31	6.1	1.1	4.7	0.9	4.6	1.0	2.9	0.4	2.9	0.4	173	246
	DC1-1 (0-1.1.8) [#]	SSH0000SVF	Drill core	51.6	102	13	45	8.6	1.7	6.5	1.2	6.2	1.4	3.8	0.5	3.9	0.6	246.4	204
	DC1-2 (0.18-0.3)	SSH0000SVG	Drill core	53.1	105	14	48	8.8	1.6	6.5	1.1	5.8	1.3	3.6	0.5	3.7	0.5	252.6	152
	DC1-3 (0.3-0.49)	SSH0000SVH	Drill core	50	99.3	13	45	8.6	1.5	6.7	1.1	5.9	1.3	3.6	0.5	3.7	0.5	240.8	165
	DC1-4 (0.49-0.61)	SSH0000SVI	Drill core	49.8	96.4	13	43	8.3	1.5	6.4	1.1	5.9	1.3	3.6	0.5	3.5	0.5	234.5	171
	DC1-5 (0.61-0.79)	SSH0000SVJ	Drill core	57	113	15	53	9.7	1.9	7.9	1.4	7.0	1.5	4.2	0.6	4.1	0.7	276.4	194
	DC1-8 (1.1-1.2)	SSH0000SVM	Drill core	53.9	107	15	51	9.7	1.9	7.8	1.3	7.0	1.4	3.9	0.6	4	0.6	264.2	179
	DC1-11 (1.5-1.7)	SSH0000SVP	Drill core	53.2	103	14	49	9.8	1.8	7.8	1.3	6.9	1.5	4.2	0.6	4.1	0.6	257.5	186
	DC1-14 (2.4-2.6)	SSH0000SVS	Drill core	53.5	106	14	49	10.1	1.9	8.1	1.4	7.0	1.5	4.2	0.6	4.2	0.6	261.9	195
	DC1-17 (3.4-3.5)	SSH0000SVV	Drill core	49.6	101	13	46	8.9	1.7	7.2	1.2	6.1	1.3	3.7	0.5	3.6	0.5	244.8	173
	DC1-20 (4.3-4.5)	SSH0000SVY	Drill core	44.2	92.5	12	44	10.1	2.3	9.9	1.7	8.2	1.6	4.3	0.6	4.4	0.6	236.7	171
	DC1-23 (5.2-5.4)	SSH0000SW1	Drill core	49.7	96.3	13	46	9.1	1.8	8.0	1.3	6.9	1.4	3.9	0.6	3.9	0.6	241.9	203
	DC1-26 (6.1-6.3)	SSH0000SW4	Drill core	49.5	98.8	13	46	8.7	1.7	7.2	1.2	6.3	1.3	3.8	0.6	3.7	0.6	242.1	172
	DC1-29 (10.7-10.9)	SSH0000SW7	Drill core	45.9	88.7	12	42	8.3	1.7	6.8	1.2	5.7	1.2	3.4	0.5	3.6	0.5	221	170
	DC1-32 (15.2-15.4)	SSH0000SWA	Drill core	46.3	88.1	12	41	8	1.5	6.5	1.1	5.5	1.2	3.5	0.5	3.4	0.5	219.6	172
	DC1-35 (19.8-20.0)	SLB 0000SWD	Deepest soil	47.7	89.7	13	44	8.6	1.7	7.1	1.2	6.0	1.3	3.7	0.5	3.6	0.5	229.5	155
	DC1-37 (22.9-23.0)	SLB 0000SWF	Deepest soil	44	84.6	11	39	7.7	1.5	6.2	1.1	5.2	1.1	3.1	0.4	3.2	0.5	209	153
	DC1-38 (24.4-24.6)	SLB 0000SWG	Deepest soil	33.2	66.4	9	33	7.6	1.6	7.2	1.2	6.3	1.3	3.4	0.5	3.3	0.5	175	231
	Average DC1	Local bedrock ^b	51	99	13	46	9.0	1.7	7.3	1.2	6.3	1.4	3.8	0.5	3.8	0.6	244	178	
	AF-1-15	Deepest soil	47	106	11	44	8.7	1.67	7.56	1.12	6.51	1.28	3.62	0.5	3.6	0.5	243	146	
	SLB 000 02X	SLB 000 02X	Deepest soil	48	94	12	39	7.4	1.5	5.6	0.9	5.6	1.1	3.5	0.5	3.3	0.5	223	151
	SLB 000 03J	SLB 000 03J	Deepest soil	45	71	11	37	7.1	1.4	5.1	0.8	5.1	1.1	3.4	0.5	3.2	0.5	213	177
	AF-1-17	Local bedrock ^b	69	241	18	72	15.7	1.39	15.3	2.33	13	2.57	7.01	1.05	6.9	1.08	468	159	
	MT-09-39	SSH0000PO	Deepest soil	69	126	15	59	11.7	2.6	14.8	2.4	15.0	3.3	7.3	1.3	7.7	1.1	338	882
	TSW-1163	SSH00005CD	Local outcrop ^b	53	108	13	45	8.6	1.6	6.5	1.1	7.3	1.6	4.7	0.8	4.9	0.8	257	311
	TSW-1164	SSH00005D	Local outcrop ^b	54	116	14	48	8.9	1.7	6.5	1.1	7.1	1.6	4.5	0.7	4.8	0.7	269	338
	TSW-1165	SSH00005E	Local outcrop ^b	49	98	12	42	8.7	1.8	7.2	1.2	7.5	1.6	4.7	0.8	4.8	0.7	240	217
	Average	SSH00005ES	Parent ^b	52	107	13	45	8.7	1.7	6.7	1.1	7.3	1.6	4.6	0.7	4.8	0.7	255	289
	Sidev	SLB 000 03J	Deepest soil	3	9	1	3	0.2	0.1	0.4	0.1	0.2	0.0	0.1	0.0	0.1	0.0	17	64
	TN	SSH0000S2	Deepest soil	53	112	14	49	9.2	1.7	8.2	1.3	7.9	1.6	4.7	0.7	4.4	0.7	268	268
	ALD-11-432	SSH0000SHJ	Shale chip ^b	52	103	12	48	8.6	1.7	8.3	1.2	7.3	1.6	4.6	0.7	4.4	0.7	254	261
	ALD-10-432	SSH00006Q	Local outcrop ^b	56	114	15	51	10.0	1.9	8.0	1.3	7.9	1.7	4.7	0.7	4.7	0.7	277	256
	TSW-1212	SSH00006R	Local outcrop ^b	53	105	13	45	8.6	1.6	6.8	1.1	7.1	1.5	4.5	0.7	4.5	0.7	254	247
	TSW-1213	SSH00006S	Local outcrop ^b	55	112	14	49	9.5	1.9	7.6	1.2	7.7	1.6	4.5	0.7	4.6	0.7	270	272
	TSW-1214	SSH00006T	Local outcrop ^b	54	109	14	48	9.2	1.8	7.7	1.2	7.5	1.6	4.6	0.7	4.6	0.7	264	259
	AL	ALD-11-508	SSH00000TR	2	5	1	2	0.7	0.1	0.7	0.1	0.4	0.1	0.0	0.1	0.0	0.1	13	10
		ALD-10-2025	SSH00000SJ	56	99	18	87	21.4	4.6	17.6	1.7	6.9	1.0	2.5	0.3	2.2	0.4	338	148
			58	110	16	55	12.1	2.5	11.1	1.8	10.1	2.1	5.5	0.8	5.2	0.8	290	165	

(continued on next page)

Table 2 (continued)

Site	Sample name	IGSN ^a	Type	La	Ce	Pr	Nd	Sm	Eu	Gd	Tb	Dy	Ho	Er	Tm	Yb	Lu	REE	Zr
ALD-10-2026	SSH00008K	Local outcrop ^b	60	123	17	64	14.8	3.1	13.9	2.1	12.3	2.5	6.5	1.0	5.8	0.9	327	219	
	SSH00008M	Local outcrop ^b	51	100	13	45	9.1	1.8	7.5	1.2	7.3	1.6	4.4	0.7	4.3	0.6	247	226	
	Average	56	111	15	54	12.0	2.4	10.8	1.7	9.9	2.1	5.5	0.8	5.1	0.8	288	203		
	(parent ^b)																		
PR	Sidey	5	12	2	9	2.9	0.6	3.2	0.5	2.5	0.5	1.1	0.2	0.8	0.1	40	33		
	Deepest soil	51	61	12	55	11.8	3.7	13.3	1.9	11.1	2.2	6.4	0.9	5.6	0.9	237	114		
	SSH00003XL	Local outcrop ^b	10	23	3	15	2.8	0.8	2.9	0.4	2.3	0.5	1.5	0.2	1.4	0.2	63	49	
	SSH00003W	Local outcrop ^b	37	26	5	22	3.7	1.1	4.9	0.6	3.4	0.7	2.0	0.3	1.5	0.2	108	55	
ALD-11-93	Average	24	24	4	18	3.3	0.9	3.9	0.5	2.9	0.6	1.7	0.2	1.5	0.2	86	52		
	(parent ^b)																		
	Sidey	19	2	1	5	0.6	0.2	1.4	0.1	0.7	0.2	0.4	0.0	0.1	0.0	32	4		
	PAAS	38	80	9	34	5.6	1.1	4.7	0.8	4.7	1.0	2.9	0.4	2.8	0.4	185			

^a International Geo Sample Number, www.geosamples.org.^b Samples used to calculate the parent composition for each site.

Numbers in the parenthesis refer to the depth range of the drill core samples in m.

2.3. Soil residence time

Soil residence time (SRT) is defined here as the average time that a particle resides in one of the soil profiles after formation from parent material but before erosion at the ridge-top. The SRT is a good estimate for the duration of time soil particles remain in the zone of weathering. The SRT of all soil profiles, reported by Dere et al. (2013) and discussed in Dere (2014), are summarized in Table 1 and introduced briefly below. The maximum SRT estimated is 250 ka for the PR site, while other soils have estimated values of SRT < 100 ka. Over that time period, the climate fluctuated as glacial and interglacial intervals in North America, including the transition from the last glacial maximum (LGM) to the present (Imbrie et al., 1984; Cadwell and Muller, 2004; Clark et al., 2004). The LGM directly impacted Wales by glaciation, while PA was subjected to periglacial conditions until at least 15 ka (Ciolkosz et al., 1986; Clark and Ciolkosz, 1988; Gardner et al., 1991). Previous researchers have also found periglacial features present in VA and the Great Smoky Mountains in TN (King and Ferguson, 1960; Clark and Ciolkosz, 1988).

3. Methods

3.1. Rock and soil sampling for the Rose Hill gray shale sites

The archived samples used for this REE study were previously characterized for major chemistry, mineralogy, and soil properties (Mathur et al., 2012; Jin et al., 2013; Dere et al., 2013; Dere, 2014; Dere et al., 2016), and registered with international geo sample numbers (IGSN) at www.geosamples.org. Sampling methods are discussed briefly below. Samples were collected using a 5-cm diameter hand auger from the mineral soil surface to the depth of refusal where auger penetration is impossible. Samples were collected at 5-cm intervals in the upper 20 cm of the profile and then at 10-cm intervals below that. The organic horizon was collected separately by hand before augering and the interface between the organic and mineral horizon was defined as a depth of 0 cm. In addition to hand augering, soil pits were dug as deeply as possible (maximum depth of 2 m) and described (Soil Survey Staff, 1993). All samples were collected and analyzed in bulk, without any separation of fine fractions. To constrain parent composition, rock samples were collected from outcrops nearby and/or from soil pits or augered soils as chips. At the PA site in SSHO, 25-m drill core samples (DC-1) allowed characterization of the Rose Hill shale bedrock (Jin et al., 2010).

Soils and saprolite are operationally defined here as all the materials that can be augered or dug by hand. Soil does not retain evidence of the original structure of the rock, generally due to bioturbation, and can easily be mobilized downslope through physical erosion but saprolite retains rock structure. Beneath augerable soil lies either saprolite (in southern samples) or blade-like rock fragments of mostly in-place shale or fractured shale that has been referred to as saprock (Jin et al., 2011b). Saprock is chemically altered from bedrock, but retains an original bedrock character, i.e. bedding and structure. Different from saprolite or soil, saprock cannot be augered and is therefore referred to as the layer of “augering refusal”. At the gray shale site in PA, Jin et al. (2011b) argued that fresh bedrock was only encountered at depth of 26 m and deeper at ridges and that an intervening layer of “saprock” was found between fresh bedrock and soil. Therefore, the augerable soil in PA overlies the saprock without intervening saprolite. Similar soil/bedrock interface structures were also observed in the weathering profile in Wales. In VA, soil is developed from shale that extends directly into an underlying sandstone layer (~80 cm deep). Weathering profiles in TN, AL, and PR consist of soils overlying saprolite and hand augering did not penetrate fresh bedrock beneath the soil/saprolite. The characterization of weathering profiles is reported in Table 1. In the following discussion, “soils” collectively refer to the entire weathering profiles that were sampled, and “rocks” refers to parent materials that are not weathered.

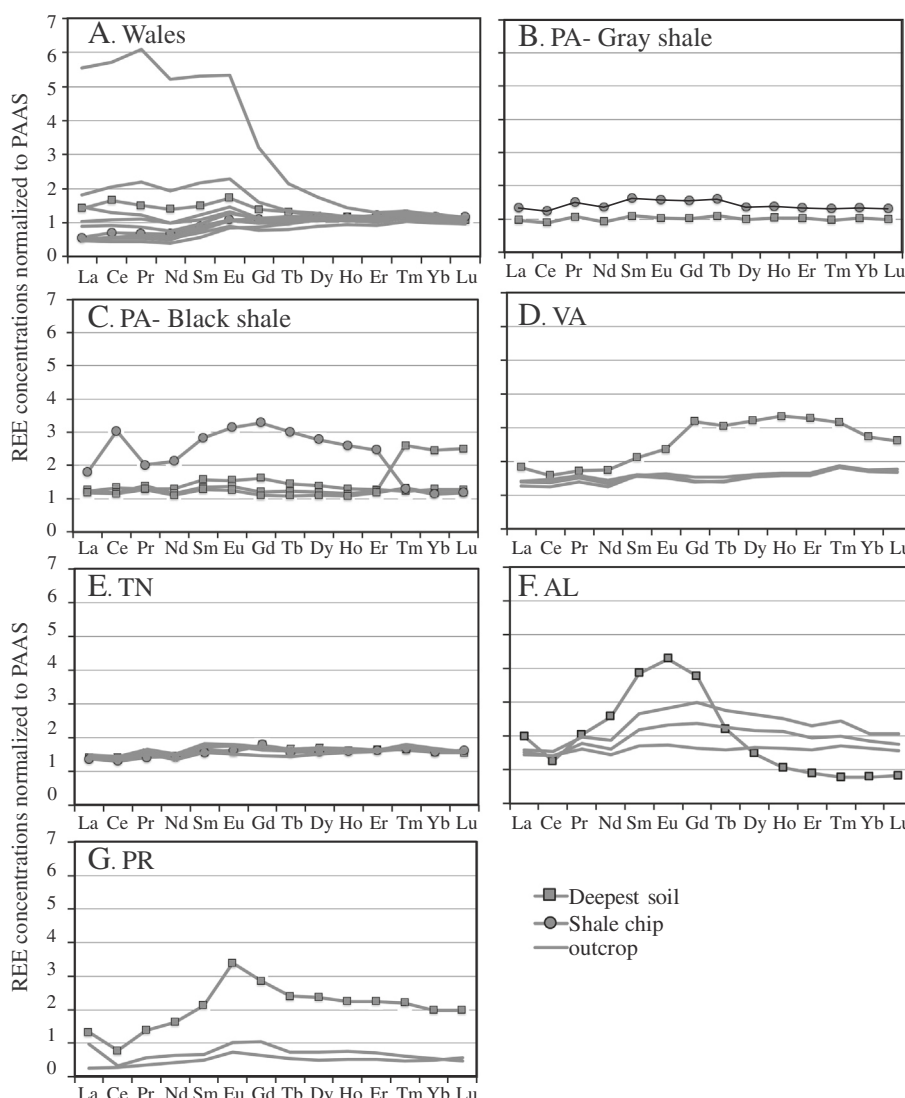


Fig. 2. REE concentrations (normalized to PAAS) of rock fragments and the deepest augered sample at each site: (A) Wales, (B) PA-gray shale, (C) PA-black shale, (D) VA, (E) TN, (F) AL, and (G) PR.

3.2. Rock, soil and soil water sampling for the Marcellus black shale site

A soil pit was dug in Huntingdon, PA for soil sample collection of the Marcellus Formation black shale (PA-BlackShale1). Rock chips from the bottom of the soil pit provided bedrock samples. In addition, soil profiles were sampled using a 5-cm diameter hand auger in Jackson Corners, central Pennsylvania, along a planar hillslope, at ridge top and valley floor locations (PA-Blackshale2 and PA-BlackShale3, respectively) (Mathur et al., 2012; Jin et al., 2013). Three nests of tension lysimeters (soil water samplers) were installed in 2010 along the same hillslope at the ridge top (MRT), mid-slope (MMS) and valley floor (MVF) positions. The MRT and MVF lysimeter nests are next to soil cores PA-BlackShale 2 and PA-BlackShale3, respectively. At each location, lysimeters were placed at 10-cm intervals for the top 60 cm and then at 20-cm intervals below that. The soil water samples were collected weekly beginning in the spring of 2010, two weeks after installation, as spring and fall are the wet seasons in central Pennsylvania. The water in the lysimeter cup is sampled, emptied and pulled to -50 centibars vacuum for the next sampling.

3.3. REE analysis

Bulk soil samples and rock fragments were air-dried and ground to pass through a 100-mesh sieve ($<150\text{ }\mu\text{m}$). REE abundances were

measured by SGS Canada Inc. (Minerals Services Laboratory at Toronto, Ontario; method IMS95A). In this analysis, 0.1 g of ground sample was fused at $950\text{ }^{\circ}\text{C}$ with lithium metaborate and re-dissolved in dilute nitric acid. Resultant solutions were analyzed by inductively coupled plasma mass spectrometry (ICP-MS) for REE and Zr (analytical details can be found at www.ca.sgs.com). For quality assessment and control, randomly selected samples were run as duplicates and the precision was estimated at $\pm 5\%$ of measured values. In addition, two USGS rock standards (BCR-2 and W-2) were analyzed as unknown samples and reported REE concentrations were compared to reference values. The relative errors observed were $<10\%$ for REE and Zr, except for Tm ($\sim 15\%$) (Appendix Table 1). A selected number of the soil samples have been digested by LiBO_2 fusion and measured by inductively coupled plasma optical emission spectrometry (ICP-OES) for Zr concentrations at the Penn State Materials Characterization Lab (MCL) and reported in Dere et al. (2013). Those reported values were consistent with the data collected by ICP-MS for the same samples from this study (Appendix Table 2).

The ceramic cups of lysimeters emplaced in the Marcellus site have a maximum pore size of $1.3\text{ }\mu\text{m}$. The soil water samples collected via these lysimeters were therefore not filtered further before major element analysis (Heidari et al., 2017). In order to investigate the transport of REE in different forms (dissolved versus colloidal), some soil waters were additionally filtered in the laboratory, often three months

Table 3
Concentrations and mass transfer coefficients of REEs as well as Zr concentrations for soils of all study sites.

Sample name	Depth	La	Ce	Pr	Nd	Sm	Eu	Gd	Tb	Dy	Ho	Er	Tm	Yb	Lu	REE	Zr
	cm	ppm	ppm	ppm	ppm	ppm	ppm	ppm	ppm	ppm	ppm	ppm	ppm	ppm	ppm	ppm	
Wales	10	46.3	107	11.3	39.6	6.7	1.33	4.8	0.73	4.39	0.88	2.51	0.37	2.6	0.38	229	
Q-0-10	20	42.6	94.2	9.67	31.2	5.5	1.27	4.52	0.78	4.51	0.95	2.71	0.43	2.9	0.43	202	
Q-10-20	30	39	90.9	9.61	33.5	6.3	1.42	5.57	0.89	4.93	1.01	2.96	0.46	3.0	0.45	159	
Q-20-30	31	41.2	93.9	9.8	34	6.7	1.43	5.56	0.9	5.26	1.08	3.26	0.47	3.1	0.45	169	
Q-30-31	35	54.	132	13.3	47.3	8.3	1.87	6.45	1.02	5.61	1.16	3.37	0.5	3.3	0.46	176	
Q-31-35	32.7	8.1	27.9	5.7	1.4	5.0	0.8	5.2	1.1	3.1	0.5	3.2	0.5	3.2	0.5	176	
PA (gray)																	
SPRT 0010	5	37.6	72	9.04	31	5.7	1.1	4.75	0.86	4.74	1.02	2.97	0.39	3.1	0.43	175	
SPRT 1020	15	42.4	82.8	10.6	36	6.8	1.2	5.47	0.98	5.34	1.13	3.34	0.45	3.3	0.52	273	
SPRT 2030	25	36.9	70.8	9.48	31.2	6.1	1.1	4.71	0.85	4.63	1.03	2.92	0.39	2.9	0.43	275	
Parent	51	99	13	46	9.0	1.7	7.3	1.2	6.3	1.4	3.8	0.5	3.8	0.6	244	246	
VA																	
MT-09-32	10	46.0	102	10.7	42.4	8.1	1.63	8.41	1.25	8.18	1.79	5.44	0.73	4.9	0.75	242	
MT-09-33	20	46.4	100	10.9	42.6	8.0	1.71	7.96	1.21	7.53	1.61	4.82	0.7	4.7	0.72	239	
MT-09-34	30	40.0	85.4	9.67	38.5	7.2	1.4	6.6	0.92	5.61	1.22	3.53	0.52	3.4	0.55	205	
MT-09-35	40	39.8	85.7	9.56	38.9	6.9	1.46	6.86	0.99	6.12	1.3	4.03	0.57	3.6	0.59	206	
MT-09-36	50	53.1	108	12.4	48.2	8.7	1.8	8.98	1.32	7.82	1.7	4.85	0.67	4.5	0.69	263	
MT-09-37	60	56.4	113	13.5	54.2	10.1	2.03	10.3	1.45	8.85	1.88	5.35	0.82	4.9	0.81	280	
MT-09-38	70	64.3	124	16.8	65.9	19.4	6.54	47.1	9.25	51.7	10.6	27.8	3.93	19.2	3.15	470	
MT-09-39	80	69.4	126	15.1	58.7	11.7	2.55	14.8	2.36	15	3.31	9.32	1.28	7.7	1.13	338	
Parent	51.5	107.5	13.2	45	8.7	1.7	6.7	1.1	7.3	1.6	4.6	0.7	4.8	0.7	255	289	
TN																	
ALD-09-17	5	39.5	84.1	9.77	33.2	5.9	1.12	5.27	0.91	5.83	1.19	3.33	0.53	3.6	0.53	195	
ALD-09-18	10	46.3	96.2	11.4	38.3	6.8	1.18	5.6	0.97	5.99	1.25	3.66	0.55	3.6	0.52	222	
ALD-09-02	20	46.6	95.6	11	38.4	6.8	1.21	5.49	0.9	5.89	1.19	3.61	0.52	3.5	0.5	221	
ALD-09-03	30	47	99.9	11.5	39.6	7.1	1.24	5.64	0.91	6.03	1.19	3.64	0.51	3.6	0.49	228	
ALD-09-04	40	49.6	108	12.6	44	8.3	1.42	6.27	1.05	6.38	1.25	3.73	0.55	3.7	0.53	247	
ALD-09-05	50	51.4	108	13	45.9	8.4	1.54	6.42	1.09	6.6	1.32	3.75	0.56	3.8	0.56	269	
ALD-09-07	70	55	116	14.4	52.3	9.6	1.68	7.37	1.1	6.29	1.27	3.66	0.55	3.7	0.55	273	
ALD-09-09	90	58.2	124	16.3	61.2	13.1	2.45	9.79	1.43	7.47	1.44	3.98	0.58	3.9	0.55	253	
ALD-09-11	110	53.5	113	13.9	50.1	9.8	1.73	7.81	1.14	6.83	1.31	3.78	0.58	3.8	0.53	268	
ALD-09-13	130	41.6	87.4	10.4	36.4	6.9	1.34	6.3	1.03	6.02	1.25	3.59	0.52	3.6	0.52	207	
ALD-09-15	150	55.6	117	13.5	46.8	8.1	1.37	6.19	0.96	6.1	1.26	3.79	0.55	3.7	0.54	222	
ALD-09-16	155	55.3	116	13.1	45.4	7.9	1.36	6.04	1	6.08	1.25	3.63	0.55	3.8	0.54	262	
ALD-09-64	170	63.9	131	15.6	52.3	9	1.54	6.4	1.07	6.19	1.3	3.7	0.54	3.7	0.57	297	
ALD-10-67	200	57.2	118	13.7	47.4	8	1.46	6.11	0.97	6.15	1.27	3.54	0.55	3.7	0.53	269	
ALD-10-70	220	60.8	125	14.6	49.6	9	1.5	6.72	1.02	6.41	1.37	3.98	0.59	3.9	0.56	285	
ALD-10-73	240	51.7	104	12.2	42.6	8.1	1.45	6.48	0.97	6.14	1.28	3.79	0.52	3.7	0.54	243	
ALD-10-75	250	51.4	108	12.4	42.8	7.9	1.46	6.21	1.04	6.28	1.26	3.65	0.53	3.5	0.49	247	
ALD-11-401	270	48.5	102	11.9	40.8	7	1.27	5.8	0.97	6.07	1.24	3.79	0.58	3.7	0.53	234	
ALD-11-404	300	49.1	105	12.2	43.1	8.3	1.58	7.16	1.15	6.77	1.4	4.14	0.63	4	0.6	245	
ALD-11-426	340	56.1	118	14.1	48.8	9.4	1.62	7.39	1.16	7.23	1.49	4.3	0.66	4.3	0.63	289	
ALD-11-429	370	59.8	125	14.8	52.2	10	1.76	8.43	1.29	8.01	1.62	4.57	0.7	4.5	0.65	268	
ALD-11-432	398	53.1	112	13.6	49.3	9.2	1.7	8.23	1.28	7.91	1.59	4.67	0.66	4.4	0.67	268	
Parent	54	109	14	48	9.2	1.8	7.7	1.2	7.5	1.6	4.6	0.7	4.6	0.7	233	259	
AL																	
ALD-10-114	10	17.5	30.8	3.7	14.7	2.6	0.54	2.62	0.37	2.39	0.54	1.58	0.24	1.6	0.26	79	
ALD-10-115	20	26.2	50.3	5.69	22.4	4	0.86	4.04	0.58	3.5	0.74	2.22	0.31	2.4	0.38	124	
ALD-10-116	30	33.5	53	7.21	28.8	5.1	0.98	4.44	0.6	3.62	0.76	2.3	0.34	2.4	0.36	143	
ALD-10-117	40	39.7	52.9	8.66	35	6.1	1.23	5.41	0.72	3.74	0.74	2.27	0.31	2.1	0.35	159	
ALD-10-118	50	53.4	65.4	11.8	48.6	8.5	1.71	6.6	0.83	4.15	0.79	2.32	0.31	2.2	0.35	207	
ALD-10-121	70	103	124	29.1	133	27.6	5.61	18.4	2.06	7.74	1.14	2.58	0.39	2.3	0.39	457	
ALD-10-123	100	96.1	124	28.6	143	31.7	7.18	24.8	2.51	9.14	1.24	2.83	0.38	2.3	0.33	474	

Table 3 (continued)

Sample name	Depth	La	Ce	Pr	Nd	Sm	Eu	Gd	Tb	Dy	Ho	Er	Tm	Yb	Lu	REE	Zr	
	cm	ppm	ppm															
ALD-10-125	120	123	163	34.2	187	47	10.2	37.1	3.68	13.4	1.8	3.81	0.45	2.7	0.41	628	173	
ALD-10-127	140	117	162	32.7	178	45.9	9.98	37.7	3.66	13.5	1.79	3.93	0.43	2.7	0.42	610	161	
ALD-10-129	155	44.6	60.2	10.9	52.7	12	2.65	10.2	1.01	4.14	0.65	1.67	0.22	1.5	0.23	203	119	
ALD-11-506	180	56.7	76.1	13.3	61.3	14.3	3.09	12	1.25	5.15	0.78	2.12	0.28	1.9	0.31	249	158	
ALD-11-508	200	75.9	99	17.9	86.9	21.4	4.63	17.6	1.7	6.85	1.04	2.52	0.31	2.2	0.35	338	148	
Parent	56	111	15	54	12.0	2.4	10.8	1.7	9.9	2.1	5.5	0.8	5.1	0.8	287.9	203		
PR	8	4.8	9.8	1.13	4.4	1.1	0.35	1.48	0.26	1.6	0.37	1.2	0.22	1.4	0.25	28	135	
ALD-11-13	10	4.5	9.2	1.02	4	1.1	0.33	1.39	0.24	1.72	0.39	1.22	0.2	1.5	0.26	27	119	
ALD-11-14	15	5.8	11.6	1.33	5.4	1.2	0.35	1.64	0.26	1.7	0.4	1.41	0.21	1.7	0.24	33	128	
ALD-11-15	20	4.3	8.9	0.92	3.8	0.9	0.27	1.18	0.23	1.59	0.39	1.37	0.22	1.6	0.28	26	128	
ALD-11-16	30	4.1	8.9	0.94	3.8	0.8	0.26	1.24	0.23	1.67	0.41	1.4	0.23	1.7	0.27	26	128	
ALD-11-17	40	4.4	9.5	0.95	3.8	0.8	0.25	1.23	0.21	1.48	0.35	1.27	0.19	1.4	0.19	26	131	
ALD-11-18	50	4.3	9.5	0.92	3.7	0.9	0.26	1.07	0.19	1.34	0.34	1.09	0.18	1.2	0.19	25	128	
ALD-11-19	111	6.2	19.6	1.47	6	1.4	0.41	1.49	0.26	1.93	0.44	1.55	0.23	1.8	0.25	43	130	
ALD-11-25	160	6.8	26.8	1.81	7.5	1.8	0.55	2.09	0.34	2.11	0.55	1.67	0.27	1.8	0.3	54	117	
ALD-11-30	210	8.8	29.4	1.35	10.3	2.2	0.59	2.26	0.35	2.34	0.55	1.69	0.26	1.9	0.29	63	120	
ALD-11-38	260	7.2	25.5	1.97	8.8	1.8	0.51	1.86	0.3	1.85	0.42	1.4	0.22	1.6	0.28	54	115	
ALD-11-43	310	7.6	29.2	2.09	9.1	2.1	0.53	1.88	0.31	1.89	0.43	1.41	0.22	1.6	0.28	59	117	
ALD-11-48	360	9.3	38.3	2.74	12.2	2.8	0.81	2.87	0.43	2.76	0.6	1.91	0.26	1.9	0.33	77	114	
ALD-11-53	410	8.5	29.7	2.5	10.8	2.5	0.71	2.59	0.42	2.61	0.58	1.8	0.27	1.8	0.3	65	125	
ALD-11-58	460	19.1	42.1	4.5	19.6	4.2	1.3	4.55	0.71	4.3	0.95	2.76	0.37	2.5	0.38	107	131	
ALD-11-63	505	22.5	45.2	5.6	24.8	5.2	1.49	5.21	0.75	4.73	0.95	2.82	0.41	2.7	0.43	123	119	
ALD-11-76	580	73.2	108	17.8	79.6	17	5.3	18.1	2.54	14.5	2.88	1.1	6.5	0.97	355	105		
ALD-11-86	632	50.6	61.4	12.2	54.9	11.8	3.66	13.3	1.86	11.1	2.23	6.4	0.89	5.6	0.86	237	114	
ALD-11-92	24	24	4	18	3.3	0.9	0.9	3.9	0.5	2.9	0.6	1.7	0.2	1.5	0.2	85.5	52	
Parent	359																	
PA-Black shale																		
AF-1-1	2	24.9	53.2	5.92	22.4	4.2	0.82	3.76	0.57	3.42	0.69	2.03	0.29	2	0.29	124	85.1	
AF-1-3	41.5	40.4	80.9	8.93	31.4	5	0.86	4.52	0.71	4.26	0.97	2.68	0.41	2.8	0.4	184	132	
AF-1-5	58	43.6	88.9	9.93	34.9	5.7	0.97	4.44	0.77	4.46	0.91	2.89	0.45	3	0.47	201	149	
AF-1-7	73.5	50	103	11.2	41.2	6.6	1.3	5.77	0.91	5.43	1.19	3.48	0.51	3.5	0.55	235	170	
AF-1-9	104	58	139	15.9	67.3	16.2	3.5	15	2.08	1.1	4.3	0.95	2.76	0.77	5.2	0.77	342	154
AF-1-11	132.5	44.9	97.8	10.5	40	7.8	1.45	6.68	1.04	5.99	1.23	3.72	0.55	3.8	0.56	226	141	
AF-1-13	150.5	46.5	103	11.4	42.7	7.7	1.54	7.04	1.04	5.92	1.22	3.63	0.49	3.7	0.59	236	150	
AF-1-15	170.5	47	106	11.4	43.8	8.7	1.67	7.56	1.12	6.51	1.28	3.62	0.5	3.6	0.55	243	146	
Parent	68.7	241	17.8	72.1	15.7	3.39	15.3	2.33	13	2.57	7.01	1.05	6.9	1.08	468	159		
PA-Black shale 2 (MVF, valley floor)																		
MVF-0-10	5	32.4	64.5	8.05	26.4	5.1	1.04	4.29	0.79	5.04	1.02	3.17	0.49	3	0.47	156	199	
MVF-10-15	10	36	71.2	8.93	29.8	5.7	1.18	4.95	0.86	5.42	1.12	3.36	0.53	3.3	0.5	173	204	
MVF-15-20	15	37.9	75.4	9.55	31.3	6.1	1.22	4.85	0.85	5.37	1.11	3.47	0.54	3.3	0.51	181	207	
MVF-20-30	20	40.4	79.9	10.1	33	6.2	1.24	4.77	0.79	4.94	1.03	3.2	0.52	3.1	0.49	190	181	
MVF-30-35	30	45.2	88.7	11.3	36.8	7.1	1.38	5.02	0.86	5.22	1.08	3.37	0.54	3.2	0.5	210	176	
MVF-35-40	35	47.5	91.3	11.5	37.7	7.2	1.39	5.08	0.86	5.32	1.07	3.22	0.51	3.2	0.52	216	160	
MVF-40-45	40	47.7	92.5	11.7	38.4	7.3	1.41	5.2	0.86	5.21	1.08	3.3	0.53	3.3	0.51	219	158	
MVF-45-52	45	45.2	87.6	11	35.9	6.8	1.35	4.86	0.79	4.85	0.99	3.12	0.51	3.1	0.49	207	154	
MVF-52-57	52	46.9	90.9	11.2	36.6	6.7	1.36	4.88	0.81	5.02	1.02	3.2	0.5	3.1	0.5	213	162	
MVF-57-62	57	50.2	94.5	11.7	38.4	7.1	1.36	5.23	0.87	5.41	1.1	3.33	0.51	3.2	0.5	223	151	
MVF-62-67	62	49.3	95	11.8	38.4	7.4	1.43	5.29	0.88	5.42	1.12	3.41	0.53	3.2	0.51	224	159	
MVF-67-72	67	52.4	98.8	12.4	40.2	7.7	1.49	5.63	0.92	5.72	1.17	3.54	0.54	3.3	0.51	234	160	
MVF-72-77	72	51.8	96.5	12.3	39.7	7.4	1.49	5.42	0.92	5.68	1.16	3.47	0.53	3.2	0.51	230	155	
MVF-77-82	77	49.2	95.6	12.2	39.5	7.5	1.52	5.69	0.96	5.89	1.19	3.66	0.57	3.4	0.52	227	153	
MVF-82-84	82	48.1	93.7	12.2	39.2	7.4	1.48	5.59	0.94	5.58	1.13	3.5	0.53	3.3	0.51	223	151	

(continued on next page)

Table 3 (continued)

Sample name	Depth	La	Ce	Pr	Nd	Sm	Eu	Gd	Tb	Dy	Ho	Er	Tm	Yb	Lu	REE	Zr
	cm	ppm															
PA-Black shale 3 (MRT, Ridge top, CEO)	5	37.2	76	9.47	31.2	6.2	1.18	4.79	0.83	5.31	1.08	3.44	0.52	3.3	0.51	181	209
MRT-0-17	17	44.7	89	11.1	36.1	6.8	1.33	4.96	0.79	4.98	1.04	3.31	0.52	3.2	0.49	208	183
MRT-17-27	27	44.6	89	11.1	37	7.2	1.34	5	0.82	4.99	1.02	3.25	0.49	3.1	0.49	209	175
MRT-27-38	38	45.4	91.8	11.5	38.4	7.4	1.43	5.3	0.84	5.06	1.03	3.29	0.51	3.1	0.5	216	178
MRT-38-50	50	45.3	90.9	11.3	36.7	6.9	1.32	4.93	0.8	5.09	1.04	3.32	0.52	3.2	0.51	212	178
MRT-50-68	68	47.2	93.5	11.7	37.9	7.3	1.38	5.17	0.84	5.21	1.07	3.35	0.53	3.3	0.54	219	179
MRT-68-83	83	45.3	91	11.3	37.2	7.1	1.36	5.1	0.84	5.14	1.06	3.37	0.52	3.2	0.51	213	177
Sample name	Ti	La	Ce	Pr	Nd	Sm	Eu	Gd	Tb	Dy	Ho	Er	Tm	Yb	Lu	REE	(Ce/Ce*)N
	%	τ	τ	τ	τ	τ	τ	τ	τ	τ	τ	τ	τ	τ	τ	τ	(Eu/Eu*)N
Wales																	
Q-0-10	0.6	0.6	0.5	0.6	0.3	0.1	0.0	-0.1	-0.1	-0.1	-0.1	-0.2	-0.1	-0.1	0.5	1.1	0.9
Q-10-20	0.4	0.4	0.2	0.2	0.0	0.0	-0.1	0.0	-0.1	-0.1	-0.1	-0.1	0.0	0.0	0.3	1.0	1.0
Q-20-30	0.2	0.3	0.2	0.2	0.1	0.1	0.1	0.1	0.0	0.0	0.0	0.0	0.0	0.0	0.2	1.1	0.9
Q-30-31	0.3	0.3	0.2	0.2	0.2	0.1	0.1	0.3	0.1	0.1	0.1	0.1	0.0	0.0	0.8	1.1	1.0
Q-31-35	0.8	0.9	0.7	0.8	0.5	0.5	0.4	0.0	0.0	0.0	0.0	0.0	0.0	0.0	0.0	1.0	1.0
Parent	0.0	0.0	0.0	0.0	0.0	0.0	0.0	0.0	0.0	0.0	0.0	0.0	0.0	0.0	0.0	0.0	1.0
PA (gray)	-0.5	-0.5	-0.6	-0.6	-0.6	-0.6	-0.6	-0.5	-0.5	-0.5	-0.5	-0.5	-0.5	-0.5	-0.5	-0.5	-0.5
SPRT 0010	-0.5	-0.5	-0.5	-0.5	-0.5	-0.5	-0.5	-0.5	-0.5	-0.5	-0.5	-0.4	-0.4	-0.4	-0.4	-0.4	1.0
SPRT 1020	-0.5	-0.5	-0.5	-0.5	-0.5	-0.5	-0.5	-0.5	-0.5	-0.5	-0.5	-0.4	-0.4	-0.4	-0.4	-0.4	0.9
SPRT 2030	0.0	0.0	0.0	0.0	0.0	0.0	0.0	0.0	0.0	0.0	0.0	0.0	0.0	0.0	0.0	0.0	1.0
Parent																	
VA																	
MT-09-32	0.72	0.1	0.2	0.0	0.1	0.1	0.2	0.5	0.4	0.4	0.4	0.4	0.4	0.2	0.2	0.2	1.1
MT-09-33	0.73	0.1	0.0	0.1	0.1	0.2	0.4	0.3	0.2	0.2	0.3	0.1	0.2	0.2	0.1	0.1	1.0
MT-09-34	0.56	0.2	0.2	0.3	0.3	0.3	0.3	0.5	0.3	0.2	0.2	0.1	0.1	0.2	0.3	1.1	0.9
MT-09-35	0.55	0.2	0.3	0.2	0.4	0.3	0.4	0.6	0.4	0.3	0.4	0.2	0.2	0.3	1.1	1.0	1.0
MT-09-36	0.68	0.3	0.3	0.2	0.4	0.3	0.4	0.7	0.5	0.4	0.4	0.4	0.2	0.2	0.2	0.3	1.0
MT-09-37	0.61	0.5	0.5	0.7	0.7	0.7	1.2	0.9	0.7	0.7	0.7	0.6	0.5	0.6	0.6	1.0	0.9
MT-09-38	0.68	0.6	0.5	0.7	0.9	1.9	4.0	8.1	9.7	8.2	7.6	6.8	4.1	4.5	4.4	0.9	1.0
MT-09-39	0.75	0.6	0.4	0.3	0.5	0.6	0.8	1.6	1.5	1.4	1.4	1.0	0.9	0.8	0.6	0.9	0.9
Parent	0.88	0.0	0.0	0.0	0.0	0.0	0.0	0.0	0.0	0.0	0.0	0.0	0.0	0.0	0.0	0.0	1.0
TN																	
ALD-09-17	-0.4	-0.4	-0.4	-0.5	-0.5	-0.5	-0.4	-0.4	-0.4	-0.4	-0.4	-0.4	-0.4	-0.4	-0.4	-0.4	1.1
ALD-09-18	-0.4	-0.3	-0.4	-0.4	-0.5	-0.4	-0.4	-0.4	-0.4	-0.4	-0.4	-0.4	-0.4	-0.4	-0.4	-0.4	1.0
ALD-09-02	-0.3	-0.3	-0.3	-0.3	-0.4	-0.4	-0.4	-0.4	-0.3	-0.3	-0.3	-0.3	-0.3	-0.3	-0.3	-0.3	1.0
ALD-09-03	-0.2	-0.2	-0.3	-0.3	-0.3	-0.3	-0.4	-0.4	-0.3	-0.3	-0.3	-0.3	-0.3	-0.3	-0.3	-0.3	1.0
ALD-09-04	-0.2	-0.1	-0.2	-0.2	-0.2	-0.3	-0.2	-0.2	-0.2	-0.2	-0.2	-0.2	-0.2	-0.2	-0.2	-0.2	1.0
ALD-09-05	-0.1	0.0	-0.1	-0.1	-0.1	-0.1	-0.2	-0.1	-0.1	-0.1	-0.1	-0.1	-0.1	-0.1	-0.1	-0.1	1.0
ALD-09-07	0.0	0.1	0.0	0.1	0.0	-0.1	0.0	0.0	0.0	0.0	0.0	0.0	0.0	0.0	0.0	0.0	1.0
ALD-09-09	0.1	0.2	0.3	0.5	0.4	0.3	0.2	0.0	0.0	0.0	0.0	0.0	0.0	0.0	0.0	0.0	1.0
ALD-09-11	-0.1	0.0	0.0	0.0	-0.1	0.0	-0.1	-0.1	-0.1	-0.1	-0.1	-0.1	-0.1	-0.1	-0.1	-0.1	1.0
ALD-09-13	0.2	0.3	0.2	0.1	0.0	-0.1	-0.1	-0.1	-0.1	-0.1	-0.1	-0.1	-0.1	-0.1	-0.1	-0.1	1.0
ALD-09-15	0.2	0.3	0.2	0.1	0.0	-0.1	0.0	0.0	0.0	0.0	0.0	0.0	0.0	0.0	0.0	0.0	1.0
ALD-09-16	0.2	0.3	0.2	0.1	0.0	-0.1	0.0	0.0	0.0	0.0	0.0	0.0	0.0	0.0	0.0	0.0	1.0
ALD-09-64	0.4	0.5	0.3	0.2	0.0	0.0	0.0	0.0	0.0	0.0	0.0	0.0	0.0	0.0	0.0	0.0	1.0
ALD-10-67	0.3	0.3	0.2	0.2	0.0	0.0	0.0	0.0	0.0	0.0	0.0	0.0	0.0	0.0	0.0	0.0	1.0
ALD-10-70	0.4	0.4	0.3	0.2	0.2	0.0	0.1	0.0	0.0	0.0	0.0	0.0	0.0	0.0	0.0	0.0	1.0
ALD-10-73	0.5	0.4	0.4	0.4	0.3	0.3	0.2	0.4	0.4	0.4	0.4	0.4	0.4	0.4	0.4	0.4	1.0
ALD-10-75	0.6	0.7	0.6	0.5	0.5	0.5	0.4	0.4	0.4	0.4	0.4	0.4	0.4	0.4	0.4	0.4	1.1

Table 3 (continued)

Sample name	Ti	La	Ce	Pr	Nd	Sm	Eu	Gd	Tb	Dy	Ho	Er	Tm	Yb	Lu	REE	(Ce/Ce*)N	(Eu/Eu*)N
%	τ	τ	τ	τ	τ	τ	τ	τ	τ	τ	τ	τ	τ	τ	τ	τ	τ	
ALD-11-401	0.1	0.2	0.1	0.0	-0.1	-0.1	-0.1	0.0	0.0	0.0	-0.2	-0.2	0.0	0.0	0.1	1.1	0.9	
ALD-11-404	-0.2	-0.1	-0.2	-0.2	-0.1	-0.2	-0.1	-0.1	-0.2	-0.2	-0.2	-0.2	-0.2	-0.2	-0.1	1.1	1.0	
ALD-11-426	-0.1	0.0	-0.1	-0.1	-0.1	-0.1	-0.1	0.0	0.0	0.0	0.0	0.0	0.0	0.0	0.0	1.0	0.9	
ALD-11-429	0.1	0.1	0.0	0.0	0.1	-0.1	0.1	0.0	0.0	0.0	0.0	0.0	0.0	0.0	0.1	1.0	0.9	
ALD-11-432	0.0	0.0	0.0	0.0	0.0	-0.1	0.0	0.0	0.0	0.0	0.0	0.0	0.0	0.0	0.0	1.0	1.0	
Parent	0.0	0.0	0.0	0.0	0.0	0.0	0.0	0.0	0.0	0.0	0.0	0.0	0.0	0.0	0.0	1.0	1.0	
AL																		
ALD-10-114	-0.8	-0.8	-0.8	-0.8	-0.8	-0.8	-0.8	-0.8	-0.8	-0.8	-0.8	-0.8	-0.8	-0.8	-0.8	-0.8	1.0	
ALD-10-115	-0.7	-0.7	-0.8	-0.8	-0.8	-0.8	-0.8	-0.8	-0.8	-0.8	-0.8	-0.8	-0.8	-0.8	-0.7	-0.7	1.0	
ALD-10-116	-0.7	-0.7	-0.7	-0.7	-0.8	-0.8	-0.8	-0.8	-0.8	-0.8	-0.8	-0.8	-0.8	-0.8	-0.7	-0.7	1.0	
ALD-10-117	-0.6	-0.6	-0.6	-0.6	-0.6	-0.6	-0.6	-0.6	-0.6	-0.6	-0.6	-0.6	-0.6	-0.6	-0.6	-0.6	1.0	
ALD-10-118	-0.3	-0.5	-0.4	-0.4	-0.3	-0.5	-0.5	-0.5	-0.6	-0.6	-0.7	-0.7	-0.7	-0.7	-0.6	-0.4	0.7	
ALD-10-121	0.5	-0.1	0.6	1.0	0.9	0.4	0.0	-0.3	-0.5	-0.6	-0.6	-0.6	-0.6	-0.6	-0.6	0.3	1.2	
ALD-10-123	0.9	0.3	1.1	2.0	2.0	2.3	1.6	0.7	0.0	-0.3	-0.4	-0.5	-0.5	-0.5	-0.5	0.6	1.2	
ALD-10-125	1.6	0.7	1.6	3.0	3.6	3.9	3.0	1.6	0.6	0.2	-0.4	-0.4	-0.4	-0.4	-0.4	1.6	1.1	
ALD-10-127	1.6	0.8	1.7	3.1	3.8	4.2	3.4	1.7	0.7	0.1	-0.1	-0.3	-0.3	-0.3	-0.3	1.7	1.1	
ALD-10-129	0.4	-0.1	0.2	0.7	0.9	0.6	0.0	-0.3	-0.5	-0.5	-0.5	-0.5	-0.5	-0.5	-0.5	0.2	0.7	
ALD-11-506	0.3	-0.1	0.1	0.4	0.5	0.6	0.4	0.0	-0.3	-0.5	-0.5	-0.5	-0.5	-0.5	-0.5	0.1	0.7	
ALD-11-508	0.9	0.2	0.6	1.2	1.5	1.6	1.2	0.4	-0.1	-0.3	-0.4	-0.4	-0.4	-0.4	-0.4	0.6	1.1	
Parent	0.0	0.0	0.0	0.0	0.0	0.0	0.0	0.0	0.0	0.0	0.0	0.0	0.0	0.0	0.0	1.0	1.0	
PR																		
ALD-11-13	-0.9	-0.8	-0.9	-0.9	-0.9	-0.9	-0.9	-0.9	-0.9	-0.9	-0.9	-0.9	-0.9	-0.9	-0.9	-0.9	1.0	
ALD-11-14	-0.9	-0.8	-0.9	-0.9	-0.9	-0.9	-0.9	-0.9	-0.9	-0.9	-0.9	-0.9	-0.9	-0.9	-0.9	-0.9	1.0	
ALD-11-15	-0.9	-0.8	-0.9	-0.9	-0.9	-0.9	-0.9	-0.9	-0.9	-0.9	-0.9	-0.9	-0.9	-0.9	-0.9	-0.9	0.9	
ALD-11-16	-0.9	-0.8	-0.9	-0.9	-0.9	-0.9	-0.9	-0.9	-0.9	-0.9	-0.9	-0.9	-0.9	-0.9	-0.9	-0.9	1.0	
ALD-11-17	-0.9	-0.8	-0.9	-0.9	-0.9	-0.9	-0.9	-0.9	-0.9	-0.9	-0.9	-0.9	-0.9	-0.9	-0.9	-0.9	1.0	
ALD-11-18	-0.9	-0.8	-0.9	-0.9	-0.9	-0.9	-0.9	-0.9	-0.9	-0.9	-0.9	-0.9	-0.9	-0.9	-0.9	-0.9	1.0	
ALD-11-19	-0.9	-0.8	-0.9	-0.9	-0.9	-0.9	-0.9	-0.9	-0.9	-0.9	-0.9	-0.9	-0.9	-0.9	-0.9	-0.9	1.0	
ALD-11-25	-0.9	-0.7	-0.9	-0.9	-0.9	-0.9	-0.9	-0.9	-0.9	-0.9	-0.9	-0.9	-0.9	-0.9	-0.9	-0.9	1.0	
ALD-11-30	-0.9	-0.5	-0.8	-0.8	-0.8	-0.8	-0.8	-0.7	-0.7	-0.7	-0.7	-0.6	-0.6	-0.5	-0.5	-0.8	2.6	
ALD-11-38	-0.8	-0.7	-0.7	-0.8	-0.7	-0.7	-0.7	-0.7	-0.7	-0.7	-0.7	-0.6	-0.6	-0.5	-0.5	-0.7	3.1	
ALD-11-43	-0.9	-0.5	-0.8	-0.8	-0.8	-0.7	-0.7	-0.7	-0.7	-0.7	-0.7	-0.6	-0.6	-0.5	-0.5	-0.7	2.6	
ALD-11-48	-0.9	-0.5	-0.8	-0.8	-0.8	-0.7	-0.7	-0.7	-0.7	-0.7	-0.7	-0.6	-0.6	-0.5	-0.5	-0.7	2.8	
ALD-11-53	-0.8	-0.3	-0.7	-0.7	-0.6	-0.6	-0.6	-0.6	-0.6	-0.6	-0.6	-0.5	-0.5	-0.5	-0.5	-0.6	3.0	
ALD-11-58	-0.8	-0.5	-0.7	-0.8	-0.7	-0.7	-0.7	-0.7	-0.7	-0.7	-0.7	-0.6	-0.6	-0.5	-0.5	-0.7	3.1	
ALD-11-63	-0.7	-0.3	-0.6	-0.6	-0.5	-0.5	-0.5	-0.5	-0.4	-0.4	-0.4	-0.4	-0.4	-0.3	-0.3	-0.5	1.1	
ALD-11-76	-0.6	-0.2	-0.4	-0.4	-0.3	-0.3	-0.3	-0.4	-0.3	-0.3	-0.3	-0.3	-0.3	-0.2	-0.2	-0.4	1.6	
ALD-11-86	0.5	1.2	1.2	1.6	1.8	1.3	1.5	1.5	1.3	1.5	1.5	1.2	1.2	1.1	1.2	1.1	1.1	
ALD-11-92	0.0	0.2	0.4	0.4	0.7	0.8	0.5	0.7	0.8	0.6	0.7	0.8	0.8	0.8	0.8	1.0	1.0	
Parent	0.0	0.0	0.0	0.0	0.0	0.0	0.0	0.0	0.0	0.0	0.0	0.0	0.0	0.0	0.0	1.0	1.0	
PA-Black shale																		
AF-1-1	-0.3	-0.6	-0.4	-0.4	-0.5	-0.5	-0.5	-0.5	-0.5	-0.5	-0.5	-0.5	-0.5	-0.5	-0.5	-0.5	0.9	
AF-1-3	-0.3	-0.6	-0.5	-0.5	-0.6	-0.7	-0.6	-0.6	-0.6	-0.6	-0.6	-0.6	-0.6	-0.5	-0.5	-0.6	0.8	
AF-1-5	-0.3	-0.6	-0.4	-0.5	-0.6	-0.7	-0.7	-0.6	-0.6	-0.6	-0.6	-0.6	-0.6	-0.5	-0.5	-0.5	0.9	
AF-1-7	-0.3	-0.6	-0.4	-0.5	-0.6	-0.6	-0.6	-0.6	-0.6	-0.6	-0.6	-0.6	-0.6	-0.5	-0.5	-0.5	1.0	
AF-1-9	-0.1	-0.4	0.0	0.1	0.1	0.1	0.0	-0.1	-0.1	-0.1	-0.1	-0.1	-0.1	-0.2	-0.2	-0.2	0.7	
AF-1-11	-0.3	-0.5	-0.3	-0.4	-0.4	-0.5	-0.5	-0.5	-0.5	-0.5	-0.5	-0.5	-0.5	-0.4	-0.4	-0.4	0.9	
AF-1-13	-0.3	-0.5	-0.3	-0.3	-0.4	-0.4	-0.5	-0.5	-0.5	-0.5	-0.5	-0.5	-0.5	-0.4	-0.4	-0.4	0.6	
AF-1-15	0.0	0.0	0.0	0.0	0.0	0.0	0.0	0.0	0.0	0.0	0.0	0.0	0.0	0.0	0.0	0.0	1.0	
Parent	0.0	0.0	0.0	0.0	0.0	0.0	0.0	0.0	0.0	0.0	0.0	0.0	0.0	0.0	0.0	0.0	1.0	
PA-Black shale 2 (MVVF, valley floor)																		
MVF-0-10	-0.6	-0.8	-0.6	-0.7	-0.7	-0.7	-0.8	-0.7	-0.7	-0.7	-0.7	-0.6	-0.6	-0.6	-0.7	-0.7	1.0	
MVF-10-15	-0.6	-0.8	-0.6	-0.7	-0.7	-0.7	-0.7	-0.7	-0.7	-0.7	-0.7	-0.6	-0.6	-0.6	-0.7	-0.7	1.0	
MVF-15-20	-0.6	-0.8	-0.6	-0.7	-0.7	-0.7	-0.7	-0.7	-0.7	-0.7	-0.7	-0.6	-0.6	-0.6	-0.6	-0.6	1.0	

Table 3 (continued)

Sample name	Ti	La	Ce	Pr	Nd	Sm	Eu	Gd	Tb	Dy	Ho	Er	Tm	Yb	Lu	REE	(Ce/Ce*)N	(Eu/Eu*)N
%	τ	τ	τ	τ	τ	τ	τ	τ	τ	τ	τ	τ	τ	τ	τ	τ	τ	
MVF-20-30	-0.5	-0.7	-0.5	-0.6	-0.7	-0.7	-0.7	-0.7	-0.7	-0.6	-0.6	-0.6	-0.6	-0.6	-0.6	-0.6	1.0	
MVF-30-35	-0.4	-0.7	-0.4	-0.5	-0.6	-0.6	-0.7	-0.7	-0.6	-0.6	-0.6	-0.6	-0.6	-0.6	-0.6	-0.6	1.1	
MVF-35-40	-0.3	-0.6	-0.4	-0.5	-0.5	-0.5	-0.6	-0.7	-0.6	-0.6	-0.6	-0.5	-0.5	-0.5	-0.5	-0.5	1.1	
MVF-40-45	-0.3	-0.6	-0.3	-0.5	-0.5	-0.5	-0.6	-0.7	-0.6	-0.6	-0.6	-0.5	-0.5	-0.5	-0.5	-0.5	1.0	
MVF-45-52	-0.3	-0.6	-0.4	-0.5	-0.5	-0.5	-0.6	-0.7	-0.6	-0.6	-0.6	-0.5	-0.5	-0.5	-0.5	-0.5	1.1	
MVF-52-57	-0.3	-0.6	-0.4	-0.5	-0.5	-0.5	-0.6	-0.7	-0.7	-0.6	-0.6	-0.5	-0.5	-0.5	-0.6	-0.6	1.1	
MVF-57-62	-0.2	-0.6	-0.3	-0.4	-0.5	-0.5	-0.6	-0.6	-0.6	-0.6	-0.6	-0.5	-0.5	-0.5	-0.5	-0.5	1.0	
MVF-62-67	-0.3	-0.6	-0.3	-0.5	-0.5	-0.5	-0.6	-0.7	-0.6	-0.6	-0.6	-0.5	-0.5	-0.5	-0.5	-0.5	1.0	
MVF-67-72	-0.2	-0.6	-0.3	-0.4	-0.5	-0.5	-0.6	-0.6	-0.6	-0.6	-0.6	-0.5	-0.5	-0.5	-0.5	-0.5	1.0	
MVF-72-77	-0.2	-0.6	-0.3	-0.4	-0.5	-0.5	-0.5	-0.6	-0.6	-0.6	-0.6	-0.5	-0.5	-0.5	-0.5	-0.5	1.1	
MVF-77-82	-0.3	-0.6	-0.3	-0.4	-0.5	-0.5	-0.6	-0.6	-0.6	-0.6	-0.6	-0.5	-0.4	-0.4	-0.5	-0.5	1.1	
MVF-82-84	-0.3	-0.6	-0.3	-0.4	-0.5	-0.5	-0.5	-0.5	-0.5	-0.5	-0.5	-0.5	-0.5	-0.5	-0.5	-0.5	1.1	
PA-Black shale 3 (MRT, Ridge top, CEC)																		
MRT-0-17	-0.6	-0.8	-0.6	-0.7	-0.7	-0.7	-0.8	-0.8	-0.7	-0.7	-0.7	-0.6	-0.6	-0.6	-0.6	-0.7	1.0	
MRT-17-22	-0.4	-0.7	-0.5	-0.6	-0.6	-0.6	-0.7	-0.7	-0.7	-0.6	-0.6	-0.6	-0.6	-0.6	-0.6	-0.6	1.0	
MRT-27-38	-0.4	-0.7	-0.4	-0.5	-0.6	-0.6	-0.6	-0.7	-0.7	-0.6	-0.6	-0.6	-0.6	-0.6	-0.6	-0.6	1.0	
MRT-38-50	-0.4	-0.7	-0.4	-0.5	-0.6	-0.6	-0.6	-0.7	-0.7	-0.6	-0.6	-0.6	-0.6	-0.6	-0.6	-0.6	1.0	
MRT-50-68	-0.4	-0.7	-0.4	-0.5	-0.6	-0.7	-0.7	-0.7	-0.7	-0.6	-0.6	-0.6	-0.6	-0.6	-0.6	-0.6	1.0	
MRT-68-83	-0.4	-0.7	-0.4	-0.5	-0.6	-0.6	-0.6	-0.7	-0.7	-0.6	-0.6	-0.6	-0.6	-0.6	-0.6	-0.6	1.0	
MRT-83-135	-0.4	-0.7	-0.4	-0.5	-0.6	-0.6	-0.6	-0.7	-0.7	-0.6	-0.6	-0.6	-0.6	-0.6	-0.6	-0.6	1.0	

later, using a syringe nylon filter with a 0.45-μm membrane. Filtered and unfiltered samples were acidified using ultra-pure concentrated nitric acid and measured for REE concentrations on a ThermoFisher Scientific XS 2 quadrupole ICP-MS at the MCL. Concentrations of dissolved organic carbon (DOC) and major elements, including dissolved Mg^{2+} , Ca^{2+} , Na^+ , K^+ , Cl^- , SO_4^{2-} , NO_3^- , and soil water pH values and Cu isotopes of the same water samples were reported previously in Mathur et al. (2012), Jin et al. (2013), and Heidari et al. (2017).

3.4. Characterization of soil cation exchangeable capacity (CEC)

Cation concentrations in the soil exchangeable pools were characterized following the same procedure as Jin et al. (2010). Specifically, about 2.5 g of an untreated soil sample were weighed into a 50-ml centrifuge tube and 25 ml of 0.1 M $BaCl_2$ –0.1 M NH_4Cl solution were added. The slurry was shaken vigorously on an end-to-end shaker table for 15 min, and then centrifuged at 2500 rpm for 20 min. The solution was filtered, weighed and analyzed for Ca, Na, K, Mg, Mn, Na, Si and Sr by ICP-OES for major elements at the Low-Temperature Geochemistry Laboratory of the University of Texas at El Paso. Standards were prepared in the same 0.1 M $BaCl_2$ –0.1 M NH_4Cl matrix solutions. Cation exchange capacity (CEC) was calculated for each soil using the measured cation concentrations and reported on an equivalent basis. For VA site, soils from a duplicate core were used for CEC characterization.

4. Results

4.1. REE in shale parent materials

A core (DC-1) drilled at the northern ridge at SSHO (in the PA-gray shale site) allowed characterization of the parent bedrock: total REE content in DC-1 is 220–276 ppm (244 ppm on average; Table 2). Rock chips (AF-1-17) from the bottom of the PA-BlackShale1 pit provided bedrock samples for the Marcellus Formation (Mathur et al., 2012; Jin et al., 2013); total REE content is ~468 ppm, about a factor of 2 higher than that of the Rose Hill Formation (PA-gray shale) (Table 2).

Unlike the shale parent materials in the PA sites that have been well characterized for their REE contents, shale from all the other locations have only been studied for major element compositions and mineralogy (Dere et al., 2013; Dere et al., 2016). The major elemental chemistry of these shale bedrock samples varies little among sites except for Ca (Dere et al., 2013); however, REE contents vary significantly from 63 to 966 ppm (Table 2). Among all six gray shale sites, Wales and PR bedrock samples have the most variable REE contents.

As an alternative to bedrock from local outcrops and rock chips in soil pits, the deepest soils may be considered as the least altered materials for the study of elemental mobility (Table 2). We evaluate such a possibility here. For the Wales and TN sites, average rock fragments and the deepest soil have similar REE concentrations, but at the PA sites, for both gray and black shale, total REE contents are much higher in the rocks than those in the deepest soils. In contrast, the deepest soils in VA, AL or PR have much higher REE concentrations than their rock counterparts (Table 2).

Concentrations of different REE in rocks and the deepest soils are normalized to Post-Archean Australian Shale (PAAS), a well-known reference shale unit (Fig. 2). Overall, the bedrock patterns from all sites are relatively flat, indicating a similar distribution of light, middle and heavy REE as the PAAS, except for two outliers from Wales with high values of light REE (LREE), two outliers from AL with high enrichment of middle REE (MREE), and one outlier from PA-black shale with depletions of heavy REE (HREE).

The deepest soils, however, show variable patterns with respect to PAAS: the deepest soil samples from the Wales, PA and TN sites show similar REE contents and distribution patterns as the rock fragments (Table 2; Fig. 2); those at one PA black shale site are more enriched in MREE; the deepest soils from VA and PR are more enriched in MREE

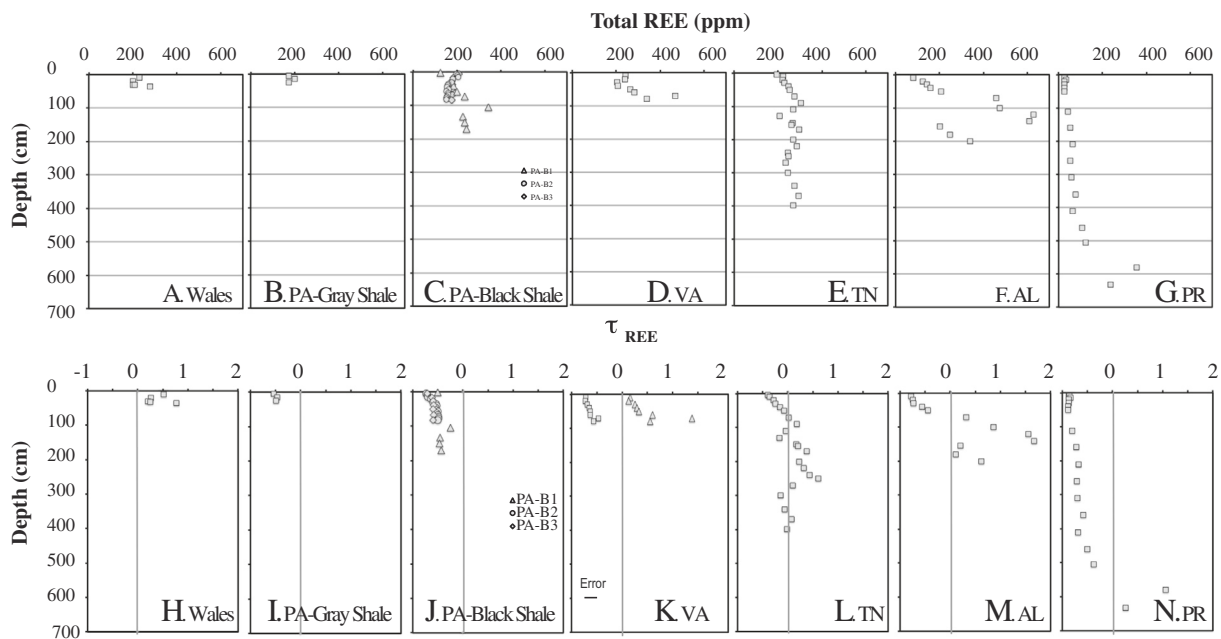


Fig. 3. Concentrations and mass transfer coefficients (τ_{Zr}) of total REE in soils for each site: (A, H) Wales, (B, I) PA-gray shale, (C, J) PA-black shale, (D, K) VA, (E, L) TN, (F, M) AL, and (G, N) PR. Three soil profiles were sampled at the PA-Black Shale site. Zr was used as the immobile element. For VA soils, mass transfer coefficients were re-calculated using Ti as the immobile element (triangles in L). See text for details. Error bar in mass transfer coefficients is shown in (K).

and HREE; the deepest soil from the AL site is more enriched in MREE but depleted in HREE. In addition, the deepest soils from VA, AL, and PR sites have much higher REE contents than the assumed parent bedrock materials, respectively, and also exhibit different REE patterns from the bedrock (Fig. 2). Hence, we conclude that in this study, our selected deepest soil samples from VA, AL, and PR are not representative of the parent materials in terms of REE content or pattern. Therefore, in the following discussion, the average concentrations of multiple rock samples whenever available from each site are used as estimates of the original REE content in parent materials.

4.2. Total REE contents in soil profiles

Three northern sites on the shale transect (Wales, PA, VA) have relatively thin soil profiles with soil thickness ranging from 30 to 80 cm (Table 1). In contrast, three southern sites (TN, AL, PR) have soils up to 600 cm thick. For the black shale sites in PA, soils are thicker than their gray shale counterparts, ranging from 84 cm to 170 cm.

Total REE contents vary significantly with depth in each profile and also among the seven soil profiles (Table 3; Fig. 3). In general, REE contents decrease toward the surface except in TN where limited variation in REE concentrations with depth was observed. Compared to the Wales and PA gray sites, higher REE contents for the PR, AL, PA-BlackShale1 and VA sites are observed at depth just above the depth of auger refusal (~70 cm at VA, ~130 cm at PA-BlackShale1, ~120 cm at AL and ~600 cm at PR). In addition, soil profiles in the PA black shale profile show more variability in REE contents (124–342 ppm) compared to the PA gray shale site (173–200 ppm).

The mass transfer coefficient, τ , was calculated to assess REE mobility. The τ values can be indicative of depletion or enrichment of a certain element after taking into account changes in concentrations of other elements in the soils based on concentrations of immobile element i (Brimhall and Dietrich, 1987; Anderson et al., 2002):

$$\tau_{i,j} = \frac{C_{j,w}C_{i,p}}{C_{j,p}C_{i,w}} - 1 \quad (1)$$

Positive $\tau_{i,j}$ values indicate enrichment of element j (total or individual REE for this study) in the weathered soils (w) with respect to

parent (p), negative values mean depletion and zero means element j is immobile. Moreover, if τ is negative, the absolute value of τ equals the fraction of element j that was lost from the soil. Likewise, the relative enrichment factor for element j equals τ if τ is positive. The method is highly contingent upon proper identification of the parent material (p) and the immobile element (i). In this study, the local outcropping bedrock samples were assumed to be parent materials as discussed above. The outcrop samples are homogeneous for each site with respect to REE chemistry, except for those from Wales. Thus, we used the average rock composition from each site for the τ calculation excluding the outliers (Table 2). Zr was used as the immobile element, i , as suggested by previous studies of the Rose Hill Formation shale at SSHO and the Marcellus Formation shale (Jin et al., 2010; Jin et al., 2013; Dere et al., 2013; Dere, 2014; Dere et al., 2016).

The $\tau_{\text{Zr},\text{REE}}$ (labeled τ_{REE} hereafter) values were computed for all profiles (Table 3; Fig. 3). The Wales site has positive τ_{REE} values, indicative of an addition profile (assuming that the parent has been identified correctly). Interestingly, all soils in the PA sites, regardless of black or gray shale, have negative τ_{REE} values as low as -0.8 , suggesting significant loss of REE during chemical weathering (assuming that the parent has been identified correctly). Similarly, the VA site also shows a typical depletion profile, with negative τ_{REE} values at all depths. The other three southern sites (TN, AL, and PR), however, have negative τ_{REE} values at the soil surface but positive τ_{REE} values at depth (Fig. 3), showing a typical depletion-addition profile (Brantley and Lebedeva, 2011). The PR site has lost more REE than other sites at the surface, as suggested by τ_{REE} values close to -1 (i.e., 100% depletion).

4.3. REE patterns in soils

To display the fractionation (relative depletion or enrichment, normalized to their bedrock abundance) of one REE relative to others during rock-soil transformation, concentrations of individual REE elements in soil samples are normalized to those of their corresponding parent material (the average rock composition) using the τ notation according to Eq. (1) (Fig. 4). At the Wales sites, all soils are enriched in LREE but have comparable MREE and HREE as compared to parent material (Fig. 4A). Soils at the PA-gray shale site and three PA-black shale sites show a relatively flat

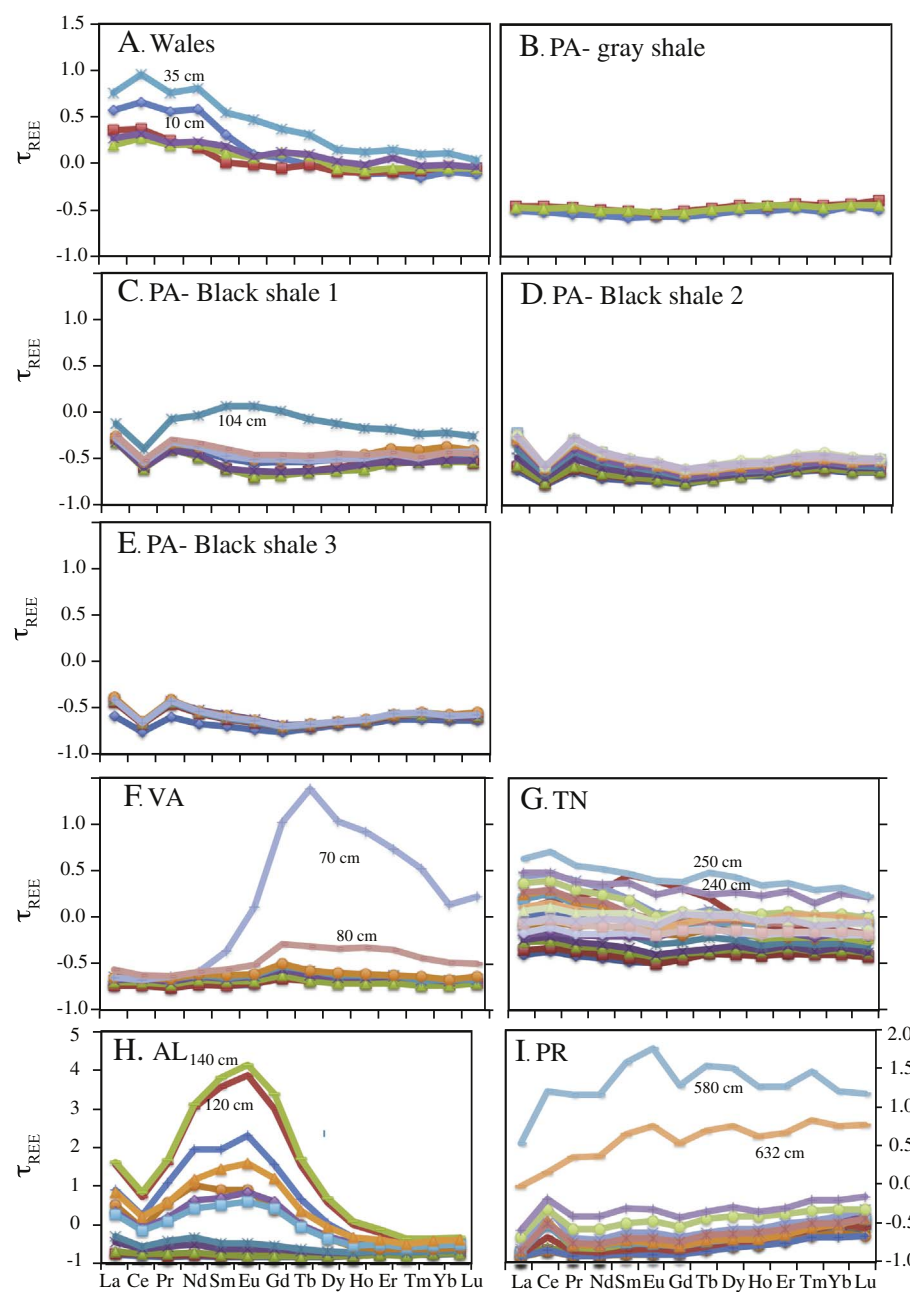


Fig. 4. Mass transfer coefficients (τ_{Z_E}) of REE with soil depth at different sites. Note that AL and PR sites have different scales.

REE pattern, with slightly more depletion in MREE than LREE and HREE (Fig. 4B, C, D, and E). One exception is a sample at 104 cm below ground surface at the PA-BlackShale1 site, which exhibits MREE enrichment. Thus, for the PA-BlackShale1 site, soils with lower REE contents are depleted in MREE, and one soil that accumulates REE is more enriched in MREE. All soils from the VA site are depleted of total REE (Fig. 3K), although less depletion is observed around the MREE (Fig. 4F). At that site, MREE are enriched compared to parent rocks for the two deepest soils (70 cm and 80 cm).

Both the total REE concentrations and the patterns in soils from the three southern sites (TN, AL, and PR) significantly deviate from their parent compositions (Fig. 3L, M, and N; Fig. 4G, H, and I). In general, soils are depleted in REE at shallow depths but are enriched in deeper soils. Interestingly, at AL site, deep soils enriched in REE (e.g., 120 cm) are enriched in MREE that are complementary to those shallow soils with REE losses (more depleted in MREE). This observation could be consistent with preferential leaching of some REE from shallow soils and precipitation in deeper soils.

4.4. Eu and Ce anomalies

Eu and Ce, each with more than one oxidation state, can fractionate differently from other REE elements due to changes in redox conditions. The $(Eu/Eu^*)_N$ and $(Ce/Ce^*)_N$ ratios are commonly calculated to evaluate Eu and Ce anomalies using the following equations (e.g., McLennan, 1989; Prudencio et al., 1995; Ma et al., 2011):

$$(Eu/Eu^*)_N = \frac{Eu_N}{(Sm_N \times Gd_N)^{0.5}} \quad (2)$$

$$(Ce/Ce^*)_N = \frac{Ce_N}{(La_N \times Pr_N)^{0.5}} \quad (3)$$

Here, the subscript N indicates REE concentrations normalized to parent composition. Soils at the PR site show a strong positive Ce anomaly (> 1), with $(Ce/Ce^*)_N$ values up to 3, while those at the PA-black shale sites and VA site demonstrate a negative Ce anomaly (< 1), with values around 0.6 (Table 3; Fig. 5A, B). In contrast, Eu shows no

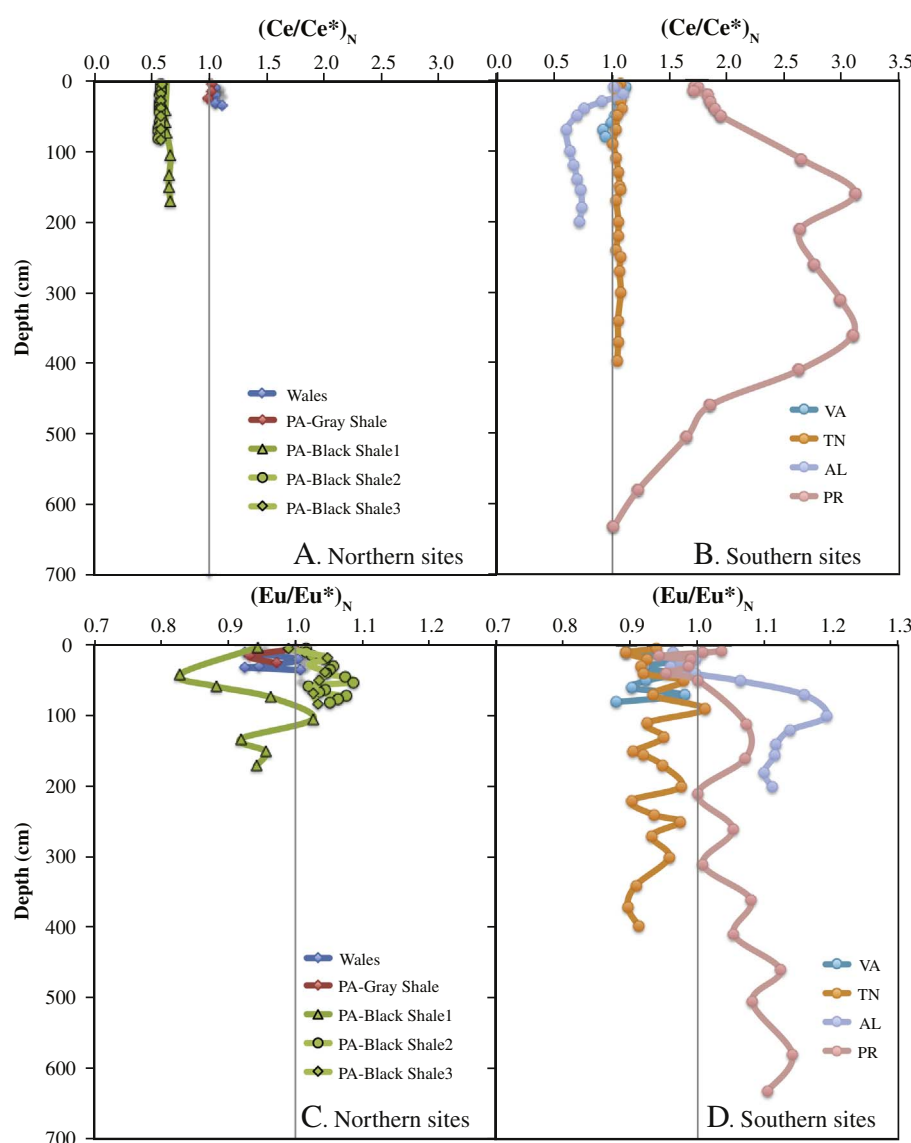


Fig. 5. Ce (A, B) and Eu (C, D) anomalies for the weathering profiles at transect sites.

apparent anomaly, with $(Eu/Eu^*)_N$ values varying little from 1 (0.9 to 1.1) among all soils (Table 3; Fig. 5C, D).

4.5. CEC and pH of soil profiles

Soil CEC values vary among sites and also with depth (Appendix Table 3). CEC is overall higher for the PR soils than at other sites. In addition, within the PR site, the CEC decreases sharply with depth. Soils from other gray shale sites have much lower CEC values, and the depth trends are also variable among sites (Appendix Fig. 1). The soil pH values, reported by Dere (2014), range from 2.8 to 3.8 for all sites except for PR where the soil is less acidic, with pH between 4.0 and 5.5. The relative concentrations of cations that are adsorbed to the exchangeable sites are soil pH-dependent: higher proportions of divalent cations are observed in soils with higher pH but Al predominates in soils at lower pH (Appendix Fig. 1). Dere et al. (2013) also reported much higher Ca for the PR shale than those in other transect sites (up to 20 wt % versus < 1 wt%). This is consistent with higher soil pH and CEC, as well as higher $(Ca + Mg)/Al$ ratios on the exchangeable sites at PR.

4.6. REE concentrations and patterns in soil waters of the Marcellus shale site

The REE concentrations of the soil waters in the black shale sites range from 0.5 to 16 ppb ($\mu\text{g/L}$), and generally decrease with depth at each site (Table 4; Fig. 6A). The REE concentrations do not show systematic variation among the three sites. The soil water pH values increase with depth from 3.5 to around 5.5 (Fig. 6B; Heidari et al., 2017). The filtered (water that passed through 0.45 μm filter) and unfiltered (water that passed through the 1.3 μm pores in the lysimeters) soil water samples have similar REE concentrations, as they all fall on a 1:1 correlation line (Appendix Fig. 2).

Ce and Eu anomalies of soil waters are calculated according to Eqs. (2) and (3), where REE concentrations are normalized to parent compositions (Fig. 6C and D). Interestingly, $(Ce/Ce^*)_N$ values of soil waters and soils are similar at PA-Black Shale sites, whereas $(Eu/Eu^*)_N$ values of soil waters are much higher than 1. In contrast, typical $(Eu/Eu^*)_N$ values of the soils are ~ 1 (Fig. 6D).

Similar to the soils, we normalized soil water REE concentrations to the parent composition for the PA-Black Shale site (Appendix Fig. 3).

Table 4

Soil water pH and REE concentration from Marcellus black shales.

Sample Date	Loca-tion	Depth	pH	La	Ce	Pr	Nd	Sm	Eu	Gd	Tb	Dy	Ho	Er	Tm	Yb	Lu	Y	REE
			cm	ppb															
5/14/2010	MMS	10	4.18	1.9	5.8	0.58	2.5	0.52	0.14	0.51	0.07	0.38	0.08	0.24	0.03	0.22	0.04	2.1	13.01
5/21/2010	MMS	10	4.10	1.4	4.0	0.38	1.6	0.33	0.09	0.32	0.05	0.26	0.05	0.16	0.02	0.14	0.02	1.4	8.82
5/28/2010	MMS	10	4.21	1.9	4.9	0.47	1.9	0.39	0.11	0.40	0	0.32	0.06	0.18	0.02	0.16	0.02	1.7	10.88
5/14/2010	MMS	20	3.86	1.2	2.4	0.26	1.1	0.21	0.09	0.23	0.03	0.17	0.04	0.10	0.01	0.08	0.01	1.1	5.93
5/21/2010	MMS	20	3.77	0.64	1.3	0.14	0.57	0.11	0.07	0.11	0.02	0.09	0.02	0.06	0.00	0.05	0.00	0.56	3.18
5/28/2010	MMS	20	3.85	0.59	1.2	0.13	0.57	0.11	0.07	0.13	0.02	0.10	0.02	0.05	0.00	0.04	0.00	0.52	3.03
6/23/2010	MMS	20	0.48	0.99	0.11	0.48	0.1	0.04	0.1	0.01	0.08	0.02	0.05	0	0.05	0	0.45	2.51	
5/14/2010	MMS	30	3.73	0.89	2.1	0.22	0.9	0.17	0.06	0.17	0	0.13	0.03	0.08	0.00	0.06	0.00	0.7	4.79
5/21/2010	MMS	30	3.74	0.45	1.0	0.11	0.45	0.09	0.04	0.10	0.01	0.08	0.02	0.05	0.00	0.04	0.00	0.40	2.44
5/28/2010	MMS	30	3.85	0.32	0.8	0.08	0.36	0.07	0.03	0.08	0.00	0.07	0.01	0.04	0.00	0.03	0.00	0.32	1.84
5/14/2010	MMS	40	3.92	0.58	1.4	0.13	0.57	0.12	0.07	0.13	0.02	0.10	0.02	0.07	0.00	0.06	0.00	0.68	3.27
5/21/2010	MMS	40	3.82	0.50	1.2	0.12	0.49	0.10	0.07	0.10	0.02	0.09	0.02	0.06	0.00	0.05	0.00	0.54	2.82
5/28/2010	MMS	40	3.84	0.38	0.90	0.09	0.39	0.08	0.07	0.09	0	0.07	0.01	0.04	0.00	0.04	0.00	0.43	2.16
5/14/2010	MMS	50	4.17	0.55	0.99	0.11	0.55	0.11	0.05	0.14	0.02	0.11	0.03	0.08	0.00	0.06	0.00	0.75	2.8
5/21/2010	MMS	50	3.76	0.52	0.98	0.12	0.55	0.11	0.06	0.13	0.02	0.11	0.02	0.07	0.00	0.05	0.00	0.62	2.74
5/28/2010	MMS	50	4.00	0.4	0.78	0.09	0.43	0.09	0.05	0.1	0.01	0.08	0.02	0.05	0.00	0.04	0.00	0.43	2.14
6/23/2010	MMS	50	3.85	0.4	0.84	0.1	0.5	0.1	0.04	0.12	0.02	0.1	0.02	0.06	0	0.04	0	0.53	2.34
5/14/2010	MMS	60	4.19	0.22	0.45	0.05	0.26	0.05	0.03	0.06	0	0.05	0.01	0.04	0.00	0.03	0.00	0.34	1.25
5/21/2010	MMS	60	3.94	0.25	0.51	0.06	0.30	0.06	0.03	0.07	0.00	0.06	0.01	0.04	0.00	0.03	0.00	0.33	1.42
5/28/2010	MMS	60	4.15	0.2	0.5	0.06	0.3	0.05	0.03	0.06	0.00	0.05	0.00	0.03	0.00	0.02	0.00	0.3	1.27
6/23/2010	MMS	60	4.34	0.13	0.28	0.03	0.16	0.03	0.01	0.04	0	0.03	0	0.02	0	0.02	0	0.18	0.75
5/14/2010	MMS	80	4.53	0.08	0.18	0.02	0.12	0.03	0.01	0.03	0	0.03	0.00	0.02	0.00	0.02	0.00	0.16	0.54
5/21/2010	MMS	80	4.39	0.11	0.24	0.03	0.15	0.03	0.02	0.04	0.00	0.03	0.00	0.03	0.00	0.02	0.00	0.20	0.7
5/28/2010	MMS	80	4.58	0.06	0.14	0.02	0.09	0.02	0.00	0.02	0.00	0.02	0.00	0.01	0.00	0.01	0.00	0.12	0.39
5/14/2010	MMS	100	4.44	0.29	0.68	0.07	0.34	0.07	0.03	0.07	0	0.06	0.01	0.04	0.00	0.04	0.00	0.37	1.7
5/21/2010	MMS	100	4.36	0.29	0.70	0.08	0.33	0.07	0.03	0.08	0.01	0.07	0.02	0.04	0.00	0.03	0.00	0.39	1.75
5/28/2010	MMS	100	5.26	0.70	1.5	0.17	0.7	0.16	0.06	0.18	0.03	0.15	0.03	0.08	0.00	0.07	0.00	0.8	3.86
5/21/2010	MRT	10	4.13	1.3	3.7	0.33	1.3	0.27	0.07	0.28	0.04	0.23	0.05	0.14	0.02	0.13	0.02	1.2	7.88
5/28/2010	MRT	10	4.13	0.89	2.3	0.21	0.86	0.17	0.05	0.17	0.03	0.14	0.03	0.09	0.01	0.08	0.01	0.85	5.04
6/23/2010	MRT	10	4.08	1.3	3.5	0.33	1.4	0.27	0.08	0.26	0.04	0.23	0.05	0.13	0.02	0.13	0.02	1.1	7.76
5/14/2010	MRT	20	4.35	1.2	2.5	0.26	1.0	0.19	0.06	0.20	0.03	0.15	0.03	0.09	0.01	0.07	0.00	0.9	5.79
5/21/2010	MRT	20	4.63	0.80	1.7	0.18	0.71	0.14	0.04	0.15	0.02	0.12	0.02	0.07	0.00	0.05	0.00	0.63	4
5/28/2010	MRT	20	4.74	0.8	2.3	0.17	0.7	0.14	0.04	0.15	0.03	0.11	0.02	0.06	0.00	0.05	0.00	0.72	4.57
5/14/2010	MRT	30	4.77	1.2	2.5	0.26	1.1	0.20	0.07	0.21	0.03	0.17	0.03	0.10	0.01	0.08	0.01	1.0	5.97
5/21/2010	MRT	30	4.19	0.97	2.0	0.21	0.82	0.17	0.06	0.17	0.03	0.15	0.03	0.08	0.00	0.06	0.00	0.79	4.75
5/28/2010	MRT	30	4.2	0.83	1.6	0.18	0.74	0.15	0.06	0.16	0.02	0.14	0.03	0.07	0.00	0.06	0.00	0.69	4.04
6/23/2010	MRT	30	3.98	0.96	2	0.22	0.91	0.19	0.06	0.19	0.03	0.16	0.03	0.09	0.01	0.07	0.01	0.84	4.93
5/14/2010	MRT	40	4.58	2.0	4.5	0.51	2.1	0.42	0.12	0.41	0.06	0.31	0.06	0.19	0.03	0.17	0.03	1.7	10.91
5/21/2010	MRT	40	4.31	1.5	3.4	0.37	1.5	0.30	0.09	0.28	0.04	0.22	0.04	0.13	0.02	0.12	0.02	1.2	8.03
5/28/2010	MRT	40	4.35	1.20	2.6	0.29	1.2	0.24	0.08	0.23	0.03	0.19	0.03	0.10	0.01	0.10	0.01	0.89	6.31
6/23/2010	MRT	40	4.28	2	4.4	0.49	2.1	0.41	0.11	0.39	0.05	0.31	0.06	0.17	0.02	0.16	0.02	1.6	10.69
5/14/2010	MRT	50	4.34	0.55	1.3	0.16	0.75	0.16	0.05	0.18	0.03	0.15	0.03	0.09	0.01	0.07	0.01	0.83	3.54
5/28/2010	MRT	50	4.22	0.36	0.8	0.1	0.44	0.1	0.03	0.11	0.01	0.09	0.02	0.05	0.00	0.04	0.00	0.46	2.15
6/23/2010	MRT	50	4.18	0.58	1.2	0.15	0.68	0.15	0.04	0.17	0.02	0.14	0.03	0.08	0	0.07	0	0.72	3.31
5/14/2010	MRT	60	4.63	0.26	0.68	0.09	0.42	0.10	0.03	0.11	0.02	0.09	0.02	0.06	0.00	0.05	0.00	0.49	1.93
5/21/2010	MRT	60	4.35	0.25	0.67	0.08	0.40	0.09	0.03	0.10	0.02	0.08	0.02	0.05	0.00	0.04	0.00	0.43	1.83
5/28/2010	MRT	60	4.51	0.26	0.63	0.08	0.36	0.08	0.03	0.09	0.01	0.07	0.01	0.04	0.00	0.03	0.00	0.35	1.69
6/23/2010	MRT	60	4.41	0.32	0.72	0.08	0.37	0.09	0.03	0.09	0.01	0.08	0.01	0.04	0	0.03	0	0.39	1.87
5/14/2010	MRT	70	4.47	0.11	0.26	0.03	0.13	0.03	0.01	0.03	0	0.02	0.00	0.02	0.00	0.01	0.00	0.12	0.65
5/21/2010	MRT	70	4.53	0.08	0.20	0.02	0.11	0.02	0.01	0.02	0.00	0.02	0.00	0.02	0.00	0.01	0.00	0.12	0.51
5/28/2010	MRT	70	4.68	0.06	0.16	0.02	0.13	0.03	0.02	0.03	0.00	0.02	0.00	0.02	0.00	0.01	0.00	0.14	0.5
6/23/2010	MRT	70	4.49	0.09	0.19	0.03	0.13	0.03	0.01	0.03	0	0.02	0	0.02	0	0.02	0	0.14	0.57
5/14/2010	MRT	80	4.61	0.07	0.14	0.02	0.08	0.02	0.01	0.02	0	0.01	0.00	0.01	0.00	0.00	0.00	0.10	0.38
5/21/2010	MRT	80	4.55	0.20	0.36	0.04	0.16	0.03	0.02	0.04	0.00	0.04	0.00	0.02	0.00	0.02	0.00	0.20	0.93
5/28/2010	MRT	80	4.54	0.09	0.24	0.03	0.13	0.02	0.02	0.03	0.00	0.02	0.00	0.01	0.00	0.01	0.00	0.13	0.6
6/23/2010	MRT	80	4.32	0.06	0.14	0.02	0.08	0.02	0.02	0	0.02	0	0.02	0	0	0	0	0.09	0.36
7/16/2010	MRT	80	3.93	0.42	0.89	0.11	0.34	0.06	0.02	0.04	0	0.03	0	0.02	0	0.02	0	0.15	1.95
5/6/2010	MVF	10	4.23	2.6	7.1	0.64	2.7	0.54	0.15	0.57	0.08	0.48	0.10	0.32	0.04	0.30	0.05	2	

Table 4 (continued)

Sample Date	Locat-ion	Depth	pH	La	Ce	Pr	Nd	Sm	Eu	Gd	Tb	Dy	Ho	Er	Tm	Yb	Lu	Y	REE
		cm		ppb															
5/28/2010	MVF	50	4.26	0.84	1.8	0.22	1	0.21	0.07	0.24	0.03	0.20	0.04	0.12	0.01	0.09	0.01	1.1	4.88
6/23/2010	MVF	50	4.37	0.58	1.3	0.16	0.82	0.17	0.05	0.2	0.03	0.16	0.03	0.1	0.01	0.08	0.01	0.96	3.7
5/21/2010	MVF	60	5.34	0.45	0.98	0.12	0.56	0.13	0.04	0.13	0.02	0.09	0.02	0.06	0.00	0.06	0.00	0.57	2.66
5/14/2010	MVF	80	4.49	0.44	1.1	0.13	0.58	0.11	0.04	0.12	0.02	0.09	0.02	0.07	0.00	0.05	0.00	0.63	2.77
5/21/2010	MVF	80	4.4	0.41	1.0	0.12	0.53	0.10	0.04	0.12	0.02	0.11	0.02	0.07	0.00	0.05	0.00	0.63	2.59
5/28/2010	MVF	80	4.36	0.22	0.57	0.07	0.29	0.06	0.03	0.07	0	0.07	0.01	0.04	0.00	0.03	0.00	0.4	1.46
6/23/2010	MVF	80	3.87	0.24	0.59	0.07	0.31	0.07	0.02	0.08	0.01	0.07	0.02	0.05	0	0.04	0	0.43	1.57

Except for the Ce and Eu anomaly discussed above, the REE patterns are relatively flat, indicating limited REE fractionation in soil waters at the black shale site.

5. Discussion

One traditional method for determining the extent of REE mobility is to measure the change in REE concentration from an observed soil profile relative to the original concentrations in pristine parent material (April et al., 1986; Brimhall and Dietrich, 1987; Brimhall et al., 1992; White et al., 1998; Brantley et al., 2008; Brantley and White, 2009; Brantley and Lebedeva, 2011). This approach has been used to estimate the weathering extent of major elements in different lithology including granite, basalt and shale (e.g. April et al., 1986; White et al., 2001; Chadwick et al., 2003; Tuttle et al., 2003; Tuttle et al., 2009; Jin et al., 2010). For this mass transfer coefficient concept to work effectively, it is crucial to identify the parent material and determine its chemical composition. For this study, REE concentrations in parent bedrock were evaluated by calculating the mean concentrations for multiple available bedrock and outcrop samples, excluding outliers. The largest contributions to the errors in τ_{REE} calculations are from the difficulties in

identifying the parent materials, from heterogeneity of the bedrock chemistry, and from analytical errors in quantifying REE and Zr concentrations. Assuming up to 10% analytical error in $C_{j,w}$ and $C_{i,w}$, and 20% uncertainty in $C_{j,p}$ and $C_{i,p}$, we estimated the uncertainties in the overall τ_{REE} values at around ± 0.3 unit using error propagation.

5.1. Long-term REE release rates along the gray shale climosequence

As expected, our results show that soils become thicker and the degree of REE depletion at the land surface increases significantly from the northern sites to the southern sites. From north to south, the sites become warmer and wetter, and soil residence times become longer (Table 1). To quantitatively assess the REE loss, the total mass of REE depletion, $m_{j,w}$ ($\mu\text{g cm}^{-2}$), was calculated for REE ($j = \text{REE}$) in each profile using the following equation (Brimhall and Dietrich, 1987; Egli and Fitzie, 2000; Herndon et al., 2011):

$$m_{j,w} = C_{j,p}\rho_p \int_0^L \frac{\tau(z)}{\varepsilon(z) + 1} dz \quad (4)$$

Here ρ_p is the bulk density of parent materials (p), z is soil depth (cm), and L is the thickness of the entire weathering profile. The strain

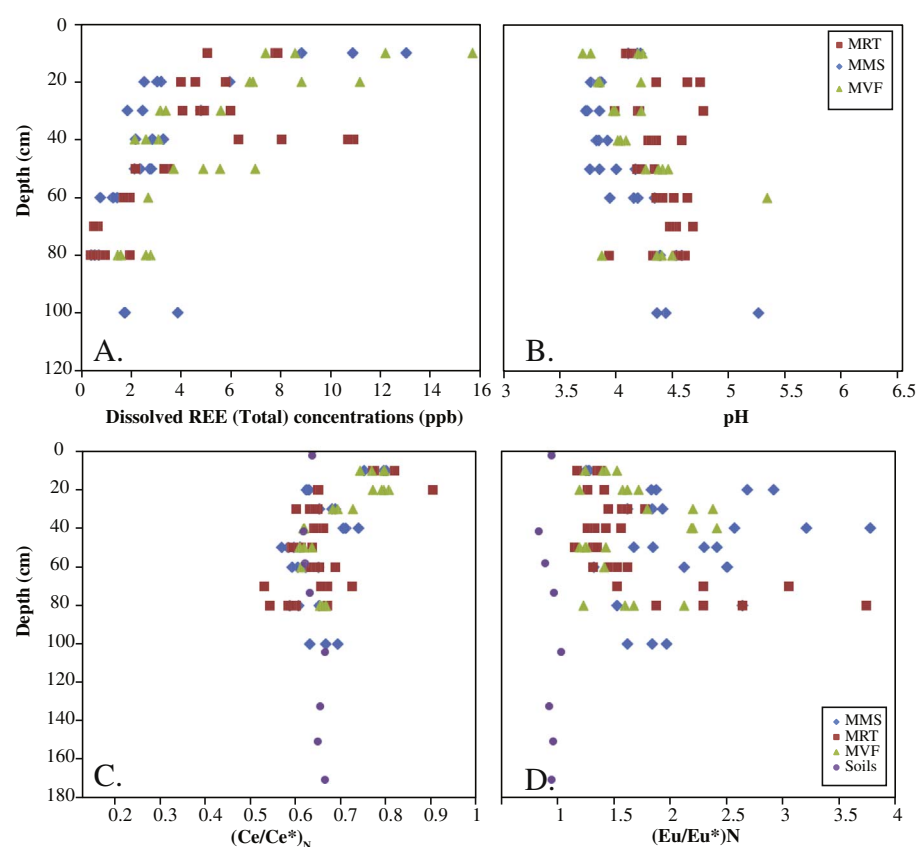


Fig. 6. Depth profiles of total REE concentrations (A), pH (B), Ce anomaly (C) and Eu anomaly (D) in soil waters from the Marcellus black shale of Pennsylvania. MRT = ridge top; MMS = mid-slope; and MVF = valley floor. The $(\text{Ce}/\text{Ce}^*)_N$ and $(\text{Eu}/\text{Eu}^*)_N$ values of the soil profile at the same site are plotted for reference.

Table 5

Mass and rates of REE depletion in soil profiles.

Site	Samples	Depth cm	C _{REE} ppm	C _{Zr} ppm	τ _{REE}	Depth interval (cm)	Bulk density (g cm ⁻³)	Strain	M (μg cm ⁻²)	R (μg cm ⁻² ka ⁻¹)
Wales	Q-0-10	10	229	159	0.52	10	0.88	1.20		
	Q-10-20	20	202	169	0.26	10	1.10	0.65		
	Q-20-30	30	200	176	0.20	10	1.24	0.42		
	Q-30-31	31	207	175	0.25	1	1.25	0.41		
	Q-31-35	35	279	166	0.77	4	1.28	0.45	2227	223
	Parent		167	176	0.00		1.75	0.00		
PA	SPRT 0010	5	175	273	−0.53	10	0.99	0.15		
(Gray Shale)	SPRT 1020	15	200	275	−0.47	10	1.21	−0.06		
	SPRT 2030	25	173	246	−0.49	10	1.33	−0.05	−6300	−371
	Parent		244	178	0.00		1.75	0.00		
PA	AF-1-1	2	124	85.1	−0.50	2	0.89	2.69		
(Black Shale)	AF-1-3	41.5	184	132	−0.53	39.5	1.44	0.46		
	AF-1-5	58	201	149	−0.54	16.5	1.51	0.24		
	AF-1-7	73.5	235	170	−0.53	15.5	1.55	0.06		
	AF-1-9	104	342	154	−0.24	30.5	1.60	0.13		
	AF-1-11	132.5	226	141	−0.46	28.5	1.63	0.21		
	AF-1-13	150.5	236	150	−0.46	18	1.64	0.13		
	AF-1-15	170.5	243	146	−0.43	20	1.65	0.15	−50,464	−2968
	Parent		468	159	0.00		1.75	0.00		
VA	MT-09-32	10	242	976	−0.72	10	1.05	−0.51		
	MT-09-33	20	239	977	−0.72	10	1.23	−0.58		
	MT-09-34	30	205	742	−0.69	10	1.33	−0.49		
	MT-09-35	40	206	672	−0.65	10	1.40	−0.46		
	MT-09-36	50	263	800	−0.63	10	1.45	−0.56		
	MT-09-37	60	284	871	−0.63	10	1.49	−0.61		
	MT-09-38	70	470	1000	−0.47	10	1.52	−0.67		
	MT-09-39	80	338	882	−0.57	10	1.54	−0.63	−52,450	−1116
	Parent		255.5	289	0.00		1.75	0.00		
TN	ALD-09-17	5	195	317	−0.40	5	1.12	0.28		
	ALD-09-18	10	222	343	−0.36	5	1.20	0.10		
	ALD-09-02	20	221	305	−0.29	10	1.31	0.13		
	ALD-09-03	30	228	297	−0.24	10	1.39	0.10		
	ALD-09-04	40	247	289	−0.16	10	1.44	0.09		
	ALD-09-05	50	252	269	−0.08	10	1.48	0.14		
	ALD-09-07	70	273	263	0.02	20	1.54	0.12		
	ALD-09-09	90	304	253	0.18	20	1.57	0.14		
	ALD-09-11	110	268	273	−0.04	20	1.60	0.04		
	ALD-09-13	130	207	245	−0.17	20	1.62	0.14		
	ALD-09-15	150	265	222	0.17	20	1.63	0.25		
	ALD-09-16	155	262	213	0.21	5	1.63	0.30		
	ALD-09-64	170	297	212	0.38	15	1.64	0.30		
	ALD-10-67	200	269	216	0.22	30	1.66	0.27		
	ALD-10-70	220	285	213	0.31	20	1.66	0.28		
	ALD-10-73	240	243	167	0.43	20	1.67	0.62		
	ALD-10-75	250	247	151	0.61	10	1.67	0.79		
	ALD-11-401	270	234	209	0.10	20	1.68	0.29		
	ALD-11-404	300	245	280	−0.14	30	1.69	−0.04		
	ALD-11-426	340	275	289	−0.06	40	1.69	−0.07		
	ALD-11-429	370	293	268	0.07	30	1.70	0.00		
	ALD-11-432	398	268	268	−0.02	28	1.70	−0.01	5845	25
	Parent		264	259	0.00		1.75	0.00	−4678 ^a	−20 ^a
AL	ALD-10-114	10	79	258	−0.78	10	1.04	0.32		
	ALD-10-115	20	124	337	−0.74	10	1.14	−0.08		
	ALD-10-116	30	143	372	−0.73	10	1.22	−0.22		
	ALD-10-117	40	159	258	−0.56	10	1.28	0.08		
	ALD-10-118	50	207	264	−0.45	10	1.33	0.02		
	ALD-10-121	70	457	244	0.32	20	1.40	0.04		
	ALD-10-123	100	474	180	0.86	30	1.47	0.35		
	ALD-10-125	120	628	173	1.56	20	1.50	0.37		
	ALD-10-127	140	610	161	1.67	20	1.53	0.45		
	ALD-10-129	155	203	119	0.20	15	1.54	0.94		
	ALD-11-506	180	249	158	0.11	25	1.57	0.44		
	ALD-11-508	200	338	148	0.61	20	1.58	0.52	25,198	195
	Parent		288	203	0.00		1.75	0.00	−16536 ^a	−128 ^a
PR	ALD-11-13	8	28	135	−0.87	8	0.96	−0.30		
	ALD-11-14	10	27	119	−0.86	2	0.99	−0.23		
	ALD-11-15	15	33	128	−0.84	5	1.06	−0.33		
	ALD-11-16	20	26	128	−0.88	5	1.12	−0.36		
	ALD-11-17	30	26	128	−0.88	10	1.21	−0.41		
	ALD-11-18	40	26	131	−0.88	10	1.28	−0.45		
	ALD-11-19	50	25	128	−0.88	10	1.33	−0.46		
	ALD-11-25	111	43	130	−0.80	61	1.50	−0.53		
	ALD-11-30	160	54	117	−0.72	49	1.56	−0.50		
	ALD-11-38	210	63	120	−0.68	50	1.60	−0.52		

(continued on next page)

Table 5 (continued)

Site	Samples	Depth cm	C _{REE} ppm	C _{Zr} ppm	τ _{REE}	Depth interval (cm)	Bulk density (g cm ⁻³)	Strain	M (μg cm ⁻²)	R (μg cm ⁻² ka ⁻¹)
	ALD-11-43	260	54	115	-0.72	50	1.62	-0.51		
	ALD-11-48	310	59	117	-0.70	50	1.64	-0.53		
	ALD-11-53	360	77	114	-0.59	50	1.66	-0.52		
	ALD-11-58	410	65	125	-0.68	50	1.67	-0.56		
	ALD-11-63	460	107	131	-0.50	50	1.67	-0.58		
	ALD-11-76	505	123	119	-0.37	45	1.68	-0.54		
	ALD-11-86	580	355	105	1.06	75	1.69	-0.49		Rate
	ALD-11-92	632	237	114	0.26	52	1.69	-0.53	-77,480	-306
Parent		86	52	0.00			1.75	0.00	-105003 ^a	-415 ^a

^a M and R are recalculated for only shallow soils where depletion is observed.

factor, $\epsilon(z)$, is a volume change factor for depth z of the profile and can be calculated as:

$$\epsilon(z) = \frac{V_w}{V_p} - 1 = \frac{C_{i,p}\rho_p}{C_{i,w}\rho_w} - 1 \quad (5)$$

Here ρ_w is the bulk density of the weathered soil (w). Positive ϵ values indicate soil expansion while negative ϵ values indicate soil compaction. If ϵ is 0, this suggests that soil genesis is isovolumetric (Brimhall and Dietrich, 1987; Anderson et al., 2002). Negative $m_{j,w}$ values mean overall depletion of element j from the entire soil profile while positive values mean net accumulation. Once $m_{j,w}$ is calculated, a time-integrated total elemental release rate, R_j ($\mu\text{g cm}^{-2} \text{ka}^{-1}$), can be determined if the soil residence time (SRT) is known (White, 2002; Brantley and White, 2009; Brantley and Lebedeva, 2011):

$$R_j = \frac{m_{j,w}}{\text{SRT}} \quad (6)$$

Similar exercises using these equations have been reported for major elements at the same sites (Dere et al., 2013, 2016; Dere, 2014). In this study, R_{REE} (i.e. the release rate for all REE) ranges from +220 to $-3000 \mu\text{g cm}^{-2} \text{ka}^{-1}$, with the greatest depletion observed at the PA-black shale site ($-2986 \mu\text{g cm}^{-2} \text{ka}^{-1}$) and the greatest accumulation of REE in Wales ($223 \mu\text{g cm}^{-2} \text{ka}^{-1}$) (Table 5).

Evaluation of REE mobility in weathering environments helps to quantify fluxes from continents to rivers to oceans at different temporal scales and could elucidate geochemical behaviors at global scales (Berner and Berner, 1995). The REE have long been considered to be immobile elements similar to Ti and Zr (Rudnick and Gao, 2003). Surprisingly, the values of m_{REE} and R_{REE} reported here are consistent with REE mobility. Indeed, this study highlights extensive release of REE during shale weathering, especially under warm and humid conditions. If m_{REE} and R_{REE} values from this study can be extrapolated to other shale-underlain terrains, an important flux of REE is expected from land to ocean.

The orders of magnitude difference in m_{REE} and R_{REE} observed in this study also could be consistent with a high variability in REE release and transport during shale weathering as a function of climate. Correlations between mineral dissolution rates and environmental variables such as MAP and MAT have been reported for major minerals or elements in rock types such as shale, basalt and granite (White and Blum, 1995; Williams et al., 2010; Rasmussen et al., 2011; Dere et al., 2013). MAP or P_{eff} is a proxy of water availability, as water can transport weathering products out of soils and promote further mineral dissolution. MAT dictates soil temperature where higher temperatures generally increase both the solubility and the rate constants for dissolution of minerals. It is commonly expected that combined high precipitation and air temperature enhance the weathering rates of individual minerals or major elemental leaching (e.g., White and Blum, 1995; Williams et al., 2010). However, R_{REE} and m_{REE} are not observed here to correlate positively with climate conditions (Table 5). Below we discuss several possible explanations for this observation.

First, it is always possible that large contributions from atmospheric deposition could obscure the weathering signature because aeolian deposition is known to contribute to soil development (e.g., Chadwick et al., 1999; Monastra et al., 2004; Muhs and Benedict, 2006; Derry and Chadwick, 2007; Reynolds et al., 2010; Lawrence et al., 2013). Numerous studies have used REE concentrations and patterns to help identify the provenance of dust and quantify their fluxes into lands and oceans (e.g., Greaves et al., 1994; Greaves et al., 1999; Tang et al., 2013). Thus, the REE depletion identified in the study soils here may be hard to interpret because of the possible overprint by REE addition through dust inputs. Such aeolian deposition is generally hard to detect except when positive τ_{REE} and R_{REE} values are observed especially in the top soil profile. For example, dust deposition may explain the observations for the Wales site (Fig. 3). Major elements reported in the Wales soils, however, show depletion profiles, except for Fe (Dere et al., 2013; Dere et al., 2016). Thus, in this case, if dust has contributed, then the hypothetical dust end member must have relatively high REE concentrations compared to its Zr concentrations to significantly modify soil REE budget, but have no detectable impacts on major elements. In addition to dust, sea aerosols may also contribute to soil REE. Precipitation chemistry at Plynlimon, Wales was monitored for over 10 years for major and trace elements (Neal et al., 2013). REE concentrations reported at that site range widely (La up to $4 \mu\text{g/L}$; Ce up to $22 \mu\text{g/L}$; Pr up to $0.16 \mu\text{g/L}$). Using the average concentrations in rain waters (La: $0.04 \mu\text{g/L}$; Ce: $0.38 \mu\text{g/L}$; Pr: $0.004 \mu\text{g/L}$) and annual precipitation rate of 250 cm , we can estimate the REE loading by rain, on the order of $100 \mu\text{g cm}^{-2} \text{ka}^{-1}$. The high accumulation rate of REE by rain at Wales is probably due to its close proximity to the ocean. This flux is expected to decrease quickly with distance from the ocean source. This exercise suggests that rain fall alone is not enough to explain the high accumulation REE rates ($\sim 220 \mu\text{g cm}^{-2} \text{ka}^{-1}$), and thus dust has contributed REE significantly at Wales.

Second, major elements in soils mainly reside in major minerals (e.g., Na and Ca from plagioclase); REE, as a group of trace elements, may be present as coatings or impurities dispersed in multiple minerals, instead of a single mineral. Thus, the release of REE from soils is likely to depend on the relative reactivity and abundance of multiple REE-bearing minerals or coatings. Given this, we expect that REE are released in step-wise reactions: REE in younger soils are likely to be lost dominantly through the dissolution of the most reactive mineral phase; this will continue until that mineral is depleted, and the second most reactive mineral will contribute to the next step of REE release. For such a case, the slope of the REE release will likely be controlled by both the REE content and the dissolution kinetics of the REE-containing minerals, instead of climate conditions.

Third, REE mobilized through mineral dissolution can be partially retained in a soil profile. REE solubility is low, and dissolved REE can be easily adsorbed to mineral surfaces (clays, iron oxyhydroxides, etc.) or co-precipitated with secondary minerals (Compton et al., 2003; Galan et al., 2007; Ma et al., 2011; Yusoff et al., 2013). The depletion-addition profiles observed in the southern sites are interpreted to be good

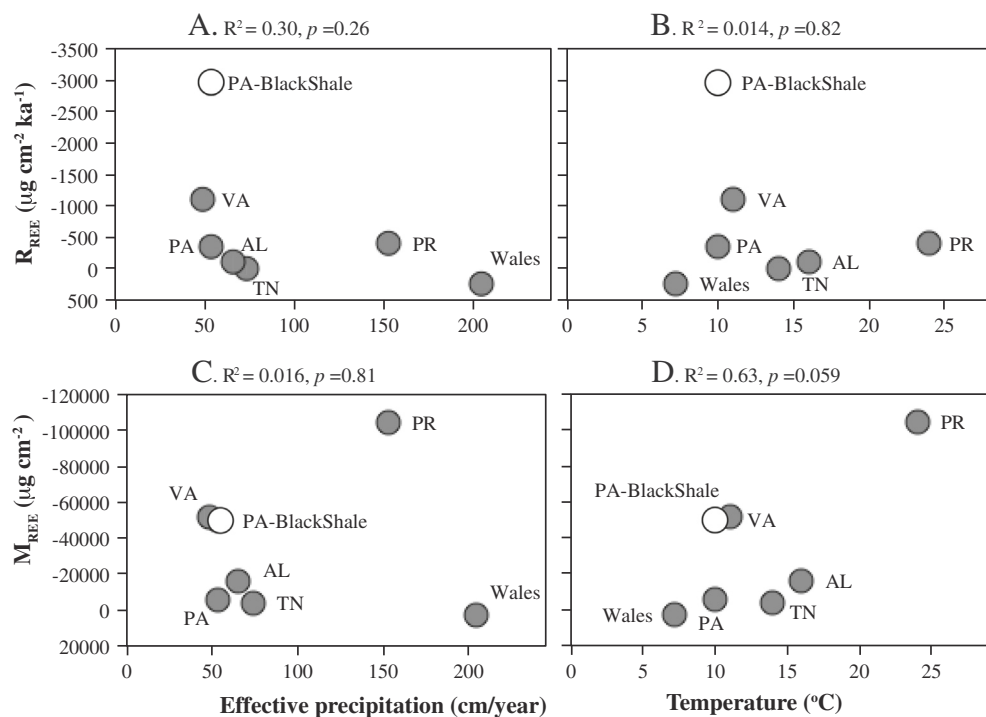


Fig. 7. The mass (M_{REE}) and rate (R_{REE}) of REE depletion at each site are plotted as a function of effective precipitation (cm/year) and mean annual temperature ($^{\circ}\text{C}$).

examples of loss of REE from shallow soils followed by movement and re-precipitation in deeper soils. Re-precipitation at depth could be caused by an increase in pH, a decrease in dissolved organic matter (DOM) concentration, or an increase in ionic strength of pore waters, as discussed below. Interestingly, the depletion-addition profiles are not observed in the northern sites, possibly because the northern soils are generally less weathered and shallower, and thus the pH shift, and changes in DOM and porewater ionic strength are not as pronounced.

Depletion-addition profiles are commonly observed in Spodosols when Al or Fe are mobilized as DOM-chelates and then are precipitated as secondary phases when the DOM is consumed in deeper soils (e.g., Brantley and Lebedeva, 2011). REE also have a strong affinity to DOM so REE can behave similarly to Fe and Al (Viers et al., 2000; Dia et al., 2000). In addition, REE solubility decreases as pH increases (e.g., Moller and Bau, 1993; Johannesson et al., 2000; Ma et al., 2011). As soil weathering extent decreases with depth, soil pH typically increases, leading to REE accumulation in deeper soils. Both pH- and DOM-controlling mechanisms might be important for the forested sites described here except for PR, where pH is slightly higher throughout the soil profile due to Ca buffering in the soil exchangeable sites. REE are also particle active and adsorb strongly to mineral surfaces (Ohlander et al., 1996; Galan et al., 2007; Bao and Zhao, 2008; Yusoff et al., 2013). This strong affinity to reactive surfaces such as those of secondary Al- and Fe-oxyhydroxides also means that REE can be sorbed to particles, then transported and re-deposited if particle agglomeration occurs with increasing ionic strength in soil waters.

Because of the re-deposition of soluble REE in deeper soils, the calculated m_{REE} and R_{REE} for the profiles of the AL and PR sites underestimate the REE loss rates from mineral dissolution in the upper soils. To correct for this, m_{REE} and R_{REE} were recomputed only for those soil depths where REE depletion is observed (Table 5). Still, the losses do not show strong correlation with temperature or precipitation (R^2 and P -values reported in Fig. 7).

Finally, soil chemistry can be impacted by the heterogeneity in overlying lithologic units. For example, at the VA site, the high value of m_{REE} might be related to the nature of the site and its previously overlying rock units. Specifically, the VA soils have unusually high Zr concentrations compared to the other sites (up to 1000 ppm; Table 3).

This Zr concentration is much higher than soils and bedrock at the other sites or even the bottom of the residual shale soil profile in VA. Instead, Zr concentrations in VA soils are within the range of sandstone units just above the Rose Hill shale (Dere et al., 2013). Thus it is possible that the high Zr in these soils might have been inherited from the sandstone that was originally present above the shale. As hypothesized previously, in this case, sandstone-derived Zr was incorporated into the shale-derived soils during denudation of the ridge (Dere et al., 2013). Based on this argument, Dere et al. (2013) used Ti as the immobile element and corrected for potential Ti losses to determine a corrected mass transfer coefficient of major elements in the shale-derived soil in VA. When we applied the same correction using Ti as the immobile element, all VA soils showed positive τ_{REE} values. Thus, we concluded that REE may also have been contributed by the overlying sandstone. For such a case, positive R_{REE} and m_{REE} may be a legacy of the previously present sandstone (Table 3).

5.2. Comparison of black and gray shale weathering sites

The two PA sites have similar MAT and MAP but the black shale soils experienced more REE depletion than the gray shale soils (Fig. 7). This is in agreement with differences observed in major elements between the two sites (Mathur et al., 2012; Brantley et al., 2013), suggesting faster mineral dissolution in OM- and sulfide-rich black shale than gray shale under similar climate conditions (Tuttle et al., 2002; Goldhaber et al., 2002; Petsch et al., 2005). It has previously been shown that exposed fossil organic carbon is quickly altered during early stages of black shale weathering through oxidation, hydrolysis and microbial consumption (Clayton and Swetland, 1978; Littke et al., 1991; Keller and Bacon, 1998; Petsch et al., 2000; Petsch et al., 2005; Jaffe et al., 2002; Copard et al., 2007; Jin et al., 2013). The depletion of organic carbon starts to occur at depths of many meters in black shale and is accompanied by opening of pores that increase permeability (Kennedy et al., 2002; Fischer and Gaupp, 2005), making initially weathered shale easily accessible to oxygenated fluids. Thus, black shale weathers more quickly than organic poor shale.

Pyrite is a ubiquitous mineral in black shale (Williams and Keith, 1963) and highly reactive when exposed to O_2 , producing strong

sulfuric acid to accelerate other weathering reactions. Indeed, reaction transport models that simulate chemical weathering reactions in Marcellus shale identified pyrite as the first mineral to react (Heidari et al., 2017). Similarly, studies on weathering of the Alum shale in Sweden showed that pyrite dissolution was the first alteration reaction (Rose and Cravotta, 1998; Feng et al., 2002; Falk et al., 2006). Furthermore, oxidation of sulfide minerals such as pyrite has been well documented even at the landscape scale (Chigira and Sone, 1991; Salomons, 1995; Chigira and Oyama, 1999; Evangelou, 2001). Acidic conditions in soils developed on black shale will enhance the weathering of clays and other minerals, thus releasing more REE and retaining dissolved REE in soil waters. This serves as another reason why REE dissolution rates are higher in black shale than those in gray shale under similar climatic conditions as observed in this study.

In addition, the pH values of the weathering profiles have important implications for REE mobility through secondary Fe phases, because of the relatively large surface area of Fe(III)-oxyhydroxide available for adsorption. At SSHO, the pH of weathering solutions remains neutral due to buffering capacity of carbonate minerals, and the oxidative dissolution of pyrite is accompanied by precipitation of Fe oxide and oxyhydroxide, retaining REE (Jin et al., 2010; Brantley et al., 2013). If the soil pH is low, Fe phases become unstable and the trace elements including REE are liberated, as observed in other studies (Jeng, 1991; Tuttle et al., 2002; Goldhaber et al., 2002; Falk et al., 2006). This might be what we observed in the Marcellus black shale site.

5.3. Short-term and long-term REE weathering processes at the black shale site

For the PA black shale (Marcellus Formation), REE are characterized in both the weathering residuum (soils) and the solutes (soil waters). Despite the limited number of samples, this new dataset allows us to examine the release, transport and fractionation at short versus long time scales. REE in aquatic ecosystems have been intensively studied, focusing on their mobility and fractionation as controlled by pH, redox conditions, and dissolved organic carbon concentrations, as well as by their adsorption to mineral surfaces (Nesbitt, 1979; Elderfield et al., 1990; Sholkovitz, 1993, 1995; Nesbitt and Markovics, 1997; Shiller, 1997, 2010; Johannesson and Zhou, 1999; Land et al., 1999; Ingris et al., 2000; Viers et al., 2000; Aubert et al., 2001; Hannigan and Sholkovitz, 2001; Moller, 2002; Compton et al., 2003; Bau et al., 2004; Johannesson et al., 2004; Andersson et al., 2006; Stille et al., 2006; Kato et al., 2011; Ma et al., 2011; Yusoff et al., 2013; Vázquez-Ortega et al., 2015). At this site, REE concentration-depth profiles in soil waters correlate well with soil water pH (Fig. 6), because pH is a strong determinant of REE mobility and REE concentrations decrease as pH increases with depth. In addition, although DOM concentrations have not been reported for these samples, DOM typically decreases with depth. For example, DOM decreases with depth at SSHO (Andrews et al., 2011). REE complexation with dissolved organic molecules could also be a mechanism for REE transport and redistribution (Viers et al., 2000; Dia et al., 2000). Thus soil water studies on Marcellus shales confirm our discussion above that both DOM concentrations and pH values control solubility and retention of REE in soils.

Below, a simple mass balance calculation is considered relating the time scales needed to leach REE out of soils at the observed rates, based on soil water REE concentrations. Central Pennsylvania receives 100 cm of precipitation annually and about half is lost to evaporation and transpiration (Jin et al., 2011a). Thus, the water flux that infiltrates and discharges to streams is about 50 cm yr⁻¹, or 0.5 m³ m⁻² yr⁻¹. Using an average REE concentration for soil water of 6 µg/L (or 6 mg m⁻³) as observed in the three Marcellus soils at 10 cm to 80 cm depth (Table 4, Fig. 6A), the annual REE flux today is estimated at about 3 mg m⁻² yr⁻¹. If a soil pedon were to lose half of its 500 ppm REE from the top 30 cm of the profile (assuming soil bulk density is 1.2 g cm⁻³), the total mass depletion is calculated as 30 cm × 1.2 g

cm⁻³ × 250 ppm, equivalent to 90 g REE m⁻². The time required to remove this REE at today's release rate is (90 g m⁻²)/(3 mg m⁻² yr⁻¹), ~30 ka. This timescale is very similar to the soil residence time that has been estimated for central Pennsylvania at SSHO: values for residence time range from 7 to 15 ka for two ridgetop sites (Ma et al., 2010; West et al., 2013).

The REE release rates at short timescales (annually, as quantified above as water flux) is 3 mg m⁻² yr⁻¹, or 0.3 mg cm⁻² ka⁻¹, lower than rates calculated over long timescales (thousands of years, as quantified by bulk soil chemistry) at ~3 mg cm⁻² ka⁻¹. This is consistent with the previous suggestion that the release of REE during shale weathering decreases with time, as controlled by the reactivity and REE contents of REE-bearing minerals. It is expected that reactive trace minerals dissolved first to release REE quickly (captured by long-term REE release rates), followed by slow release by clay dissolution (captured by short-term REE release rates). Reaction sequence for major minerals on Marcellus shale are confirmed by more sophisticated reactive transport models that simulate the evolution of soil chemistry (major elements), mineralogy and porosity to match the field data (Heidari et al., 2017).

5.4. Mineral-specific REE concentrations and patterns

Previous studies indicate aqueous REE signatures are inherited from rock REE during weathering and enhanced mobility of certain REE can be due to preferred dissolution of REE-rich trace minerals (Lev and Filer, 2004; Moller, 2002; Ma et al., 2011; Yusoff et al., 2013). REE are enriched in black shale and are largely associated with phosphates, carbonate, and clay minerals during and post-depositional and diagenetic processes (Lev and Filer, 2004). These REE-rich primary minerals therefore play key roles in REE mobility and fractionation depending on the inherent differences in patterns of mineral distribution (Möller and Giese, 1997; Moller, 2002; Ma et al., 2011; Yusoff et al., 2013). To model the variation of m_{REE} with time and predict the REE output for a watershed, it will be necessary to quantify mineral-specific REE concentrations and patterns in the future.

Below, we will examine behaviors of REE at different soil depth ranges that are defined by characteristic reactions of dominant mineral(s). This is to observe correlations between REE mobility and mineral depletion that might indirectly point to the importance of specific minerals in containing and releasing REE. The major elements in the Wales rock fragments ($n = 10$) show relatively constant concentrations (Dere et al., 2013; Dere, 2014). However, the same set of samples varies in REE concentrations and patterns (Fig. 2; Table 2), as well as loss on ignition (LOI). This observation could indicate that trace metal abundance and organic matter content in gray shale may be very sensitive to local geochemical conditions such as redox at the time of deposition. For example, previous studies have identified phosphates as major REE-bearing phases at SSHO in PA and their dissolution has controlled REE patterns and concentrations in soils and soil waters (Ma et al., 2011).

In contrast to the REE depletion observed at the bottom of augered soil samples at the Wales site, Dere et al. (2016) detected no depletion of Al, Si, Mg, or Fe (no indication of clay dissolution) at depth in the TN, VA, AL and PR sites. These observations are consistent with REE residing in mineral phases other than clays are mobilized during weathering. Similarly, τ_{REE} is almost constant with depth at the PA-gray shale site (SSHO), indicating that clay dissolution, the dominant chemical reactions in those soils, contributes little to REE depletion. In fact, up to 60% of the REE depletion observed in soils at SSHO ($\tau = \sim -0.6$) was attributed to dissolution of phosphate minerals by Ma et al. (2011).

Pyrite, ankerite, plagioclase, and organic matter are shown to have much deeper weathering fronts at SSHO, the gray shale site (Brantley et al., 2013). In contrast, other than the uppermost 0.3 m, the REE concentrations show little variation in the deep drill core (DC1) at SSHO down to 25 m (Table 2; Ma et al., 2011). Apparently, the loss of pyrite and organic matter in the gray shale at depth did not cause loss of

REE flux. Alternatively, minerals such as ankerite can be present in high abundance, but they contain little REE. These observations also justify the use of rock fragments from the augered cores or nearby outcrops as parent materials: some reactions occur quickly when fresh shales are exposed, for example as outcrops, the REE depletion may be limited. In addition, previous studies have identified unweathered cores surrounded by thick rinds in shallow and extensively altered soils (Colman, 1982; Graham et al., 2010; Engel et al., 2016). Similarly, shale chips collected from this study, maybe altered surficially, have bulk of rock volume intact, especially REE-rich phosphate minerals, and it is thus reasonable to assume they are close to parent bedrock in both REE concentrations and patterns.

The two soil profiles on the black shale (Marcellus Formation) show similar degrees of REE depletion (same τ values at surface soils in Fig. 3) even though PA-BlackShale2 is on the ridge top and PA-Black-Shale3 is at the valley floor along a planar transect. This is somewhat surprising in that we have previously observed (Jin et al., 2010) that soils that lie downslope from the ridgeline on shale tend to show greater depletion. Similar degrees of chemical depletion observed in shallow soils from PA-BlackShale2 (ridge top site) and PA-BlackShale3 (valley floor site) could be consistent with early depletion in REE followed by very little loss of REE.

5.5. REE fractionation during shale weathering

As discussed above, REE fractionation in soils could be due to preferential leaching of certain REE-rich minerals. Several environmental factors are also known to control REE fractionation during redistribution including soil pH, complexation with dissolved organic matter, adsorption and re-precipitation. Systematic fractionation of REE (preferential mobility of one subgroup of REE relative to others) commonly occurs during weathering, transport and deposition (Nesbitt, 1979; Elderfield et al., 1990; Nesbitt and Markovics, 1997; Shiller, 1997; Land et al., 1999; Viers et al., 2000; Aubert et al., 2001; Hannigan and Sholkovitz, 2001; Compton et al., 2003; Bau et al., 2004; Johannesson et al., 2004; Andersson et al., 2006; Stille et al., 2006). For example, MREE are more soluble than LREE and HREE under acidic conditions (e.g., Moller and Bau, 1993; Johannesson et al., 2000).

Soils at the northern sites have all experienced lower degrees of weathering and minimal REE losses compared to the southern sites (Dere et al., 2013; Fig. 3). Indeed, more REE are depleted from southern soils and REE fractionation is more systematic. For the PR and AL sites, particularly, LREE and MREE are more depleted in shallow soils but enriched in the deeper soils. High contents of clays and Fe-oxy-hydroxides are present in these soil profiles (Dere et al., 2013; Dere et al., 2016), in agreement with much higher CEC in the PR site observed in this study. Thus we suggest that elemental fractionation within the REE group is induced when soluble REEs are adsorbed to secondary Fe phases and clays at depth. In fact, clays and Fe and Al oxy-hydroxides are well-known to adsorb and act as carriers for REE in weathering profiles (Ohlander et al., 1996; Galan et al., 2007; Bao and Zhao, 2008; Yusoff et al., 2013). For Fe oxy-hydroxides, LREE adsorb more strongly than HREE (White, 2000; Compton et al., 2003). Thus it is reasonable that deeper soils show more enriched contents in LREE than HREE.

Soils from the VA site, however, are more depleted in HREE at shallow depths and enriched in the deeper soil profile. REE with higher atomic numbers form more stable solution complexes (Wood, 1990; Lee and Byrne, 1993; Luo and Byrne, 2004). Such variations in stability could result in solutes enriched in HREE, leaving behind a LREE-enriched residuum. Thus it is possible that REE are mobilized by chelation with other ions including dissolved organic matter for the VA site.

Ce and Eu have more than one oxidation state giving rise to redox-induced Ce and Eu anomalies that record changes in redox conditions during geological processes (Brookins, 1989; McLennan, 1989; Prudencio et al., 1995; Bau, 1999; Patino et al., 2003; Ma et al., 2011). The Ce anomaly observed in PR and AL probably points to the

fluctuation in redox conditions at these sites due to high MAP and thick soil profiles. Dere et al. (2013) and Dere et al. (2016) have reported redoximorphic features in these soils. For the AL site, $(Ce/Ce^*)_N$ is around 0.5, lower than 1, suggesting preferential loss of Ce relative to other REE. As Ce^{3+} is much more soluble than Ce^{4+} , it is likely that Ce^{4+} in shale is reduced to Ce^{3+} and lost under more reducing environments in soil profiles. A similar negative Ce anomaly is observed at the PA-black shale sites, but not for the PA-gray shale site. The difference suggests more reducing conditions in the black shale soils, even under the same climate conditions, probably due to fast consumption of O_2 by organic matter oxidation. Interestingly, a positive Ce anomaly is observed in PR, which might be related to high soil pH that lowers the solubility of MREE.

Eu anomalies are typically associated with plagioclase dissolution as Eu^{3+} can be reduced to Eu^{2+} and substituted into plagioclase for Ca. Given the errors and uncertainties associated with $(Eu/Eu^*)_N$ calculations, soils show no obvious Eu anomaly. Only soil waters from the Marcellus Formation shale site exhibit positive Eu anomalies. Different $(Eu/Eu^*)_N$ values in soils versus soil waters is consistent with the low abundance of plagioclase in the soils (< 2 wt%); however, plagioclase dissolves much faster than other mineral phases such as clays, and thus soil water shows higher $(Eu/Eu^*)_N$ than the soils.

6. Summary

We conducted a systematic investigation of REE mobility and fractionation during shale weathering along a climosequence from six weathering study sites in the eastern USA, Puerto Rico and Wales for REE concentrations and cation exchange pools (including Ca, Mg, K, Na, Al, Fe). In addition, soil and soil water samples were collected in a black shale weathering site to characterize REE mobility from an organic-rich shale end member. Mass balance models were applied to quantify the release rates of REE from each site. The results show that REEs are significantly released during shale weathering, especially under warm and humid conditions. Both mean annual temperature and precipitation probably impact the dissolution rates of REE-bearing minerals, and thus the overall loss of REE, but no simple correlations with MAT or MAP were observed. However, REE fractionation is more pronounced in southern sites under warm and humid conditions and these southern sites also show depletion from upper layers and accumulation in deep layers. Overall, REE mobility is a complicated function of the REE-hosting minerals and their reactivity, possible dust inputs, and the effects of translocation and re-deposition of REE from overlying units. In addition, REEs can be dissolved near the land surface and re-deposited at depth as DOC, pH, and clay surface area change due to weathering processes. In two PA sites experiencing similar climate conditions, REE are more depleted from a soil on black shale than on gray shale.

This study improves our understanding of the geochemical behaviors of these critical elements during chemical weathering. Shale weathering on continents is an important component of global REE cycling at Earth's surface. Future studies are needed to fully characterize REE transport and deposition during shale weathering, especially those that identify REE-bearing trace minerals on microscopic scales or REE mobilization by natural waters.

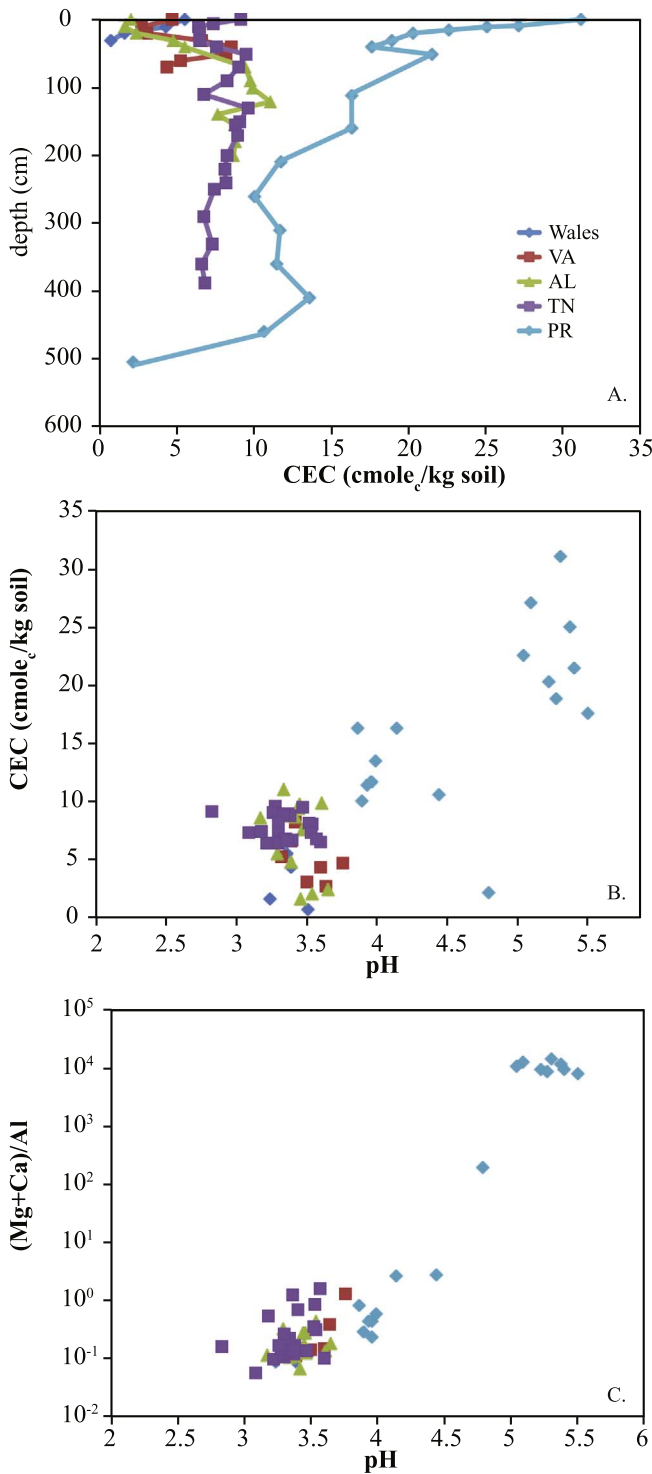
Acknowledgements

We want to acknowledge laboratory assistance from Alex Marone, Laura Liermann, and Henry Gong for ICP-MS analysis. We also thank the Centre for Ecology and Hydrology, including B. Reynolds, S. Grant, D. Robinson, I. Robinson, D. Norris, and B. Emmett, for assistance with Plynlimon samples and data. Sample collection assistance from A. Adames-Corraliza, R. April, N. Bingham, G. Carlson, D. Dere, K. Downey, T. Frederick, M. Friday, P. Grieve, D. Harbor, E. Heider, D. Keller, E. Knapp, K. Lease, L. Leidel, S. Lemon, L. Mann, G. Marshall, L.

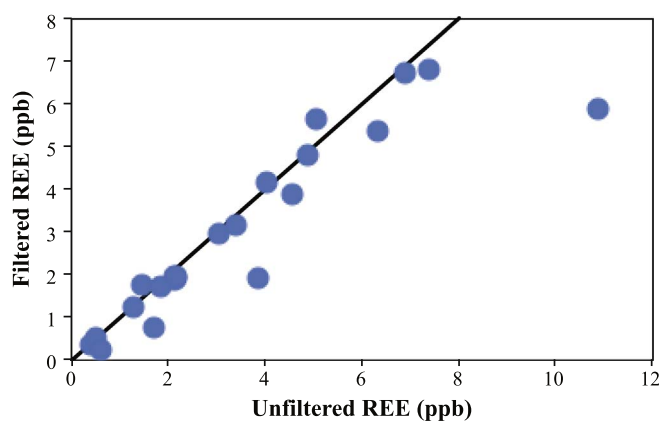
McKay, T. Miller, J. Moskal, J. Morales, R. Ruiz-Velez, M. Townsend, L. Vazquez-Albelo, D. Vazquez-Ortiz, M. Wagaw, F. Washington, N. West, D. Wilson, and J. Williams is also acknowledged. Financial support is from the U.S. Geological Survey (USGS), Department of the Interior, under USGS award number G12AP20050, and from a seed grant

through Penn State's (NSF EAR – 1239285 and EAR – 1331726) CZO to LM. We thank Dr. Jerome Gaillardet for editorial handling of this manuscript and two anonymous reviewers for their constructive comments.

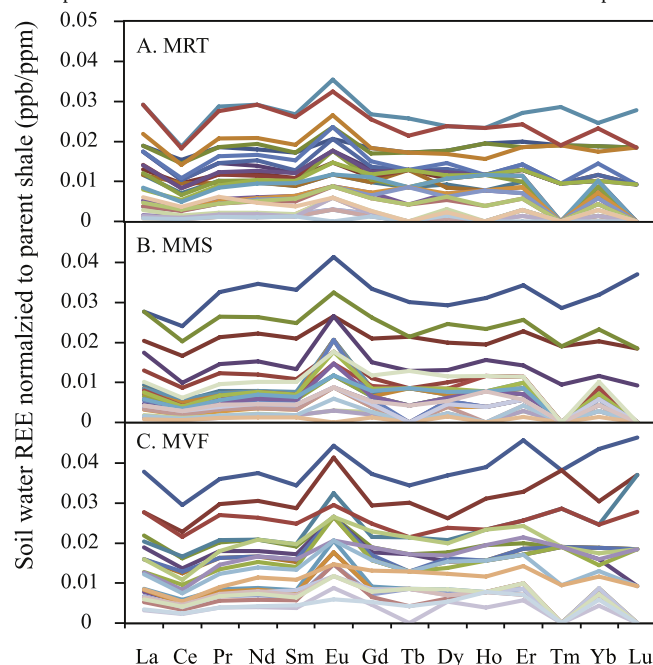
Appendix A



Appendix Fig. 1. Depth profiles of soil CEC at transect sites (A). The CEC (B) and its composition $((\text{Mg} + \text{Ca}) / \text{Al}$ ratios) (C) are correlated with pH.



Appendix Fig. 2. Comparison of REE concentrations in filtered and unfiltered soil water samples from Pennsylvania.



Appendix Fig. 3. REE patterns in soil waters from the Marcellus black shale in Pennsylvania, normalized to parent black shale. MRT = ridge top; MMS = mid-slope; and MVF = valley floor.

Appendix Table 1
QA/QC for REE analysis of rock standards.

	La	Ce	Pr	Nd	Sm	Eu	Gd	Tb	Dy	Ho	Er	Tm	Yb	Lu	Total REE	Zr
Detection Units	0.1 ppm	0.1 ppm	0.05 ppm	0.1 ppm	0.1 ppm	0.05 ppm	0.1 ppm	0.05 ppm	0.5 ppm							
Rock Standards																
W-2	10.7	22.9	2.98	12.9	3.1	1.06	3.93	0.58	3.81	0.8	2.33	0.31	2	0.32	67.72	88.3
Certified value	10	23		13	3.3	1		0.63	3.6	0.76	2.5	0.38	2.1	0.33		100
Diff. %	7%	0.4%		1%	6%	6%		8%	6%	5%	7%	20%	5%	3%		12%
BCR-2	23.2	48.8	6.48	26.6	5.7	1.9	6.81	1.07	5.89	1.22	3.4	0.5	3	0.51	135.08	181
Certified value	25	53	6.8	28	6.7	2	6.8	1.07		1.33		0.54	3.5	0.51		188
Diff. %	7%	8%	5%	5%	16%	5%	0%	0%		9%		8%	15%	0.0%		4%
Sco-1	28.5	54.1	6.62	26.1	4.8	1	4.62	0.64	4.05	0.83	2.31	0.31	2.2	0.32	136.4	164
Certified value	30	62	6.6	26												160
Diff. %	5%	14%	0.3%	0.4%												2%
ALD-11-16	4.3	8.9	0.92	3.8	0.9	0.27	1.18	0.23	1.59	0.39	1.37	0.22	1.6	0.28	25.95	128
REP-ALD-11-16	4.2	9.1	0.97	3.9	0.8	0.28	1.29	0.22	1.6	0.41	1.41	0.23	1.6	0.26	26.27	124
Diff. %	2%	2%	5%	3%	12%	4%	9%	4%	1%	5%	3%	4%	0.0%	7%	1%	3%

ALD-10-58	28.2	69.5	7.04	25.1	4.9	1.02	4.16	0.7	4.25	0.85	2.5	0.38	2.5	0.35	151.45	304
REP-ALD-10-58	29.1	72.2	7.25	25.8	5	1.08	4.26	0.7	4.5	0.87	2.43	0.4	2.5	0.37	156.46	334
Diff. %	3%	4%	3%	3%	2%	6%	2%	0.0%	6%	2%	3%	5%	0.0%	6%	3%	9%
Ave	5%	6%	3%	2%	9%	5%	4%	3%	4%	5%	4%	9%	5%	4%	2%	6%

Appendix Table 2

Zr concentrations of same soil samples run by ICP OES and ICP-MS (ppm).

Sample	Depth cm	Zr				Zr ICP-OES
		ICP-MS				
Wales						
Q-0-10	10		159			166
Q-10-20	20		169			168
Q-20-30	30		176			172
Q-30-31	31		175			170
Q-31-35	35		166			158
VA						
MT-09-32	10		976			984
MT-09-33	20		977			661
MT-09-34	30		742			718
MT-09-35	40		672			836
MT-09-36	50		800			772
MT-09-37	60		871			808
MT-09-38	70		1000			1244
MT-09-39	80		882			908
TN						
ALD-09-17	5		317			315
ALD-09-18	10		343			375
ALD-09-02	20		305			350
ALD-09-03	30		297			310
ALD-09-04	40		289			300
ALD-09-05	50		269			285
ALD-09-07	70		263			280
ALD-09-09	90		253			265
ALD-09-11	110		273			270
ALD-09-13	130		245			255
ALD-09-15	150		222			215
ALD-09-16	155		213			245
ALD-09-64	170		212			209
ALD-10-67	200		216			218
ALD-10-70	220		213			217
ALD-10-73	240		167			180
ALD-10-75	250		151			160
ALD-11-401	270		209			230
ALD-11-404	300		280			238
ALD-11-426	340		289			270
ALD-11-429	370		268			277
ALD-11-432	398		268			254
AL						
ALD-10-114	10		258			314
ALD-10-115	20		337			331
ALD-10-116	30		372			380
ALD-10-117	40		258			265
ALD-10-118	50		264			236
ALD-10-121	70		244			224
ALD-10-123	100		180			197
ALD-10-125	120		173			187
ALD-10-127	140		161			168
ALD-10-129	155		119			129
ALD-11-506	180		158			153
ALD-11-508	200		148			172
PR						
ALD-11-13	8		135			139
ALD-11-14	10		119			153

ALD-11-15		15		128			142
ALD-11-16		20		128			150
ALD-11-17		30		128			142
ALD-11-18		40		131			134
ALD-11-19		50		128			141
ALD-11-25		111		130			130
ALD-11-30		160		117			133
ALD-11-38		210		120			132
ALD-11-43		260		115			127
ALD-11-48		310		117			122
ALD-11-53		360		114			127
ALD-11-58		410		125			155
ALD-11-63		460		131			152
ALD-11-76		505		119			127
ALD-11-86		580		105			130
ALD-11-92		632		114			120

Appendix Table 3
CEC, pH and exchangeable cation concentrations in soils of all study sites.

Sample name	IBGC ^a	Depth range	Depth	pH	CEC	Al	Ca	Fe	K	Mg	Mn	Na	Si	Sr	
		cm	cm		cmol _c /Kg										
PlynQ 0-10	SSH000SSM	Wales	0–10	0	3.36	5.5	14.4	0.3	1.8	1.1	1.2	0.5	1.1	0.0	0.0
PlynQ 10-20	SSH0000HE	Wales	10–20	10	3.39	4.3	9.3	0.2	0.1	0.7	0.5	6.0	0.8	0.0	0.0
PlynQ 20-30	SSH0000HF	Wales	20–30	20	3.24	1.6	3.9	0.1	0.0	0.3	0.2	1.6	0.3	0.0	0.0
PlynQ 31-35	SSH0000HH	Wales	31–35	31	3.51	0.8	2.0	0.1	0.0	0.2	0.2	0.4	0.2	0.0	0.0
ALD-11-300	SSH0000Q4	VA	0–10	0	3.76	4.7	4.1	4.6	0.0	1.8	1.1	10.7	0.0	0.1	0.0
ALD-11-301	SSH0000Q5	VA	10–20	10	3.64	2.7	4.3	1.3	0.0	0.6	0.5	5.0	0.0	0.1	0.0
ALD-11-302	SSH0000Q6	VA	20–30	20	3.50	3.1	7.6	0.8	0.0	0.4	0.3	2.6	0.0	0.1	0.0
ALD-11-303	SSH0000Q7	VA	30–40	30	3.39	6.7	19.5	1.3	0.0	0.7	0.9	1.2	0.0	0.1	0.0
ALD-11-304	SSH0000Q8	VA	40–50	40		8.5	24.7	1.5	0.0	0.9	2.2	1.2	0.0	0.2	0.0
ALD-11-305	SSH0000Q9	VA	50–60	50	3.42	8.2	24.1	0.8	0.0	0.9	2.8	0.6	0.0	0.2	0.0
ALD-11-306	SSH0000QA	VA	60–70	60	3.32	5.3	15.5	0.3	0.0	0.6	2.0	0.3	0.0	0.1	0.0
ALD-11-307	SSH0000QB	VA	70–75	70	3.60	4.4	12.6	0.2	0.0	0.6	1.7	0.6	0.0	0.1	0.0
ALD-09-17	SSH0000QC	TN	0–5	0	2.83	9.2	25.5	2.8	0.8	2.0	1.5	1.1	0.0	0.0	0.0
ALD-09-18	SSH0000QD	TN	5–10	5	3.09	7.4	22.4	0.6	0.1	1.7	0.7	0.8	0.0	0.1	0.0
ALD-09-02	SSH0000QG	TN	10–20	10	3.22	6.4	18.5	0.8	0.0	2.0	1.0	1.1	0.0	0.1	0.0
ALD-09-03	SSH0000QH	TN	20–30	20	3.30	6.5	17.6	0.7	0.0	2.7	1.2	2.4	0.0	0.2	0.0
ALD-09-04	SSH0000QI	TN	30–40	30	3.60	6.5	18.9	0.5	0.0	2.3	1.6	0.7	0.0	0.2	0.0
ALD-09-05	SSH0000QJ	TN	40–50	40	3.30	7.6	22.1	0.7	0.0	2.3	2.4	0.1	0.0	0.2	0.0
ALD-09-07	SSH0000QL	TN	50–70	50	3.47	9.5	27.9	0.4	0.0	2.6	3.4	0.1	0.0	0.2	0.0
ALD-09-09	SSH0000QN	TN	70–90	70	3.37	9.0	26.7	0.2	0.0	2.4	3.1	0.0	0.0	0.3	0.0
ALD-09-11	SSH0000QP	TN	90–110	90	3.30	8.3	24.5	0.1	0.0	2.2	2.9	0.0	0.0	0.3	0.0
ALD-09-13	SSH0000QR	TN	110–130	110	3.35	6.8	19.8	0.1	0.0	1.7	2.7	0.0	0.0	0.3	0.0
ALD-09-15	SSH0000QT	TN	130–150	130	3.28	9.6	28.0	0.1	0.0	2.4	4.2	0.0	0.2	0.2	0.0
ALD-09-16	SSH0000QU	TN	150–155	150	3.26	9.1	26.1	0.1	0.0	2.5	4.4	0.1	0.2	0.2	0.0
ALD-09-64	SSH0000QY	TN	155–170	155	3.38	8.9	25.3	0.1	0.0	2.5	4.3	0.0	0.2	0.3	0.0
ALD-09-67	SSH0000R1	TN	170–200	170	3.34	8.9	24.6	0.1	0.0	2.6	5.5	0.1	0.3	0.3	0.0
ALD-09-70	SSH0000R4	TN	200–220	200	3.30	8.2	22.1	0.1	0.0	2.7	5.9	0.1	0.4	0.2	0.0
ALD-09-73	SSH0000R8	TN	220–240	220	3.54	8.1	20.9	0.1	0.0	2.7	6.8	0.2	0.5	0.3	0.0
ALD-09-75	SSH0000R9	TN	240–250	240	3.52	8.2	20.5	0.1	0.0	2.7	7.4	0.4	0.5	0.3	0.0
ALD-11-401	SSH0000RP	TN	250–270	250	3.18	7.4	16.5	0.3	0.0	3.5	9.1	0.1	0.8	0.4	0.0
ALD-11-404	SSH0000RS	TN	290–300	290	3.40	6.7	14.1	0.2	0.0	3.1	9.6	0.2	0.6	0.3	0.0
ALD-11-426	SSH0000RW	TN	330–340	330	3.53	7.3	14.0	0.3	0.0	3.4	12.2	0.5	0.7	0.3	0.0
ALD-11-429	SSH0000RZ	TN	360–370	360	3.36	6.7	10.7	0.2	0.0	3.9	13.5	0.6	0.7	0.3	0.0
ALD-11-432	SSH0000S2	TN	388–398	388	3.57	6.9	9.5	0.5	0.0	4.6	15.5	0.8	0.7	0.3	0.0
ALD-11-114	SSH0000T3	AL	0–10	0	3.54	2.1	4.5	1.5	0.0	1.2	0.5	0.9	0.0	0.0	0.0
ALD-11-115	SSH0000T4	AL	10–20	10	3.46	1.7	3.9	0.7	0.0	0.9	0.4	0.9	0.0	0.0	0.0
ALD-11-116	SSH0000T5	AL	20–30	20	3.65	2.4	6.3	0.8	0.0	1.0	0.4	0.8	0.0	0.1	0.0
ALD-11-117	SSH0000T6	AL	30–40	30	3.39	4.8	13.2	1.3	0.0	1.9	0.9	0.8	0.0	0.1	0.0
ALD-11-118	SSH0000T7	AL	40–50	40	3.29	5.5	13.9	1.4	0.0	2.1	3.3	0.7	0.0	0.2	0.0
ALD-11-121	SSH0000TA	AL	70–80	70	3.44	9.4	25.3	0.6	0.0	1.6	6.7	0.2	0.0	0.5	0.0
ALD-11-123	SSH0000TC	AL	90–100	90	3.45	9.8	27.8	0.4	0.0	1.1	4.7	0.2	0.0	0.7	0.0
ALD-11-125	SSH0000TE	AL	100–120	100	3.61	9.9	29.0	0.3	0.0	1.2	3.7	0.1	0.0	0.7	0.0

ALD-11-127	SSH0000TG	AL	120–140	120	3.34	11.1	33.0	0.2	0.0	1.2	3.3	0.1	0.0	0.8	0.0
ALD-11-129	SSH0000TI	AL	140–155	140	3.47	7.6	22.3	0.7	0.0	1.0	2.2	0.3	0.0	0.5	0.0
ALD-11-506	SSH0000TP	AL	155–180	155	3.42	8.8	26.9	0.1	0.0	0.8	1.7	0.0	0.0	0.5	0.0
ALD-11-508	SSH0000TR	AL	180–200	180	3.38	8.8	26.1	0.6	0.0	0.9	2.4	0.1	0.0	0.7	0.0
ALD-11-510	SSH0000TT	AL	200–210	200	3.17	8.7	25.6	0.7	0.0	0.9	2.4	0.3	0.0	0.5	0.0
ALD-11-13	SSH0000VO	PR	0–8	0	5.30	31.1	0.0	133.0	0.0	7.9	16.4	0.2	1.6	0.6	0.2
ALD-11-14	SSH0000VP	PR	8–10	8	5.09	27.1	0.0	117.5	0.0	4.6	13.4	0.1	1.9	0.5	0.2
ALD-11-15	SSH0000VQ	PR	10–15	10	5.37	25.1	0.0	109.9	0.0	3.0	11.6	0.1	2.2	0.5	0.2
ALD-11-16	SSH0000VR	PR	15–20	15	5.04	22.6	0.0	98.9	0.0	2.4	10.2	0.1	2.9	0.5	0.2
ALD-11-17	SSH0000VS	PR	20–30	20	5.22	20.3	0.0	89.4	0.0	2.5	8.6	0.0	2.8	0.4	0.2
ALD-11-18	SSH0000VT	PR	30–40	30	5.27	18.9	0.0	83.9	0.0	2.7	7.3	0.0	2.4	0.3	0.1
ALD-11-19	SSH0000VU	PR	40–50	40	5.50	17.6	0.0	77.4	0.0	3.1	7.1	0.0	2.2	0.3	0.1
ALD-11-25	SSH0000W0	PR	50–111	50	5.40	21.5	0.0	83.0	0.0	9.8	16.6	0.0	4.5	0.3	0.2
ALD-11-30	SSH0000W5	PR	111–160	111	4.14	16.3	16.4	37.5	0.0	16.8	7.8	0.0	3.9	0.6	0.1
ALD-11-38	SSH0000WA	PR	160–210	160	3.86	16.3	29.6	20.2	0.0	18.1	4.7	0.0	3.7	0.6	0.0
ALD-11-43	SSH0000WF	PR	210–260	210	3.96	11.7	25.5	9.3	0.0	12.8	2.4	0.0	2.8	0.5	0.0
ALD-11-48	SSH0000WK	PR	260–310	260	3.89	10.1	23.6	5.3	0.0	12.4	1.6	0.0	1.7	0.4	0.0
ALD-11-53	SSH0000WP	PR	310–360	310	3.96	11.7	29.0	5.0	0.0	12.0	1.9	0.1	2.3	0.4	0.0
ALD-11-58	SSH0000WU	PR	360–410	360	3.93	11.5	25.6	8.4	0.0	10.0	3.1	0.1	3.2	0.3	0.0
ALD-11-63	SSH0000WZ	PR	410–460	410	3.99	13.6	28.1	10.0	0.0	10.6	7.4	0.1	4.6	0.3	0.1
ALD-11-76	SSH0000X5	PR	460–505	460	4.44	10.7	10.5	18.9	0.0	9.6	10.3	0.1	5.6	0.3	0.2
ALD-11-86	SSH0000XF	PR	505–580	505	4.79	2.2	0.0	0.8	0.0	4.2	1.2	0.0	13.5	0.0	0.0

References

- Amiotte-Suchet, P., Probst, J., Ludwig, W., 2003. Worldwide distribution of continental rock lithology: implications for the atmospheric/soil CO₂ uptake by continental weathering and alkalinity river transport to the oceans. *Glob. Biogeochem. Cycles* 17, 1038. <http://dx.doi.org/10.1029/2002GB001891>.
- Anderson, S.P., Dietrich, W.E., Brimhall, G.H., 2002. Weathering profiles, mass-balance analysis, and rates of solute loss: linkages between weathering and erosion in a small, steep catchment. *GSA Bull.* 114, 1143–1158.
- Andersson, K., Dahlqvist, R., Turner, D., Stolpe, B., Larsson, T., Ingri, J., Andersson, P., 2006. Colloidal rare earth elements in a boreal river: changing sources and distributions during the spring flood. *Geochim. Cosmochim. Acta* 70, 3261–3274.
- Andrews, D.M., Lin, H., Zhu, Q., Jin, L., Brantley, S.L., 2011. Hot spots and hot moments of dissolved organic carbon export and soil organic carbon storage in the Shale Hills Critical Zone Observatory. *Vadose Zone J.* 10, 943–954. <http://dx.doi.org/10.2136/vzj2010.0149>.
- April, R.H., Hluchy, M.M., Newton, R.M., 1986. Chemical weathering in two Adirondack watersheds: past and present-day rates. *Geol. Soc. Am. Bull.* 97, 1232–1238.
- Aubert, D., Stille, P., Probst, A., 2001. REE fractionation during granite weathering and removal by water and suspended loads: Sr and Nd isotopic evidence. *Geochim. Cosmochim. Acta* 65, 387–406.
- Bao, Z., Zhao, Z., 2008. Geochemistry of mineralization with exchangeable REY in the weathering crusts of granitic rocks in South China. *Ore Geol. Rev.* 33 (3–4), 519–535.
- Bau, M., 1999. Scavenging of dissolved yttrium and rare earths by precipitating iron oxyhydroxide: experimental evidence for Ce oxidation, Y-Ho fractionation, and lanthanide tetrad effect. *Geochim. Cosmochim. Acta* 63, 67–77.
- Bau, M., Alexander, B., Chesley, J.T., Dulski, P., Brantley, S.L., 2004. Mineral dissolution in the Cape Cod aquifer, Massachusetts, USA: I. Reaction stoichiometry and impact of accessory feldspar and glaucocrite on strontium isotopes, solute concentrations, and REY distribution. *Geochim. Cosmochim. Acta* 68, 1199–1216.
- Berner, E.K., Berner, R.A., 1995. Global Environment: Water, Air, and Geochemical Cycles. Prentice Hall.
- Birkeland, P.W., 1999. Soils and Geomorphology. Oxford University Press, New York, pp. 430.
- Bockheim, J.G., 1980. Solution and use of chronofunctions in studying soil development. *Geoderma* 24, 71–85.
- Brantley, S.L., Lebedeva, M., 2011. Learning to read the chemistry of the regolith to understand the critical zone. *Annu. Rev. Earth Planet. Sci.* 39, 387–416.
- Brantley, S.L., White, A.F., 2009. Approaches to modeling weathered regolith. *Rev. Mineral. Geochem.* 70, 435–484.
- Brantley, S.L., Bandstra, J., Moore, J., White, A.F., 2008. Modeling chemical depletion profiles in regolith. *Geoderma* 145, 494–504.
- Brantley, S.L., Holleran, M.E., Jin, L., Bazilevskaya, E., 2013. Probing chemical reactions underlying the Shale Hills Critical Zone Observatory, Pennsylvania (U.S.A.): nested weathering reaction fronts. *Earth Surf. Process. Landf.* <http://dx.doi.org/10.1002/esp.3415>.
- Brimhall, G.H., Dietrich, W.E., 1987. Constitutive mass balance relations between chemical composition, volume, density, porosity, and strain in metasomatic hydrochemical systems: results on weathering and pedogenesis. *Geochim. Cosmochim. Acta* 51, 567–587.
- Brimhall, G.H., Chadwick, O.A., Lewis, C.J., Compston, W., Williams, I.S., Danti, K.J., Dietrich, W.E., Power, M.E., Hendricks, D., Bratt, J., 1992. Deformational mass transport and invasive processes in soil evolution. *Science* 255, 695–702.
- Brookins, D.G., 1989. Aqueous geochemistry of rare earth elements. *Rev. Mineral.* 21, 201–225.
- Cadwell, D.H., Muller, E.H., 2004. New York glacial geology, U.S.A. In: Ehlers, J., Gibbard, P.L. (Eds.), Quaternary Glaciations – Extent and Chronology. Part II: North America. Elsevier, Netherlands, pp. 201–205.
- Chadwick, O.A., Derry, L.A., Vitousek, P.M., Huebert, B.J., Hedin, L.O., 1999. Changing sources of nutrients during four million years of ecosystem development. *Nature* 397, 491–497.
- Chadwick, O.A., Gavenda, R.T., Kelly, E.F., Ziegler, K., Olson, C.G., Elliott, W.C., Hendrick, D.M., 2003. The impact of climate on the biogeochemical functioning of volcanic soils. *Chem. Geol.* 202, 195–223.
- Chakhmouradian, A.R., Wall, F., 2012. Rare earth elements: minerals, mines, magnets, (and more). *Elements* 8, 333–340.
- Chigira, M., Oyama, T., 1999. Mechanism and effect of chemical weathering of sedimentary rocks. *Eng. Geol.* 55, 3–14.
- Chigira, M., Sone, K., 1991. Chemical weathering mechanisms and their effects on engineering properties of soft sandstone and conglomerate cemented by zeolite in a mountainous area. *Eng. Geol.* 30, 195–219.
- Ciolkosz, E.J., Crone, R.C., Sevon, W.D., 1986. Periglacial Features in Pennsylvania. *Agron. Ser. 92 PA. State Univ.* (52 p).
- Clark, C.D., Gibbard, P.L., Rose, J., 2004. Pleistocene glacial limits in England, Scotland and Wales. In: Ehlers, J., Gibbard, P.L. (Eds.), Quaternary Glaciations – Extent and Chronology. Part I: Europe. Elsevier, Netherlands, pp. 47–82.
- Clark, G.M., Ciolkosz, E.J., 1988. Periglacial geomorphology of the Appalachian highlands and interior highlands south of the glacial border – a review. *Geomorphology* 1, 191–220.
- Clayton, J.L., Swetland, P.J., 1978. Subaerial weathering of sedimentary organic matter. *Geochim. Cosmochim. Acta* 42, 305–312.
- Colman, S.M., 1982. Clay mineralogy of weathering rinds and possible implications concerning the sources of clay minerals in soil. *Geology* 10, 370–375.
- Compton, J.S., White, R.A., Smith, M., 2003. Rare earth element behavior in soils and salt pan sediments of a semi-arid granitic terrain in the Western Cape, South Africa. *Chem. Geol.* 201, 239–255.
- Copard, Y., Amiotte-Suchet, P., Di-Giovanni, C., 2007. Storage and release of fossil organic carbon related to weathering of sedimentary rocks. *Earth Planet. Sci. Lett.* 258, 345–357.
- Dere, A.L., 2014. Shale Weathering Across a Latitudinal Climosequence. PhD thesis The Pennsylvania State University (302 pages).
- Dere, A.L., White, T.S., April, R.H., Reynolds, B., Miller, T.E., Knapp, E.P., McKay, L.D., Brantley, S.L., 2013. Climate dependence of feldspar weathering in shale soils along a latitudinal gradient. *Geochim. Cosmochim. Acta* 122, 101–126. <http://dx.doi.org/10.1016/j.gca.2013.08.001>.
- Dere, A.L., White, T.S., April, R.H., Brantley, S.L., 2016. Mineralogical transformations and soil development in shale across a climosequence. *Soil Sci. Soc. Am. J.* 80, 623–636. <http://dx.doi.org/10.2136/sssaj2015.05.0202>.
- Derry, L.A., Chadwick, O.A., 2007. Contributions from earth's atmosphere to soil. *Elements* 3 (5), 333–338.
- Dia, A., Gratu, G., Olivie-Lauquet, G., Riou, C., Molenat, J., Curmi, P., 2000. The distribution of rare earth elements in groundwaters: Assessing the role of source-rock composition, redox changes and colloidal particles. *Geochim. Cosmochim. Acta* 64, 4131–4151.
- Egli, M., Fitze, P., 2000. Formulation of pedogenic mass balance based on immobile elements: a revision. *Soil Sci.* 165, 437–443.
- Elderfield, H., Upstill-Goddard, R., Sholkovitz, E.R., 1990. The rare earth elements in

- rivers, estuaries, and coastal seas and their significance to the composition of ocean waters. *Geochim. Cosmochim. Acta* 54, 971–991.
- Engel, J.M., Ma, L., Sak, P.B., Gaillardet, J., Ren, M., Engle, M.A., Brantley, S.L., 2016. Quantifying chemical weathering rates along a precipitation gradient on Basse-Terre Island, French Guadeloupe: new insight from U-series isotopes in weathering rinds. *Geochim. Cosmochim. Acta* 195, 29–67.
- Evangelou, V.P., 2001. Pyrite microencapsulation technologies: principles and potential field application. *Ecol. Eng.* 17, 165–178.
- Falk, H., Lavergne, U., Bergback, B., 2006. Metal mobility in alum shale from Oland, Sweden. *J. Geochem. Explor.* 90, 157–165.
- Feng, G., Wu, L., Letey, J., 2002. Evaluating aeration criteria by simultaneous measurement of oxygen diffusion rate and soil-water regime. *Soil Sci.* 167, 495–503.
- Fischer, C., Gaupp, R., 2005. Change of black shale organic material surface area during oxidative weathering: implications for rock-water surface evolution. *Geochim. Cosmochim. Acta* 69, 1213–1224.
- Gaillardet, J., Dupré, B., Louvat, P., Allègre, C.J., 1999. Global silicate weathering and CO₂ consumption rates deduced from the chemistry of large rivers. *Chem. Geol.* 159, 3–30.
- Galan, E., Fernández-Caliani, J.C., Miras, A., Aparicio, P., Marquez, M.G., 2007. Residence and fractionation of rare earth elements during kaolinization of alkaline per-aluminous granites in NW Spain. *Clay Miner.* 42, 341–352.
- Gardner, T.W., Ritter, J.B., Shuman, C.A., Bell, J.C., Sasowsky, K.C., Pinter, N., 1991. A periglacial stratified slope deposit in the valley and ridge province of central Pennsylvania, USA: sedimentology, stratigraphy and geomorphic evolution. *Permafro. Periglac. Process.* 2, 141–162.
- Goldhaber, M.B., Hatch, J.R., Callender, E.C., Irwin, E.R., Tuttle, M.L., Ayuso, R.A., Lee, L., Morrison, J.M., Grosz, A., Atkins, J.B., Black, D.D., Zappia, H., Pashin, J.C., Diehl, S.F., Sanzolone, R.F., Ruppert, L.F., Kolker, A., Finkelman, R.B., Bevins, H.E., 2002. Impact of Elevated Arsenic in Coal on the Geochemical Landscape of the Eastern U.S. Sixth International Symposium on the Geochemistry of the Earth's Surface (GES-6), Honolulu, Hawaii.
- Graham, R.C., Rossi, A.M., Hubbert, K.R., 2010. Rock to regolith conversion: producing hospitable substrates for terrestrial ecosystems. *GSA Today* 20, 4–9.
- Greaves, M.J., Statham, P.J., Elderfield, H., 1994. Rare-earth element mobilization from marine atmospheric dust into seawater. *Mar. Chem.* 53, 255–260.
- Greaves, M.J., Elderfield, H., Sholkovitz, E.R., 1999. Aeolian sources of rare earth elements to the western Pacific Ocean. *Mar. Chem.* 68, 31–37.
- Hannigan, R.E., Sholkovitz, E.R., 2001. The development of middle rare earth element enrichments in freshwaters: weathering of phosphate minerals. *Chem. Geol.* 175, 495–508.
- Heidari, P., Li, L., Jin, L., Brantley, S.L., 2017. Understanding controls of Marcellus Shale weathering using reactive transport modeling. *Geochim. Cosmochim. Acta*.
- Herndon, E.M., Jin, L., Brantley, S.L., 2011. Soils reveal widespread manganese enrichment from industrial inputs. *Environ. Sci. Technol.* 45 (1), 241–247.
- Imbrie, J., Hays, J.D., Pisias, N.G., Prell, W.L., Shackleton, N.J., 1984. The orbital theory of Pleistocene climate: support from a revised chronology of the marine ⁸⁷O record. In: Berger, J.A., Hays, J., Kukla, G., Saltzman, B. (Eds.), Milankovitch and Climate. Reidel, Dordrecht, Netherlands.
- Ingris, J., Widerlund, A., Land, M., Gustafsson, O., Andersson, P., Ohlander, B., 2000. Temporal variations in the fractionation of the rare earth elements in a boreal river; the role of colloidal particles. *Chem. Geol.* 166, 23–45.
- Jacobson, A.D., Blum, J.D., Chamberlain, C.P., Craw, D., Koons, P.O., 2003. Climatic and tectonic controls on chemical weathering in the New Zealand Southern Alps. *Geochim. Cosmochim. Acta* 67, 29–46.
- Jaffe, L.A., Peucker-Ehrenbrink, B., Petsch, S.T., 2002. Mobility of rhenium, platinium group elements and organic carbon during black shale weathering. *Earth Planet. Sci. Lett.* 198, 339–353.
- Jeng, A.S., 1991. Weathering of some Norwegian alum shales: I. Laboratory simulations to study acid generation and the release of sulphate and metal cations (Ca, Mg and K). *Acta Agric. Scand.* 41, 13–35.
- Jenny, H., 1941. Factors of Soil Formation. McGraw Hill, NY (281 p).
- Jin, L., Ravella, R., Ketchum, B., Heaney, P., Brantley, S.L., 2010. Mineral weathering and elemental transport during hillslope evolution at the Susquehanna/Shale Hills Critical Zone Observatory. *Geochim. Cosmochim. Acta* 74, 3669–3691.
- Jin, L., Andrews, D.M., Holmes, G.H., Lin, H., Brantley, S.L., 2011a. Open the “Black Box”: water chemistry reveals hydrological controls on weathering in the Susquehanna Shale Hills Critical Zone Observatory. *Vadose Zone J.* 10, 928–942.
- Jin, L., Rother, G., Cole, D.R., Mildner, D.F.R., Duffy, C.J., Brantley, S.L., 2011b. Characterization of deep weathering and nanoporosity development in shale – a neutron study. *Am. Mineral.* 96, 198–512.
- Jin, L., Mathur, R., Rother, G., Cole, D.R., Bazilevskaya, E., Williams, J., Carone, A., Brantley, S.L., 2013. Porosity and chemical fingerprints of a black shale (Marcellus Formation) as it weathers at the land surface. *Chem. Geol.* 356, 50–63.
- Johannesson, K.H., and Zhou (1999). Origin of middle rare earth element enrichments in acid waters of a Canadian high Arctic Lake. *Geochim. Cosmochim. Acta* 63, 153–165.
- Johannesson, K.H., Zhou, X., Guo, C., Stetzenbach, K.J., Hodge, V.F., 2000. Origin of rare earth element signatures in groundwaters of circumneutral pH from southern Nevada and eastern California, USA. *Chem. Geol.* 164, 239–258.
- Johannesson, K.H., Tang, J., Daniels, J.M., Bounds, W.J., Burdige, D.J., 2004. Rare earth element concentrations and speciation in organic-rich blackwaters of the Great Dismal Swamp, Virginia, USA. *Chem. Geol.* 209, 271–294.
- Kato, Y., Fujinaga, K., Nakamura, K., Takaya, Y., Kitamura, K., Ohta, J., Toda, R., Nakashima, T., Iwamori, H., 2011. Deep-sea mud in the Pacific Ocean as a potential resource for rare-earth elements. *Nat. Geosci.* 4, 535–539.
- Keller, C.K., Bacon, D.H., 1998. Soil respiration and georespiration distinguished by transport analyses of vadose CO₂, ¹³CO₂, and ¹⁴CO₂. *Glob. Biogeochem. Cycles* 12, 361–372.
- Kennedy, M.J., Pevear, D.R., Hill, R.J., 2002. Mineral surface control of organic carbon in black shale. *Science* 295, 657–660.
- King, P.B., Ferguson, H.W., 1960. Geology of Northeasternmost Tennessee. U.S. Geol. Survey Prof. Paper 311 (136 p).
- Kynicky, J., Smith, M.P., Xu, C., 2012. Diversity of rare earth deposits: the key example of China. *Elements* 8 (5), 361–368.
- Land, M., Ohlander, B., Ingris, J., Thunberg, J., 1999. Solid speciation and fractionation of rare earth elements in a spodosol profile from northern Sweden as revealed by sequential extraction. *Chem. Geol.* 160, 121–138.
- Lawrence, C.R., Reynolds, R.L., Ketterer, M.E., Neff, J.C., 2013. Aeolian controls of soil geochemistry and weathering fluxes in high-elevation ecosystems of the Rocky Mountains, Colorado. *Geochim. Cosmochim. Acta* 107, 27–46.
- Lee, J.H., Byrne, R.H., 1993. Complexation of trivalent rare earth elements (Ce, Eu, Gd, Tb, Yb) by carbonate ions. *Geochim. Cosmochim. Acta* 57, 295–302.
- Lev, S.M., Filer, J.K., 2004. Assessing the impact of black shale processes on REE and the U-Pb isotope system in the southern Appalachian Basin. *Chem. Geol.* 206, 393–406.
- Littke, R., Klussmann, U., Krooss, B., Leythaeuser, D., 1991. Quantification of loss of calcite, pyrite, and organic matter due to weathering of Toarcian black shales and effects on kerogen and bitumen characteristics. *Geochim. Cosmochim. Acta* 55, 3369–3378.
- Long, K., 2010. The geology of rare earth elements. *Geology.com*. Retrieved from. <http://geology.com/usgs/renee-geology/>.
- Luo, Y.R., Byrne, R.H., 2004. Carbonate complexation of yttrium and the rare earth elements in natural waters. *Geochim. Cosmochim. Acta* 68, 691–699.
- Ma, L., Chabaux, F., Pelt, E., Blaes, E., Jin, L., Brantley, S.L., 2010. Regolith production rates calculated with uranium-series isotopes at Susquehanna/Shale Hills Critical Zone Observatory. *Earth Planet. Sci. Lett.* 297, 211–225.
- Ma, L., Jin, L., Brantley, S.L., 2011. How mineralogy and slope aspect affect REE release and fractionation during shale weathering in the Susquehanna/Shale Hills Critical Zone Observatory. *Chem. Geol.* 290, 31–49.
- Ma, L., Konter, J., Herndon, E., Jin, L., Steinboeck, G., Sanchez, D., Brantley, S.L., 2015a. Quantifying an early signature of the industrial revolution from Pb concentrations and isotopes in soils of Pennsylvania, USA. *Anthropocene*. <http://dx.doi.org/10.1016/j.ancene.2014.12.003>.
- Ma, L., Teng, F., Jin, L., Ke, S., Yang, W., Gu, H., Brantley, S.L., 2015b. Mg isotope fractionation during shale weathering in the Shale Hills Critical Zone Observatory: accumulation of light Mg isotopes in soils by clay mineral transformation. *Chem. Geol.* 397, 37–50.
- Mariano, A.N., Mariano Jr., A., 2012. Rare earth mining and exploration in North America. *Elements* 8 (5), 369–376.
- Mathur, R., Jin, L., Paul, J., Prush, V., Ebersole, C., Fornadel, A., Williams, J., Brantley, S.L., 2012. Insights into the weathering processes of black shale through Cu isotopes and concentrations of the Marcellus Formation shale, Pennsylvania. *Chem. Geol.* 304–305, 175–184.
- McLennan, S.M., 1989. Rare earth elements in sedimentary rocks: influence of provenance and sedimentary processes. *Rev. Mineral.* 21, 169–200.
- Millero, F.J., 1992. Stability constants for the formation of rare earth inorganic complexes as a function of ionic strength. *Geochim. Cosmochim. Acta* 56, 3123–3132.
- Moller, P., 2002. The distribution of rare earth elements and yttrium in water-rock interactions: field observations and experiments. In: Stoerber, I., Bucher, K. (Eds.), Water-Rock Interaction. Kluwer Academic Publishers, Netherlands, pp. 97–123.
- Moller, P., Bau, M., 1993. Rare-earth patterns with positive cerium anomaly in alkaline lake waters from Lake Van, Turkey. *Earth Planet. Sci. Lett.* 117, 671–676.
- Möller, P., Giese, U., 1997. Determination of easily accessible metal fractions in rocks by batch leaching with acid cation exchange resin. *Chem. Geol.* 137, 41–55.
- Monastra, V., Derry, L.A., Chadwick, O.A., 2004. Multiple sources of lead in soils from a Hawaiian chronosequence. *Chem. Geol.* 209, 215–231.
- Muhs, D., Benedict, J., 2006. Eolian additions to late Quaternary alpine soils, Indian Peaks Wilderness Area, Colorado Front Range. *Arct. Alp. Res.* 38, 120–130.
- Neal, C., Kirchner, J., Reynolds, B., 2013. Plynlimon Research Catchment Hydrochemistry. NERC Environmental Information Data Center <http://dx.doi.org/10.5285/44095e17-43b0-45d4-a781-aab4f72da025>.
- Nesbitt, H.W., 1979. Mobility and fractionation of rare earth elements during weathering of a granodiorite. *Nature* 279, 206–210.
- Nesbitt, H.W., Markovics, G., 1997. Weathering of granodioritic crust, long-term storage of elements in weathering profiles, and petrogenesis of siliciclastic sediments. *Geochim. Cosmochim. Acta* 61, 1653–1670.
- Ohlander, B., Land, M., Ingris, J., Widerlund, A., 1996. Mobility of rare earth elements during weathering of till in northern Sweden. *Appl. Geochem.* 11, 93–99.
- Patino, L.C., Velbel, M.A., Price, J.R., Wade, J.A., 2003. Trace element mobility during spheroidal weathering of basalts and andesites in Hawaii and Guatemala. *Chem. Geol.* 202, 343–363.
- Petsch, S.T., Berner, R.A., Eglington, T.I., 2000. A field study of the chemical weathering of ancient sedimentary organic matter. *Org. Geochem.* 31, 475–487.
- Petsch, S.T., Edwards, K.J., Eglington, T.I., 2005. Microbial transformations of organic matter in black shales and implications for global biogeochemical cycles. *Palaeogeogr. Palaeoclimatol. Palaeoecol.* 219, 157–170.
- Prudencio, M.I., Gouveia, M.A., Sequeira Braga, M.A., 1995. REE distribution in present-day and ancient surface environments of basaltic rocks (central Portugal). *Clay Miner.* 30, 239–248.
- Rasmussen, C., Brantley, S., Richter, D., Blum, A., Dixon, J., White, A.F., 2011. Strong climate and tectonic control on plagioclase weathering in granitic terrain. *Earth Planet. Sci. Lett.* 301, 521–530.
- Reynolds, R.L., Mordecai, J.S., Rosenbaum, J.G., Ketterer, M.E., Walsh, M.K., Moser, K.A., 2010. Compositional changes in sediment of subalpine lakes, Uinta Mountains (Utah): evidence for the effects of human activity on atmospheric dust inputs. *J.*

- Paleolimnol. 44, 161–175.
- Rose, A.W., Cravotta, C.A., 1998. Coal mine drainage prediction and pollution prevention in Pennsylvania. Pennsylvania Department of Environmental Protection catalog # TN321.C6 1998. <http://www.techtransfer.osmre.gov/NTTMainsite/Library/pub/cmdppp.shtml>.
- Rudnick, R.L., Gao, S., 2003. Composition of the Continental Crust. Treatise on Geochemistry. 3. pp. 1–64.
- Salomons, W., 1995. Environmental impact of metals derived from mining activities: processes, predictions, prevention. *J. Geochem. Explor.* 52, 5–23.
- Shiller, A.M., 1997. Dissolved trace elements in the Mississippi river: seasonal, inter-annual, and decadal variability. *Geochim. Cosmochim. Acta* 61, 4321–4330.
- Shiller, A.M., 2010. Dissolved rare earth elements in a seasonally snow-covered, alpine/subalpine watershed, Loch Vale, Colorado. *Geochim. Cosmochim. Acta* 74, 2040–2052.
- Sholkovitz, E.R., 1993. The geochemistry of rare earth elements in the Amazon river estuary. *Geochim. Cosmochim. Acta* 57, 2181–2190.
- Sholkovitz, E.R., 1995. The aquatic chemistry of rare earth elements in rivers and estuaries. *Aquat. Geochem.* 1, 1–34.
- Soil Survey Staff, 1993. National Soil Survey Handbook, Title 430-VI. U.S. Govt. Printing Office, Washington, D.C.
- Stille, P., Steinmann, M., Pierret, M.-C., Gauthier-Lafaye, F., Chabaux, F., Viville, D., Pourcelot, L., Matera, V., Aouad, G., Aubert, D., 2006. The impact of vegetation on REE fractionation in stream waters of a small forested catchment (the Strengbach case). *Geochim. Cosmochim. Acta* 70, 3217–3230.
- Tang, Y., Han, G., Wu, Q., Xu, Z., 2013. Use of rare earth element patterns to trace the provenance of the atmospheric dust near Beijing, China. *Environ. Earth Sci.* 68, 871–879. <http://dx.doi.org/10.1007/s12665-012-1791-z>.
- Thomas, E., Lin, H., Duffy, C., Sullivan, P., Holmes, G.H., Brantley, S., Jin, L., 2013. Spatiotemporal patterns of water stable isotope compositions at the Shale Hills Critical Zone Observatory: linkages to subsurface hydrologic processes. *Vadose Zone J.* <http://dx.doi.org/10.2136/vzj2013.01.0029>.
- Thornthwaite, C.W., 1948. An approach toward a rational classification of climate. *Geogr. Rev.* 38, 55–94.
- Tuttle, M.L.W., Goldhaber, M.B., Ruppert, L.F., Hower, J.C., 2002. Arsenic in rocks and stream sediments of the Central Appalachian Basin, Kentucky. U.S. Geol. Surv. Open File Rep. 02–28.
- Tuttle, M.L.W., Breit, G.N., Goldhaber, M.B., 2003. Geochemical data from New Albany Shale, Kentucky: a study of metal mobility during weathering of black shales. U.S. Geol. Surv. Open File Rep. 03–207, 1–57.
- Tuttle, M.L.W., Breit, G.N., Goldhaber, M.B., 2009. Weathering of the New Albany Shale, Kentucky: II. Redistribution of minor and trace elements. *Appl. Geochem.* 24, 1565–1578.
- US Department of the Interior and US Geological Survey, 2011. Mineral Commodity Summaries 2011. US Government Printing Office.
- Vázquez-Ortega, A., Perdrial, J., Harpold, A., Zapata-Ríos, X., Rasmussen, C., McIntosh, J., Schaap, M., Pelletier, J.D., Brooks, P.D., Amistadi, M.K., Chorover, J., 2015. Rare earth elements as reactive tracers of biogeochemical weathering in forested rhyolitic terrain. *Chem. Geol.* 391, 19–32.
- Viers, J., Dupré, B., Braun, J.-J., Deberdt, S., Angeletti, B., Ngoupayou, J.N., Michard, A., 2000. Major and trace element abundances, and strontium isotopes in the Nyong basin rivers (Cameroon): constraints on chemical weathering processes and elements transport mechanisms in humid tropical environments. *Chem. Geol.* 169, 211–241.
- West, A.J., Galy, A., Bickle, M., 2005. Tectonic and climatic controls on silicate weathering. *Earth Planet. Sci. Lett.* 235, 211–228.
- West, N., Kirby, E., Bieman, P., Slingerland, R., Ma, L., Rood, D., Brantley, S.L., 2013. Regolith production and transport at the Susquehanna Shale Hills Critical Zone Observatory: part 2 - insights from meteoric ^{10}Be . *J. Geophys. Res. Earth Surf.* 118, 1–20.
- White, A.F., 2002. Determining mineral weathering rates based on solid and solute weathering gradients and velocities: application to biotite weathering in saprolites. *Chem. Geol.* 190, 69–89.
- White, A.F., Blum, A.E., 1995. Effects of climate on chemical weathering in watersheds. *Geochim. Cosmochim. Acta* 59, 1729–1747.
- White, A.F., Blum, A.E., Schulz, M.S., Vivit, D.V., Stonestrom, D.A., Larsen, M., Murphy, S.F., Eberl, D., 1998. Chemical weathering in a tropical watershed, Luquillo Mountains, Puerto Rico: I. Long-term versus short-term weathering fluxes. *Geochim. Cosmochim. Acta* 62, 209–226.
- White, A.F., Bullen, T.D., Schulz, M.S., Blum, A.E., Huntington, T.G., Peters, N.E., 2001. Differential rates of feldspar weathering in granitic regolith. *Geochim. Cosmochim. Acta* 65, 847–869.
- Williams, E.G., Keith, M.L., 1963. Relationship between sulfur in coals and the occurrence of marine roof beds. *Econ. Geol.* 58, 720–729.
- Williams, J.Z., Bandstra, J.Z., Pollard, D., Brantley, S.L., 2010. The temperature dependence of feldspar dissolution determined using a coupled weathering-climate model for Holocene-aged loess soils. *Geoderma* 156, 11–19.
- Wood, S.A., 1990. The aqueous geochemistry of the rare-earth elements and yttrium: 1. Review of available low-temperature data for inorganic complexes and the inorganic REE speciation of natural waters. *Chem. Geol.* 82, 159–186.
- Yesavage, T., Fantle, M.S., Vervoort, J., Mathur, R., Jin, L., Liermann, L.J., Brantley, S.L., 2012. Fe cycling in the Shale Hills Critical Zone Observatory, Pennsylvania: an analysis of microbiology, chemical weathering, and Fe isotope fractionation. *Geochim. Cosmochim. Acta* 99, 18–38.
- Yusoff, Z.M., Ngwenya, B.T., Parsons, I., 2013. Mobility and fractionation of REEs during deep weathering of geochemically contrasting granites in a tropical setting, Malaysia. *Chem. Geol.* 349–350, 71–86. <http://dx.doi.org/10.1016/j.chemgeo.2013.04.016>.